

TECHNISCHE UNIVERSITÄT MÜNCHEN

Lehrstuhl für Bauchemie

**Adsorption behavior and effectiveness of AMPS<sup>®</sup>-based cement  
fluid loss additives at high temperature and in combination  
with lignosulfonate and biogums**

**Nils Michael Recalde Lummer**

Vollständiger Abdruck der von der Fakultät für Chemie der Technischen Universität München zur Erlangung des akademischen Grades eines

**Doktors der Naturwissenschaften (Dr. rer. nat.)**

genehmigten Dissertation.

Vorsitzender: Univ.-Prof. Dr. Kai-Olaf Hinrichsen

Prüfer der Dissertation:

1. Univ.-Prof. Dr. Johann Peter Plank

2. Univ.-Prof. Dr. Volker Sieber

Die Dissertation wurde am 29.11.2010 bei der Technischen Universität München eingereicht und durch die Fakultät für Chemie am 01.02.2011 angenommen.

Ἄνδρα μοι ἔννεπε, Μοῦσα, πολύτροπον, ὃς μάλα πολλὰ  
πλάγχθη, ἐπεὶ Τροίης ἱερὸν πτολίεθρον ἔπερσε:...

Homer, *Odyssey*, Book 1, Lines 1 to 2

## Acknowledgments

This thesis is dedicated to my mother Ingried de Recalde. Without her love and unconditional support under all circumstances, I would not have succeeded. Kuhs la Muff!

Next, I would like to express my deep gratitude to Prof. Johann Plank for being a great doctor father and offering me a wonderful subject for research. I always enjoyed being a PhD student at the Chair for Construction Chemicals. Going to work always felt like coming home.

I especially want to thank Fatima Dugonjić-Bilić who has always been a good companion in all these years. I will miss you. Further thanks go to Daniel Bülchen, Constantin Tiemeyer and Salami Oyewole Taye; our successors in the oil field group. They have become more good friends to me than mere colleagues. I wish them all the best for their future.

I also would like to express my gratitude to Daniela Michler for her help to cope with bureaucracy in a pleasant and uncomplicated way. Gracias muchacha! For helping at laboratory experiments, my thanks go to Richard Beiderbeck and Dagmar Lettrich.

For his help regarding XRD measurements, I would like to thank Dr. Roland Sieber. I would also like to express my gratitude to Christof Schröfl for his company in the “Wuthöhle”. Thanks for being a great colleague during the CCS project go to Matthias Lesti. I would also like to thank Mirko Gruber and Friedrich von Hoessle for being the good souls of our chair.

Special thanks go to Thomas Pavlitschek for helping me with problems regarding my new computer. The collegial atmosphere felt in this chair is due to Hang Bian, Johanna de Reese, Xiaoxiao Du, Elina Dubina, Michael Glanzer, Markus Gretz, Ahmad Habbaba, Helena Keller, Holger König, Tobias Kornprobst, Zhaoyang Liu, Geok Bee Serina Ng, Vera Nilles, and Nan Zou. Thanks for your readiness to help.

Special thanks go to Dyckerhoff AG for supplying me with their oil well cement all these years which is the matrix of this thesis.

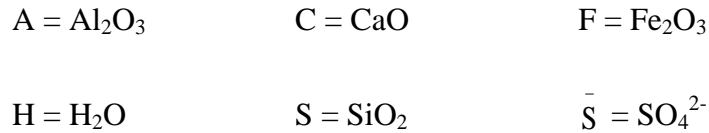
I also want to express my deep gratitude to my girlfriend Astrid Stück who always had an open and comforting ear for all the problems I encountered. Thanks for always being there for me.

## Abbreviations

AMPS <sup>®</sup>	2-acrylamido-2-methylpropane sulfonic acid
API	<i>American Petroleum Institute</i>
Bwoc	By weight of cement
Bwow	By weight of water
C	Coulomb
Da	Dalton
ESEM	Environmental scanning electron microscope
FLA	Fluid loss additive
GPC	Gel permeation chromatography
HTHP	High-temperature, high-pressure
IC	Ion chromatography
M	Molar (mol/L)
MWCO	Molecular weight cut off value
NNDMA	<i>N,N</i> -dimethyl acrylamide
Psi	Pounds per square inch
PV	Plastic viscosity
RI	Refractive index
Rpm	Rounds per minute
SEC	Size exclusive chromatography
TOC	Total organic carbon
TN	Total nitrogen
W/c ratio	Water to cement ratio
WOC	Waiting on cement
XRD	X-ray diffraction
YP	Yield point

## Chemical notation

In this work, the chemical formula of many cement compounds is expressed as a sum of oxides. In accordance to a special notation established by cement chemists, these oxides are abbreviated as follows:



Portland cement is mainly composed of four crystalline clinker phases known as tricalcium silicate ( $\text{Ca}_3(\text{SiO}_4)\text{O} = \text{C}_3\text{S}$ ), dicalcium silicate ( $\text{Ca}_2\text{SiO}_4 = \text{C}_2\text{S}$ ), tricalcium aluminate ( $\text{Ca}_9\text{Al}_6\text{O}_{18} = \text{C}_3\text{A}$ ), and tetra calcium aluminate ferrite ( $\text{Ca}_4\text{Al}_2\text{Fe}_2\text{O}_{10} = \text{C}_4\text{AF}$ ).

These phases react with water to form calcium silicate hydrates ( $x\text{CaO} \cdot y\text{SiO}_2 \cdot z\text{H}_2\text{O} = \text{C-S-H}$ ) and portlandite ( $\text{Ca}(\text{OH})_2 = \text{CH}$ ).

Further important products of cement hydration are ettringite ( $[\text{Ca}_6\text{Al}_2(\text{OH})_{12}](\text{SO}_4)_3 \cdot 26\text{H}_2\text{O} = \text{C}_3\text{A} \cdot 3\bar{\text{C}}\bar{\text{S}} \cdot \text{H}_{32}$ ) and calcium monosulfoaluminate (monosulfate) ( $[\text{Ca}_4\text{Al}_2(\text{OH})_{12}](\text{SO}_4) \cdot 6\text{H}_2\text{O} = \text{C}_3\text{A} \cdot \bar{\text{C}}\bar{\text{S}} \cdot \text{H}_{12}$ ).

## Journal publications

1. J. Plank; F. Dugonjic-Bilic; N. Recalde Lummer; S. Taye, *Working mechanism of polyvinyl alcohol cement fluid loss additive*, Journal of Applied Polymer Science, 117, **2010**, 2290.
2. J. Plank; N. Recalde Lummer; F. Dugonjic-Bilic, *Competitive adsorption between an AMPS<sup>®</sup>-based fluid loss polymer and welan gum biopolymer in oil well cement*, Journal of Applied Polymer Science, 116, **2010**, 2913.
3. J. Plank; F. Dugonjic-Bilic; N. Recalde Lummer, *Impact of the steric position of phosphonate groups in poly(N,N-dimethylacrylamide-co-2-acrylamido-2-methylpropanesulfonate-co-2-X-phosphonate) on its adsorbed conformation on cement: Comparison of vinylphosphonic acid and 2-acrylamido-2-methylpropane phosphonate modified terpolymers*, Journal of Applied Polymer Science, 115, **2009**, 1758.
4. J. Plank; F. Dugonjic-Bilic; N. Recalde Lummer, *Modification of the molar anionic charge density of acetone-formaldehyde-sulfite dispersant to improve adsorption behavior and effectiveness in presence of CaAMPS-co-NNDMA cement fluid loss polymer*, Journal of Applied Polymer Science, 111, **2009**, 2018.
5. J. Plank; A. Brandl; N. Recalde Lummer, *Effect of different anchor groups on adsorption behavior and effectiveness of poly(N,N-dimethylacrylamide-co-Ca 2-acrylamido-2-methylpropanesulfonate) as cement fluid loss additive in presence of acetone-formaldehyde-sulfite dispersant*, Journal of Applied Polymer Science, 106, **2007**, 3889.

### Conference papers and posters

1. N. Recalde Lummer; F. Dugonjic-Bilic; D. Büllichen; J. Plank, *Wichtige Zusatzmittel für die Tiefbohrzementierung*, GDCh-Monographie, 41, **2009**, 181.
2. F. Dugonjic-Bilic; J. Plank; N. Recalde Lummer, *Synthetische Wasserretentionsmittel - Chemie, Eigenschaften und Wirkmechanismus in Tiefbohrzement*, GDCh-Monographie, 41, **2009**, 43.
3. J. Plank; F. Dugonjic-Bilic; N. Recalde Lummer; D. Sadasivan, *Comparative study of the working mechanisms of chemically different cement fluid loss polymers*, **2009** SPE International Symposium on Oilfield Chemistry, The Woodlands/TX, SPE paper 121542.
4. J. Plank; N. Recalde Lummer; F. Dugonjic-Bilic, *Physico-chemical interactions perturbing the effectiveness of an ATBS-based fluid loss polymer used in oil well cementing*, **2009** SPE International Symposium on Oilfield Chemistry, The Woodlands/TX, SPE paper 121541.
5. N. Recalde Lummer; F. Dugonjic-Bilic; J. Plank, *Einfluss von Temperatur und Ionenstärke auf die Adsorption von CaAMPS-Co- und Terpolymeren an Silica*, GDCh-Monographie, 39, **2008**, 365.
6. N. Recalde Lummer; A. Brandl; F. Dugonjic-Bilic; J. Plank, *Einfluss der Temperatur auf die Wirksamkeit von Poly(N,N-Dimethylacrylamid-co-Ca 2-Acrylamido-2-methylpropan sulfonat) als Fluid Loss-Additiv in Tiefbohrzement*, GDCh-Monographie, 37, **2007**, 245.
7. A. Brandl; N. Recalde Lummer; J. Plank, *Kompetitive Adsorption anionischer Polymere an Zement: Steuerung des Adsorptionsverhaltens eines anionischen Wasserretentionsmittels durch gezielte Einführung qualitativ unterschiedlicher Ankergruppen*, GDCh-Monographie, 36, **2006**, 41.

<b>1</b>	<b>INTRODUCTION .....</b>	<b>1</b>
<b>2</b>	<b>THEORETICAL BACKGROUND .....</b>	<b>3</b>
2.1	Primary cementing .....	3
2.2	Mineralogy and properties of oil well cements .....	5
2.2.1	API classification system for oil well cements .....	6
2.2.2	Portland cement hydration .....	7
2.2.3	Rheology of cement slurries .....	15
2.2.4	Salt cement slurries .....	17
2.3	Influences of polyelectrolytes on the properties of cement slurries .....	18
2.3.1	Polyelectrolyte adsorption and zeta potential of mineral surfaces .....	18
2.3.2	Fluid loss additives .....	19
2.3.3	Microbial biopolymers .....	24
2.3.4	Cement retarders .....	28
<b>3</b>	<b>GOAL OF THIS THESIS .....</b>	<b>31</b>
<b>4</b>	<b>EXPERIMENTAL .....</b>	<b>33</b>
4.1	Materials .....	33
4.1.1	Oil well cement .....	33
4.1.2	Silica .....	35
4.1.3	Synthesis of AMPS <sup>®</sup> -based fluid loss polymers .....	37

4.2	Instruments and procedures .....	41
4.2.1	Cement characterization .....	41
4.2.2	Silica characterization .....	41
4.2.3	Polymer characterization .....	41
4.2.4	Cement slurry preparation .....	44
4.2.5	Compressive strength analysis .....	44
4.2.6	Rheology measurement .....	45
4.2.7	Fluid loss test.....	45
4.2.8	Analysis of slurry thickening time .....	46
4.2.9	Analysis of cement pore solution .....	47
4.2.10	Measurement of free water content .....	47
4.2.11	Silica slurry preparation .....	47
4.2.12	Adsorption of polymers.....	47
4.2.13	Adsorption of sulfate ions onto the silica surface .....	48
4.2.14	Adsorption of chloride ions onto the cement surface.....	48
4.2.15	Zeta potential measurement .....	49
4.2.16	Environmental scanning electron microscopy (ESEM) .....	49
<b>5</b>	<b>RESULTS AND DISCUSSION.....</b>	<b>50</b>
5.1	Cement hydration at ambient and elevated temperature .....	51
5.1.1	Impact of temperature on cement hydration and the resulting hydrates .....	51
5.1.2	Conclusions .....	55

5.2	Impact of high temperature on the adsorption behavior and effectiveness of AMPS <sup>®</sup> -based fluid loss additives.....	56
5.2.1	Synthesis and characterization of the AMPS <sup>®</sup> -based fluid loss additives .....	56
5.2.2	Temperature-dependent interaction of FLAs with cement .....	61
5.2.3	Dynamic viscosity of HTHP filtrates at elevated temperature.....	65
5.2.4	Dynamic viscosity of HTHP filtrates containing stiffer terpolymers .....	66
5.2.5	Effect of temperature on the sulfate content of cement pore solutions .....	68
5.2.6	Sulfate-dependent adsorption of FLAs on silica .....	70
5.2.7	Conformation of solved FLA polymers .....	72
5.2.8	Conclusions .....	74
5.3	Effectiveness of AMPS <sup>®</sup> -based FLAs in salt cement slurries.....	75
5.3.1	Effectiveness of CaAMPS <sup>®</sup> - <i>co</i> -NNDMA in salt cement slurries .....	75
5.3.2	Effectiveness of CaAMPS <sup>®</sup> - <i>co</i> -NNDMA- <i>co</i> -MA in salt cement slurries .....	78
5.3.3	Conclusions .....	79
5.4	Interaction between CaAMPS <sup>®</sup> - <i>co</i> -NNDMA and biopolymers.....	80
5.4.1	Interaction of CaAMPS <sup>®</sup> - <i>co</i> -NNDMA with cement.....	80
5.4.2	Interaction of microbial biopolymers with cement .....	82
5.4.3	Binary systems containing CaAMPS <sup>®</sup> - <i>co</i> -NNDMA and a free water control agent.....	84
5.4.4	Conclusions .....	91
5.5	Interaction between CaAMPS <sup>®</sup> - <i>co</i> -NNDMA and Na <sup>+</sup> lignosulfonate... 92	
5.5.1	Comparison of Ca-LS and Na-LS as cement plasticizer and retarder.....	92
5.5.2	Interaction of Na <sup>+</sup> lignosulfonate with calcium ions.....	95
5.5.3	Interaction of Na <sup>+</sup> lignosulfonate with cement.....	97
5.5.4	Adsorption behavior and effectiveness of CaAMPS <sup>®</sup> - <i>co</i> -NNDMA .....	101

# CONTENT

---

5.5.5	Adsorption behavior and effectiveness of Na <sup>+</sup> lignosulfonate.....	103
5.5.6	Conclusions .....	105
<b>6</b>	<b>SUMMARY AND OUTLOOK.....</b>	<b>106</b>
6.1	Summary.....	106
6.2	Outlook .....	110
<b>7</b>	<b>ZUSAMMENFASSUNG .....</b>	<b>111</b>
<b>8</b>	<b>APPENDIX.....</b>	<b>114</b>
<b>9</b>	<b>REFERENCES.....</b>	<b>117</b>

**1 INTRODUCTION**

The U.S. petroleum industry traditionally dates its beginning back to the drilling of the *Drake* well in 1859 [1]. However, it was not until 1903 that *Frank F. Hill* from *Union Oil Company* mixed neat Portland cement with water in a bailer and filled the resulting slurry into a borehole in the *Lompoc* field [2]. This shut off the downhole water influx above the oil sand, enabling his crew to complete the well by drilling through the isolated oil sand. This first procedure of primary cementing was named after his inventor *Hill's* dump-bailer technique which was replaced by the two-plug method introduced by *Almond A. Perkins* in 1910. In his process, a cement sheath is placed in the annulus between a tubular pipe referred to as the casing and the formations exposed to the wellbore, to provide zonal isolation in oil, gas, and water wells [3]. Here, a hydraulic seal must be created between the casing, the hardened cement, and the formation of the bore hole to ensure the integrity of the well. Since this time, it has been a major objective in primary cementing to improve methods for the separation of fluids such as water or gas occurring in one zone from oil in another section of the well. Portland cement based systems for well cementing are routinely designed to perform at temperatures ranging from below freezing in permafrost zones to 250 °C in geothermal wells. They also encounter pressure from near ambient in shallow wells to more than 1,500 bar in deep wells. In addition to severe temperatures and pressures, well cements must be designed to contend with weak or porous formations, corrosive fluids, and over-pressured formation fluids. However, only the use of cement admixtures makes it possible to accommodate to the broad range of conditions [4].

For example, fluid loss additives (FLAs) are commonly added to the cement slurry to ensure a good cement job in porous formations. In contrast, when neat cement slurry is pumped along a porous formation, its mixing water may be filtered off rapidly by the formation. The detrimental consequence is an increase in slurry viscosity resulting in incomplete cementation of the borehole and hence the loss of zonal isolation. In the 1960s, the first water-soluble fluid loss polymer was a polypeptide extracted from soybeans. Shortly thereafter, ethylene diamine carboxymethylcellulose and other cellulose derivatives were introduced. However, cellulosic fluid loss additives cause undesired viscosification of the cement slurry and show low thermal stability. Therefore, they have been replaced by synthetic polymers such as polyethylene imine and polyvinyl alcohol. Nevertheless, polymer accumulation in fish-gills limited the use

of these admixtures [5]. Nowadays, environmentally-friendly copolymers are applied to provide fluid loss control of the cement slurry, even under demanding borehole conditions such as high temperature, pressure and salinity. In comparison to cellulose-based FLAs, these water-soluble polymers provide higher thermal stability and lower viscosification of the cement slurry. In 1982, former *Hoechst AG* pioneered the technology of synthetic FLAs by introducing a terpolymer composed of 2-acrylamido-2-methylpropane sulfonic acid (AMPS<sup>®</sup>), acrylic acid, and N-methyl N-vinyl acetamide (*Hostamer*<sup>®</sup>). This copolymer can be used at borehole temperatures up to 200 °C. At low temperatures (< 100 °C), however, this polymer shows only poor FLA effectiveness. To overcome this detrimental effect, *Halliburton* established an anionic copolymer of AMPS<sup>®</sup> and *N,N*-dimethyl acrylamide (*Halad*<sup>®</sup>-344) in 1986 [6]. As these synthetic admixtures are quite expensive, their use is only cost-effective for deep wells.

Other admixtures such as sodium chloride, free water control agents and retarders are frequently used to adjust the properties of the cement slurry to the borehole conditions. Occasionally, salt cement slurries are used for the cementation of oil wells. Here, sodium chloride up to its saturation level of 36 % by weight of water is added to the slurry. For example, this procedure avoids well bore washout resulting from the osmotic dissolution of salt into the cement slurry when cementing a salt formation [7]. In contrast, free water control agents such as microbial biopolymers prevent the formation of bleeding water at the top of the cement column which would otherwise pose a serious problem for zonal isolation. Additionally, the hydration of Portland cement must be retarded to avoid premature setting of the cement slurry during pumping. Depending on the well depth, a pumping time (i.e., the period of time in which the cement slurry remains in its fluid state) of 4 to 6 hours is required [8]. The most common retarders are based on lignosulfonates [9] [10].

Needless to say that borehole conditions often require the combined use of several additives. In these multi-admixture systems, however, polymer incompatibility can considerably reduce the effectiveness of each component. Additional expenses can result from higher admixture dosages and, in the worst case, failure of the cement slurry to perform could be the consequence. Thus, studies regarding additive/additive interactions are needed to create guidelines for the formulation of improved cementing systems which provide more effective and safe cement jobs.

## **2 THEORETICAL BACKGROUND**

In this chapter, after a brief description of the procedure of primary cementing, the mineralogy of oil well cements and their hydration process are discussed. Additionally, salt cement slurry and its fields of application as well as the interaction of anionic polyelectrolytes with cement mineral surfaces are presented. Furthermore, the characteristic properties of the anionic FLA polymers used in this study and their working mechanism are specified. Special emphasis is given to admixture/admixture interactions which can influence the performance of each polymer present in the cement slurry.

### **2.1 Primary cementing**

The major objective of primary cementing is zonal isolation. To separate fluids such as water or gas in one zone from oil occurring in other zones of the well, metal liners (casing) are placed into the borehole. The space between the casing and the formation is called the annulus. Cement slurry is then pumped through the casing and pushed up the annulus. A bottom plug is placed ahead of the cement slurry to minimize contamination of cement by other fluids present in the borehole (see **Figure 1; left**) [11]. After reaching the float collar, a diaphragm in the bottom plug ruptures allowing the slurry to pass through. In contrast, the top plug possesses a solid body which indicates its contact with the float collar and the bottom plug through an increase in the pumping pressure. This indicates the end of the cementing process (see **Figure 1; right**). A waiting period referred to as waiting on cement (WOC) time is necessary to allow the cement slurry to harden. This method of drilling and cementing is repeated until the desired depth of the well is reached. Since this procedure is one of the most critical stages during the construction of a wellbore, a high quality oil well cement slurry is essential for the integrity of the wellbore.

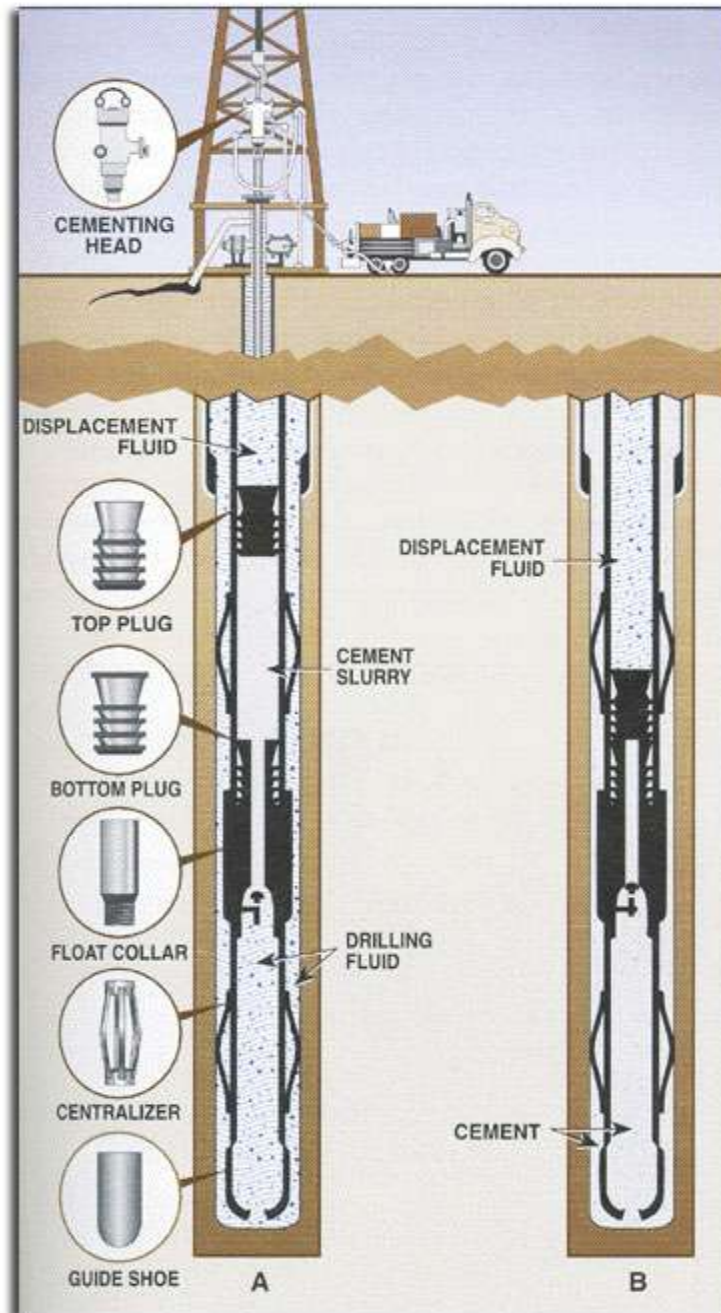


**Figure 1** Illustration of the two-plug method used in primary cementing; **left:** cementing job in progress; **right:** the top plug has successfully connected with the bottom plug and the float collar signaling the end of the cement job [12].

## 2.2 Mineralogy and properties of oil well cements

Oil well cements are generally Portland cements. This material is mainly composed of four crystalline clinker phases known as tricalcium silicate ( $\text{Ca}_3(\text{SiO}_4)\text{O} = \text{C}_3\text{S}$ ), dicalcium silicate ( $\text{Ca}_2\text{SiO}_4 = \text{C}_2\text{S}$ ), tricalcium aluminate ( $\text{Ca}_3\text{Al}_2\text{O}_6 = \text{C}_3\text{A}$ ), and tetra calcium aluminate ferrite ( $\text{Ca}_4\text{Al}_2\text{Fe}_2\text{O}_{10} = \text{C}_4\text{AF}$ ). The different characteristic appearances of the cement clinker phases observed on an optical microscope and after etching with an organic dye are illustrated in **Figure 2**.



**Figure 2** Thin section of an unhydrated oil well cement particle showing its constituents (particle size: 30  $\mu\text{m}$ ) [13].

$C_3S$  forms hexagonal or angular crystals, whereas  $C_2S$  crystallizes in spherical or rounded shapes. On the other hand, the aluminate phase  $C_3A$  appears as gray rhombohedrons.  $C_4AF$  presents the violet matrix which surrounds the rest of the cement components. Periklas ( $MgO$ ) crystallizes in small, pink hexagonal plates and free lime ( $CaO$ ) forms small, turquoise spheres, generally found in clusters.

### 2.2.1 API classification system for oil well cements

According to API specification 10 A issued by the *American Petroleum Institute* (API), there are currently eight classes of API-ISO Portland cements which are designated A to H [14]. **TABLE 1** lists them depending on the borehole depths and the temperature ranges at which they can be used.

**TABLE 1**

**Clinker composition and application ranges for API oil well cements [14]**

API Class	Typical phase composition (wt. %)				Well depth (ft)	Temperature range (°F)
	$C_3S$	$C_2S$	$C_3A$	$C_4AF$		
A	53	24	8	8	0 to 6,000	80 to 170
B	47	32	5	12	0 to 6,000	80 to 170
C	58	16	8	8	0 to 6,000	80 to 170
D	26	54	2	12	6,000 to 12,000	170 to 260
E	26	54	2	12	6,000 to 14,000	170 to 290
F	26	54	2	12	10,000 to 16,000	230 to 320
G	50	30	5	12	0 to 8,000	80 to 200
H	50	30	5	12	0 to 8,000	80 to 200

API Classes G and H cements are by far the most commonly used well cements today. They were developed in response to improved technology for slurry acceleration and retardation by chemical admixtures. Compared to the other cements, they contain less of the most reactive clinker phase  $C_3A$ . This results in higher sulfate resistance and prolonged cement hydration. In this study, an API Class G oil well cement was used.

Manufacturers of API classified cements are prohibited from adding various chemicals, even grinding agents such as glycols or acetates, to the clinker. These admixtures would improve the efficiency of grinding, but have been shown a potential to influence the effectiveness of cement additives. Consequently, oil well cements are quite coarse and possess low specific surface area in comparison to construction cements. This low surface area of  $\sim 3,000 \text{ cm}^2/\text{g}$  for API oil well cements compared to  $\sim 5,000 \text{ cm}^2/\text{g}$  for a high quality construction cement (as measured according to the method established by *Blaine*) affects the hydration behavior of the oil well cement [13].

## 2.2.2 Portland cement hydration

Upon contact with water, the clinker phases  $C_3S$ ,  $C_2S$ ,  $C_3A$ , and  $C_4AF$  display different hydration kinetics and form diverse hydration products [15]. Owing to the complexity of cement hydration, current research largely studies the behavior of individual clinker phases in an aqueous environment and relates the results to the behavior of the entire Portland cement system.

### 2.2.2.1 Hydration of $C_3S$ and $C_2S$

Through hydration of the silicate phases, amorphous gel-like calcium silicate hydrate phases (C-S-H phases in the following) and portlandite (CH) are formed (see **Figure 3**). The chemical composition of the C-S-H phases varies with the presence of silica, temperature, and water to cement (w/c) ratio [16] [17] [18]. Resulting from its high abundance in cement ( $\sim 68 \text{ wt. } \%$ ), the hydration of  $C_3S$  is largely responsible for the beginning of the set and early strength development of the cement paste.

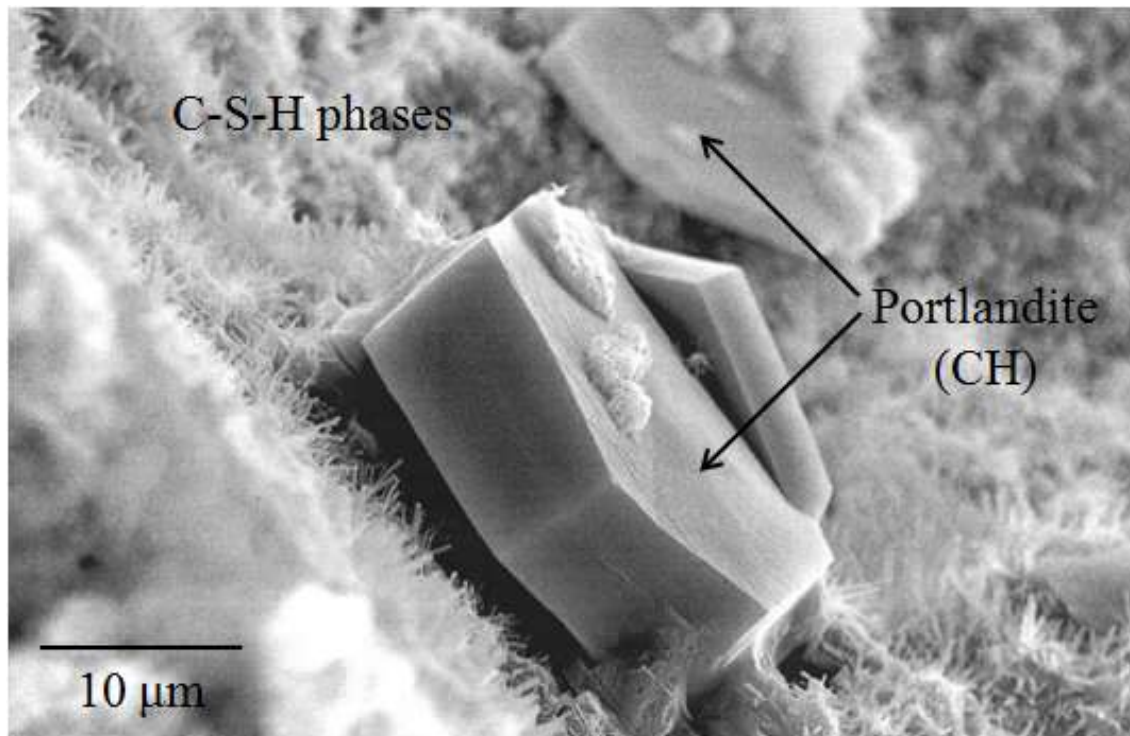


**Figure 3** SEM micrograph of hydrated  $C_3S$ . Portlandite ( $Ca(OH)_2$ ) crystallizes as hexagonal platelets resting on needles of C-S-H phases.

In comparison, the hydration of  $C_2S$  is significant only in terms of the final strength of the hardened cement. As the mechanism of  $C_2S$  hydration and its resulting C-S-H phases are very similar to those known for  $C_3S$ , only the latter will be considered here. Through calorimetric measurements, five stages of  $C_3S$  hydration can be defined: (I) the preinduction period, (II) the induction period, (III) and (IV) the acceleration and deceleration period, and (V) the diffusion period (see **Figure 4**) [19].

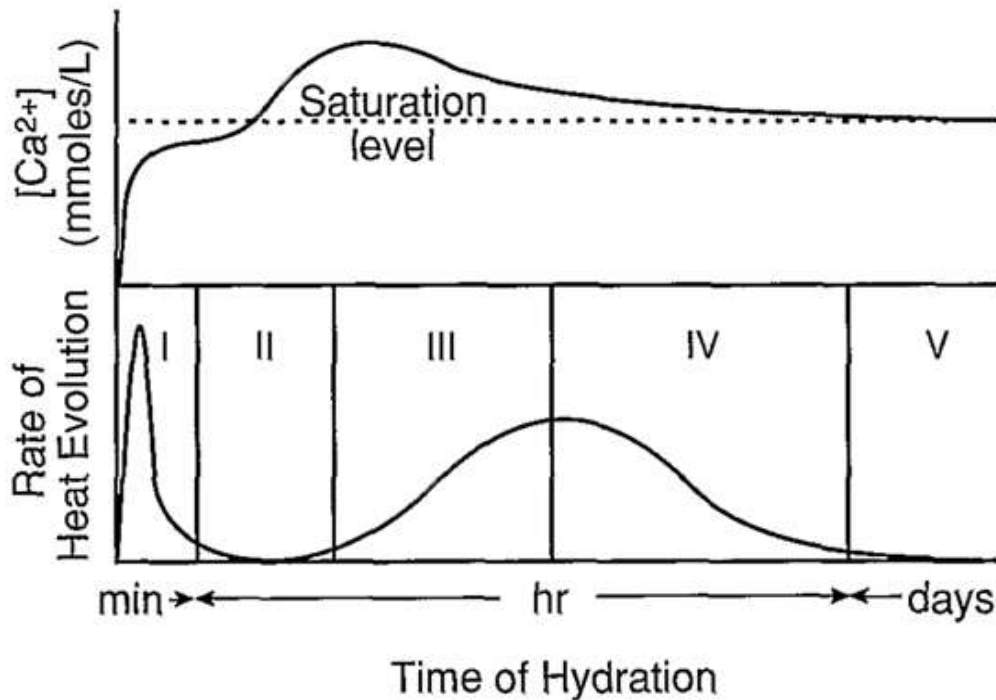


**Figure 4** Schematic representation of characteristic periods occurring during  $C_3S$  hydration [7]: (I) preinduction period, (II) induction period, (III) and (IV) acceleration and deceleration period, and (V) diffusion period.

### I Preinduction period

The preinduction period begins upon contact of  $C_3S$  with water and lasts only a few minutes. During this period,  $C_3S$  dissolution is faster than the diffusion of the reaction products away from its surface. As a result, the liquid phase surrounding the hydrating  $C_3S$  becomes supersaturated, and a layer of C-S-H phases begins to precipitate onto the surface [20].

### II Induction period

During the induction period, relatively little hydration activity can be observed. Several theories have been proposed on the mechanisms involved:

The *impermeable layer theory* postulates that C-S-H phases precipitated onto  $C_3S$  grains act as a barrier hindering the migration of water to the unhydrated surface of the clinker and the release of solvated ions into the liquid phase. Toward the end of this dormant period, the initial C-S-H layer becomes more permeable, and the hydration rate accelerates [21].

There are three principal theories to explain the increased permeability: According to *de Jong et al.*, the C-S-H layer ages and undergoes a morphological change, resulting in increased permeability [22]. Another theory holds that osmotic pressure is generated between the C-S-H layer and the unhydrated  $C_3S$  surface. Only when this gel layer eventually bursts, the unhydrated clinker is again exposed to water [23]. The third proposed mechanism involves the breakdown of the C-S-H layer because of water imbibition [24].

In contrast, the *electrical double-layer theory* assumes that the initial hydration of  $C_3S$  is incongruent. A  $SiO_2$ -rich layer adsorbs  $Ca^{2+}$  ions and creates an electrical double layer that impedes the passage of additional ions into solution. Gradually, this layer breaks down, and the hydration rate accelerates [25].

According to the theory of *nucleation of  $Ca(OH)_2$* , the surface of calcium hydroxide nuclei are poisoned by adsorbed silica ions preventing precipitation of portlandite ( $Ca(OH)_2$ ). Because the reaction of  $C_3S$  with water always produces calcium hydroxide, the resulting supersaturation of  $Ca(OH)_2$  in the liquid phase retards further hydration of  $C_3S$ . Eventually,  $\sim 1.5$  to  $2.0$  times the saturation concentration is reached, leading to the formation of stable nuclei and the precipitation of portlandite [26].

The theory of *nucleation of C-S-H* postulates the nucleation and growth of “second-stage” C-S-H phases. Those are formed when the concentration and size of their nuclei reach a critical level. At the same time, solid  $Ca(OH)_2$  starts to precipitate.

### **III and IV Acceleration and deceleration period**

These periods represent the interval of most rapid hydration. During the acceleration period, solid  $Ca(OH)_2$  crystallizes from solution and the C-S-H phases deposit into the water-filled pore space. The hydrates form a cohesive network which provides the compressive strength of the system. Eventually, hydrate deposition hinders the transportation of ions and water through this network. As a result, the hydration rate decelerates.

### **V Diffusion period**

Hydration continues at a slow pace owing to the permanently decreasing porosity of the system. Here, portlandite crystals continue to grow and engulf the hydrating  $C_3S$  grains. Thus, complete hydration can take anything between 1 and 20 years, depending on the fineness of the cement.

### 2.2.2.2 Hydration of C<sub>3</sub>A

C<sub>3</sub>A is the most reactive cement clinker phase and possesses the highest enthalpy of hydration [19]. In absence of sulfate, it quickly reacts with water to form calcium aluminate hydrates. This uncontrolled hydration of the tricalcium aluminate phase causes a severe increase of cement rheology and has a detrimental effect on cement paste workability.

Therefore, the hydration of C<sub>3</sub>A must be controlled by the addition of gypsum (CaSO<sub>4</sub>·2H<sub>2</sub>O) to the cement clinker to prolong the workability period of cement. Upon contact with water, part of the gypsum dissolves into calcium and sulfate ions. With aluminate and hydroxyl ions, they form the hydration product ettringite [27]. This hydrate precipitates onto the C<sub>3</sub>A surface, thus decreasing its hydration rate. When the supply of gypsum is exhausted, the SO<sub>4</sub><sup>2-</sup> concentration drops sharply. At a sulfate content of ~ 2.3 g/L, ettringite becomes unstable and converts to platy calcium monosulfoaluminate hydrate. As soon as the protective sulfoaluminate layer breaks down, rapid hydration resumes [28].

### 2.2.2.3 Hydration of C<sub>4</sub>AF

The calcium aluminoferrite phase is a solid solution with the general formula Ca<sub>4</sub>Al<sub>x</sub>Fe<sub>(2-x)</sub>O<sub>10</sub>, where x varies from 0 to 1.4. Under comparable conditions, the hydration products of the ferrite phase are in many respects similar to those formed by C<sub>3</sub>A. The reactivity of the ferrite phase generally declines with increasing Fe content [29]. In the absence of gypsum, the course of ferrite phase hydration is comparable to that of C<sub>3</sub>A. Through addition of gypsum, an aluminoferrite trisulfate (AFt) phase is formed (similar to ettringite) which eventually converts to aluminoferrite monosulfate [19].

## 2.2.2.4 Hydration of Portland cement

The hydration of Portland cement is a complex dissolution and precipitation process in which, unlike the hydration of the individual pure phases, the various hydration reactions proceed simultaneously at different rates. **Figure 5** shows a typical thermogram resulting from the hydration of Portland cement.

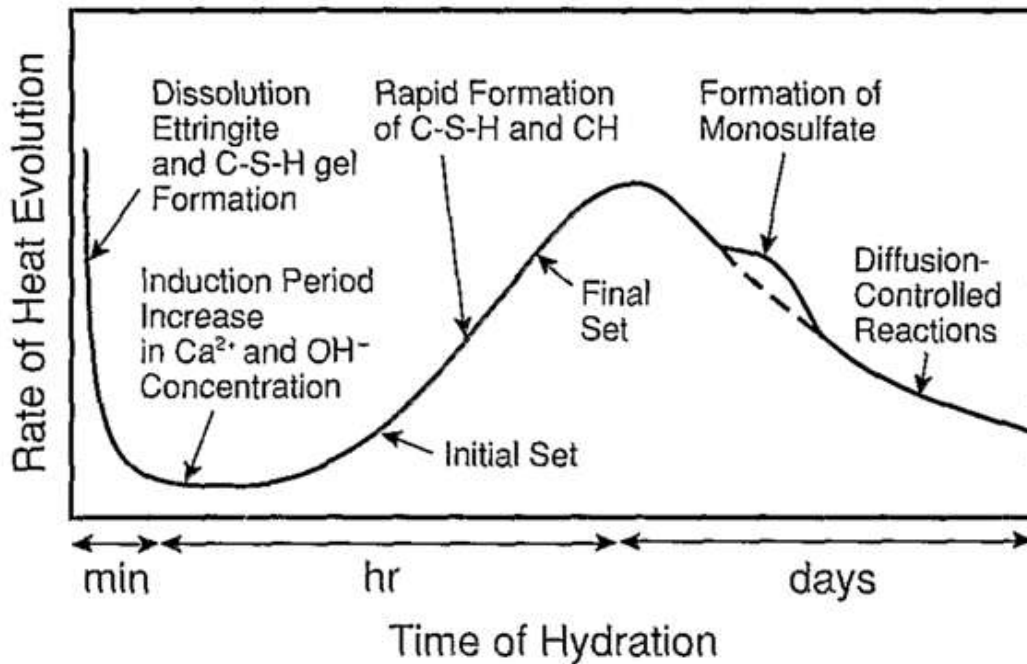


**Figure 5** Schematic representation of Portland cement hydration [7]. The formation of the different phases is indicated as rate of heat evolution as a function of time of hydration.

Although the hydration of  $C_3S$  is often used as a model for the hydration of Portland cement, it must be kept in mind that many additional parameters are involved. For example, the clinker phases influence each other regarding their hydration process. Besides, none of the clinker minerals is pure. Depending upon the composition of the raw materials, each contains foreign oxides in solid solution that alter their reactivity [30].

#### 2.2.2.5 Hydration of oil well cement at high temperature

Temperature is a key variable affecting the hydration of cement because it influences both the early hydration kinetics and the properties of the hardened cement [31]. Although cement slurry initially gains strength more rapidly when cured at increased temperature, the final strength is lower and its permeability higher. SEM studies have shown that the outer-product C-S-H gel is denser at elevated temperature, resulting from an increase in the rate of silicate polymerization. This hydrate does not fill the capillary pore space as effectively as cement cured at low temperature [32] [33]. Elevated temperature may also alter the composition of the pore solution and the equilibrium assemblage of solid phases present in the cement paste [34]. A particular important example is the relative stability of ettringite and calcium monosulfoaluminate (monosulfate). During the early periods of cement hydration, the concentration of sulfate present in the pore solution is high and, consequently, ettringite is more stable than monosulfate. As the temperature increases, monosulfate eventually becomes the favored phase resulting from its smaller enthalpy of reaction [35] [36].

At temperatures above 110 °C, a phase called alpha dicalcium silicate hydrate ( $\alpha$ -C<sub>2</sub>SH) is formed through C<sub>3</sub>S hydration [37] [38]. Compared to C-S-H phases,  $\alpha$ -C<sub>2</sub>SH provides higher crystallinity and hence higher density which results in shrinkage of the cement matrix. This effect causes a significant loss of compressive strength and severe increase of water-permeability in the hardened cement [39]. To prevent this so called *strength retrogression*, the Ca/Si molar ratio is reduced from initially 1.5 to approximately 1.0 by addition of 35 % to 40 % silica (by weight of cement). Under those conditions, a mineral phase known as tobermorite (C<sub>5</sub>S<sub>6</sub>H<sub>5</sub>) is formed instead of  $\alpha$ -C<sub>2</sub>SH, thus preserving high compressive strength and low permeability for the set cement.

As the curing temperature increases to about 150 °C, tobermorite normally converts to xonotlite ( $C_6S_6H$ ) and a minor amount of gyrolite ( $C_6S_3H_2$ ) (see **Figure 6**) [40] [41].

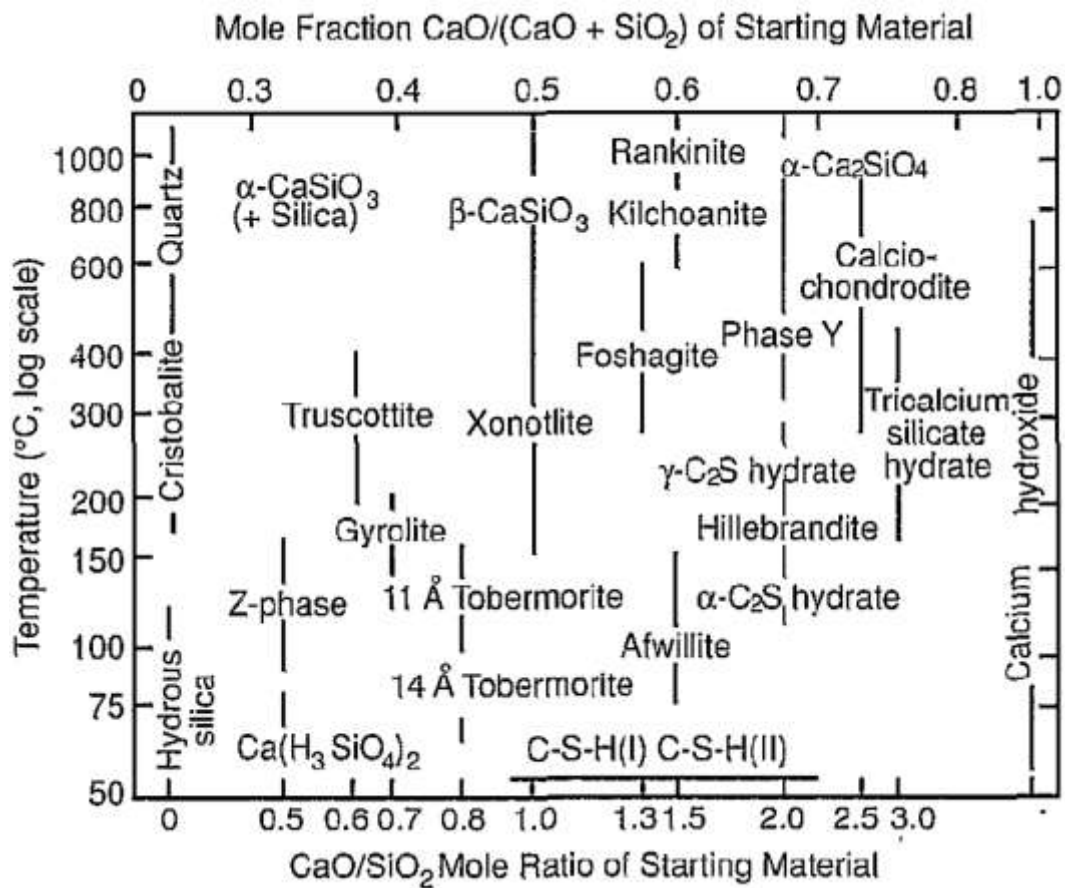


**Figure 6** Formation conditions for various calcium silicate hydrates [42].

Tobermorite sometimes persists to 250 °C, because of aluminum substitution in the lattice structure. Starting from this temperature, truscottite ( $C_7S_{12}H_3$ ) is formed [43]. At temperatures higher than 400 °C, xonotlite and truscottite dehydrate, resulting in disintegration of the set cement [44].

### 2.2.3 Rheology of cement slurries

In order to accurately design, execute, and evaluate a primary cement job, it is crucial to understand the rheological properties of the cement slurry. Here, proper rheological characterization of the slurry is essential to evaluate its mixing behavior and pumpability as well as to optimize mud removal and slurry placement.

Generally, rheology describes the relationship between stress, strain, rate of strain, and time. In a shear flow, imaginary parallel layers of liquid move in response to a shear stress to produce a velocity gradient. This gradient is referred to as shear rate and is equivalent to the rate of increase of shear strain [45]. All fluids can be characterized by their flow curves, resulting from the relation between shear stress and shear rate under constant shear. For example, *Newtonian* fluids such as water comply with the *Newtonian* model, in which the shear stress is directly proportional to the shear rate (see **Equation 1**).

$$\tau = \eta\gamma'$$

**Equation 1** Relationship between shear stress  $\tau$ , viscosity  $\eta$ , and shear rate  $\gamma'$  for *Newtonian* fluids.

In contrast, cement-based materials will flow only when the force exercised exceeds the yield point (YP). The simplest analysis, which involves solid-like behavior, is that of the *Bingham* model. There, the material is an elastic solid only at a shear stress which is smaller than the yield point, but flows at higher stresses (see **Equation 2**). Thus, YP is a measure of the flow resistance, which is the force necessary to start movement of the slurry, whereas the plastic viscosity (PV) determines the resistance of the paste against an increased speed of movement [46].

$$\tau = \tau_0 + \mu\gamma'$$

**Equation 2** Relationship between shear stress  $\tau$ , yield point  $\tau_0$ , plastic viscosity  $\mu$ , and shear rate  $\gamma'$  according to the *Bingham* model.

However, fluids do not always exhibit linear flow behavior and non-linear approximations have to be applied. *Power-law* fluids are part of a class known as pseudo-plastic fluids. Like *Newtonian* fluids, they flow immediately when a pressure gradient is applied, even though the relationship between shear rate and shear stress is not linear.

*Herschel-Bulkley* fluids combine *Power-law* and *Bingham* plastic behavior. Like *Bingham* plastic fluids, there is a yield stress that must be exceeded before flow commences. Above the yield stress, as with *Power-law* fluids, the shear-rate/shear stress relationship follows the power law. The standard equipment used to characterize the rheological properties of cement slurries and other oilfield fluids (e.g., drilling muds, spacers, fracturing fluids, etc.) is a coaxial cylinder viscometer, described by *Savins* and *Roper* in 1954 (see **Figure 7**) [47].

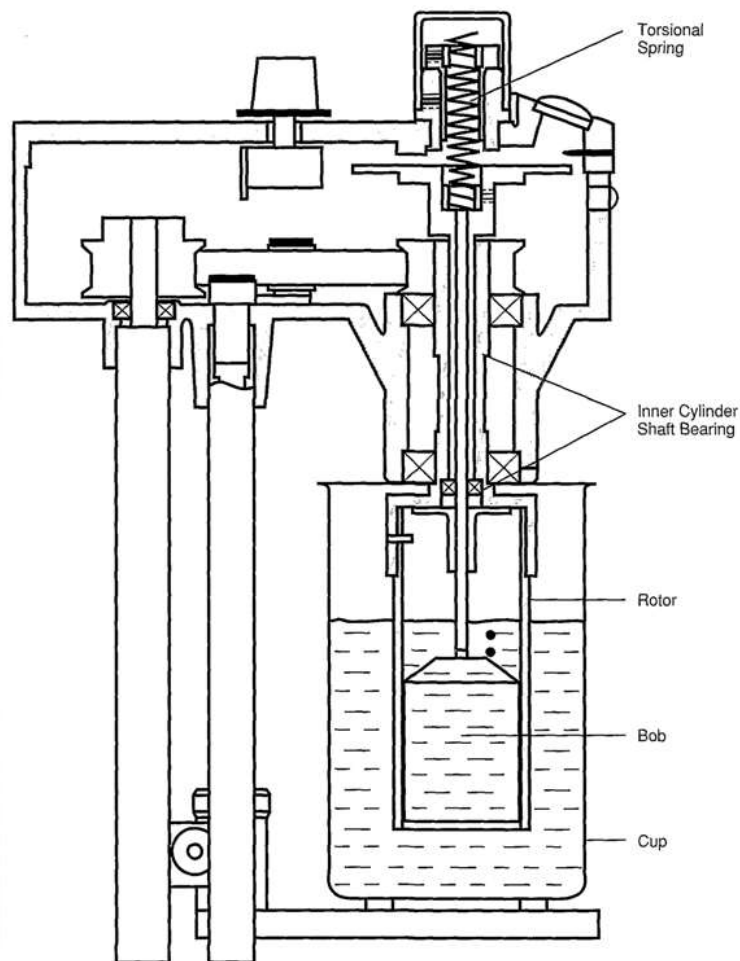


**Figure 7** Schematic drawing of a coaxial cylinder viscometer [47].

The test fluid, contained in a large cup, is sheared between an outer sleeve (the rotor) and an inner cylinder (the bob). The rotor spins at various preselected rotational speeds. The bob is attached to a torsion spring that deflects as torque is exerted by the fluid. The torsion-spring deflection is indicated on a dial that reads from 0 to 300. The dial readings are converted to shear stress in Pa while the rotational speed (shear rate) is expressed in  $\text{sec}^{-1}$ .

### **2.2.4 Salt cement slurries**

Cement systems which contain significant quantities of sodium chloride (NaCl) are commonly called “salt cements”. The salt content can either be a side effect from the use of seawater as mixing water, or result from the intentional addition of sodium chloride to the cement slurry to adjust its properties to certain borehole conditions.

#### **2.2.4.1 Seawater as mixing water**

For offshore cementing operations, seawater is the most economic and easiest available mixing fluid. Nevertheless, comparative laboratory tests have identified differences in the performance of Portland cement systems which use seawater instead of fresh water as mixing fluid: Cement slurries prepared with seawater (approximately 3 % sodium chloride) show a reduced thickening time and rheology. Furthermore, an increased tendency for slurry foaming during mixing was observed for sea water systems [7]. Thus, formulators of cement slurries have to carefully take these altered properties of salt systems into account.

#### **2.2.4.2 Sodium chloride as a cement additive**

When cementing across shale and bentonitic clay formations, cement slurries prepared with fresh water change the chemical environment surrounding the clays. This effect may induce destabilization, clay swelling, or fines migration, resulting in stuck drill pipe. Since approximately 87 % of petroleum reservoirs contain clay minerals and silica fines, freshwater cement slurries are commonly replaced by salt cement systems [48] [49]. Here, the presence of sodium chloride restricts the swelling and disintegration of water-sensitive clays.

The addition of sodium chloride is also indispensable for cementing across massive salt domes and evaporite strata. On the one hand, freshwater cement slurries can dissolve large quantities of the highly water soluble formation; on the other hand, plastic salt zones can encroach upon the casing before the cement sets [50].

Thus, salt cement slurries are routinely used to prevent the disintegration of certain formation. However, a high concentration of sodium chloride (from 10 % to 37 %) tends to over-retard the cement. It also may impede the performance of cement admixtures, especially polyelectrolytes such as dispersants and fluid loss additives which were originally developed for fresh water systems.

### 2.3 Influences of polyelectrolytes on the properties of cement slurries

Polyelectrolytes can modify the behavior of cement systems, thus allowing successful slurry placement between the casing and the formation, controlled strength development, and adequate zonal isolation during the life time of the well. The working mechanism of these polymeric admixtures is either adsorptive or non-adsorptive. Measuring the zeta potential of the mineral surface is a reliable method used to assess the adsorption of polyelectrolytes onto it [51] [52].

#### 2.3.1 Polyelectrolyte adsorption and zeta potential of mineral surfaces

##### 2.3.1.1 Zeta potential

Any charged colloidal particle which is suspended in an electrolyte solution is surrounded by a cloud of ions. This “electrical double layer” consists of two parts: one faces the surface of the colloidal particle, and the other the surrounding solution. This model is known as the “*Stern* model” or the “*Helmholtz* model”. There, the so called “shear plane” separates the liquid which adheres to the solid surface from its mobile counterpart. The zeta potential is defined as the potential difference between the shear plane and the bulk of the solution. Through zeta potential measurement, the surface charge of mineral particles can be estimated [53]. The so called zero-point-charge (i.e., the point at which the zeta potential becomes zero also referred to as isoelectric point), depends on the pH value of the surrounding solution [54].

##### 2.3.1.2 Adsorption of polyelectrolytes

The pH for the isoelectric point of silica minerals present in cement is much below the pH value of the cement slurry which exhibits a pH value of  $13.0 \pm 0.5$ . Consequently, the silicate phases  $C_2S$  and  $C_3S$  possess a negative charge. Abundant quantities of  $Ca^{2+}$  ions solved in the cement pore solution (5 to 50 mmol  $Ca^{2+}/L$  [55]) adsorb onto this negatively charged surface. Through charge overcompensation, these divalent ions form adsorption sites for anionic electrolytes on the cement surface. Here, the functionalities incorporated into the backbone of the polymers serve as anchor groups which interact with the adsorbed calcium ions electrostatically (physisorption) [56].

*Mollah et al.* described this phenomenon as a charge-controlled-reaction [57]. Therefore, the adsorption of anionic polymers onto the cement surface leads to more negative values of the zeta potential.

All macromolecules possessing poly(oxyethylene) chains but providing different end groups (hydroxyl, sulfonate, carboxylate, phosphonate and diphosphonate, respectively) show an increasing tendency to adsorb on  $\text{CaCO}_3$ , according to their capability to chelate calcium ions. This result of *Mosquet et al.* confirms that the affinity of polyelectrolytes towards adsorption sites on cement clearly depends on the quality of their anchor groups [58].

The polyelectrolytes which are most important in primary cementing are fluid loss additives (FLAs), microbial biopolymers and cement retarders. These admixtures are used for different purposes and show different working mechanisms.

### 2.3.2 Fluid loss additives

When cement slurries are placed across permeable rock formations, a filtration process may occur. Here, the aqueous phase of the slurry is pressed against the formation, leading to a filtercake buildup on the wall of the borehole (see **Figure 8; left**).

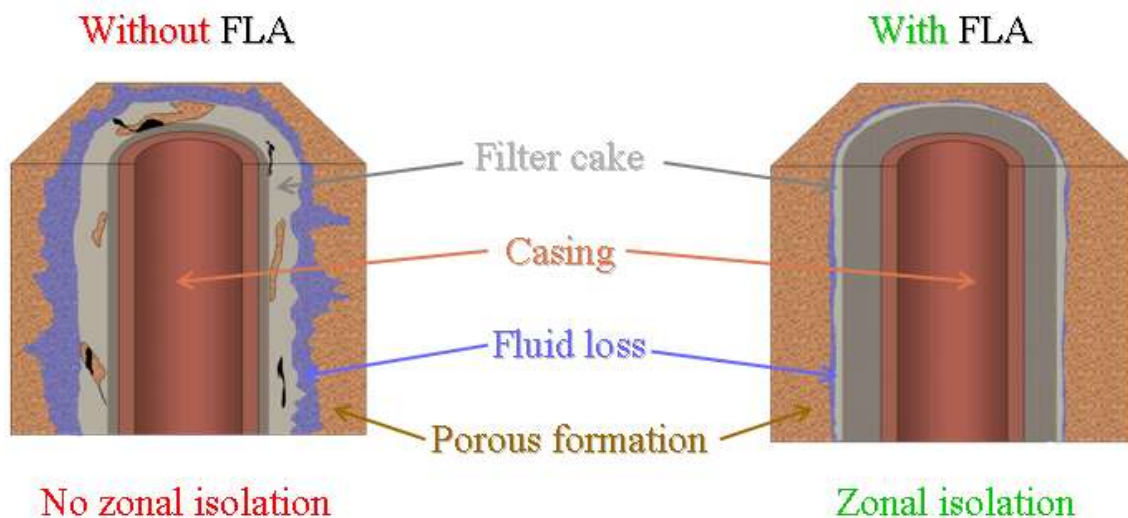


**Figure 8** Profile of a cemented wellbore; **left**: uncontrolled filtration from cement slurry leads to an incomplete cementation of the borehole; **right**: fluid loss additives (FLAs) provide fluid loss control of the cement slurry, resulting in complete filling of the annulus with cement.

This phenomenon known as fluid loss causes higher slurry viscosity and hence increased friction pressure. Additionally, the filtrate that enters the formation interacts with its minerals and modifies the rock properties (formation damage). Once the cement slurry is placed and pumping has stopped, subsequent static filtration affects the ability of the cement sheath to provide zonal isolation. To prevent these detrimental effects, fluid loss additives (FLAs) are commonly applied to the cement slurry (see **Figure 8; right**).

### 2.3.2.1 Laboratory testing of FLA effectiveness

In accordance with the procedures set forth by *the American Petroleum Institute (API)*, the efficiency of fluid loss additives is determined through a filtration test of the cement slurry in a high-temperature, high-pressure (HTHP) cell (see **Figure 9**) [59].

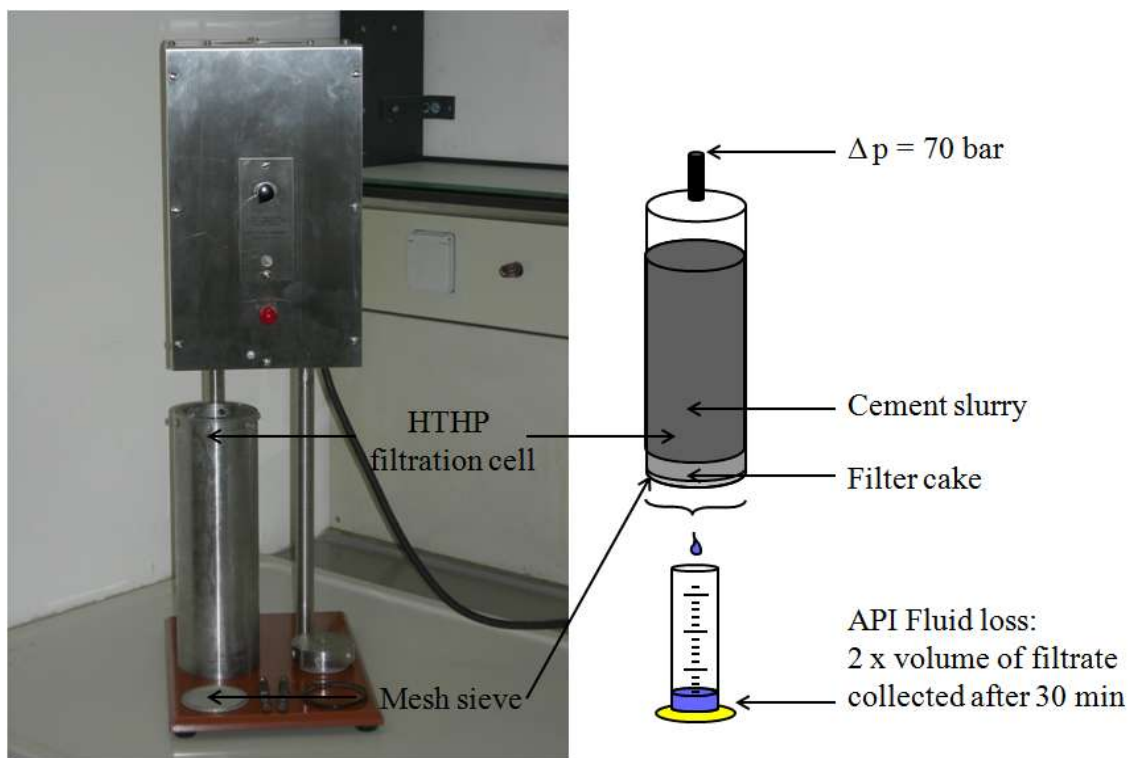


**Figure 9** High-temperature, high-pressure (HTHP) filtration cell used to test the effectiveness of fluid loss additives.

Under a differential pressure of 70 bar, filtrate is pressed out from the cement slurry through a metal sieve. Cement particles are deposited onto this sieve, forming a filtercake. The less filtrate is collected after 30 minutes, the better is the effectiveness of the respective fluid loss additive.

*Desbrières et al.* showed that filtration laws of cement slurries can be derived from *Darcy's* law (see **Equation 3**) [60] [61].

$$\frac{dV}{dt} = \frac{K_z \cdot A}{\eta} \cdot \frac{dp}{dz}$$

**Equation 3** Relationship between time-dependent volume of filtrate and characteristic properties of the cement filtercake.

Where  $dV/dt$  is the time-dependent volume of filtrate,  $K_z$  the permeability of the filtercake,  $A$  the surface area of the filtercake,  $dp$  the differential pressure,  $\eta$  the dynamic viscosity of the filtrate, and  $dz$  the thickness of an elementary layer of the filtercake.

A cake of volume  $dV_z$  is obtained when a volume  $dV$  has filtered and the relation  $dV_z = R_z \cdot dV$  is assumed ( $R_z$  being the cake volume settled by filtrate volume unit at height  $z$ ). Considering the volume  $dV_z$  of the elementary cake layer as:  $dV_z = A \cdot dz$ , the basic differential equation is as follows (**Equation 4**):

$$\frac{dV}{dt} = \frac{K_z \cdot A^2}{\eta \cdot R_z} \cdot \frac{dp}{dV}$$

**Equation 4** Relationship between time-dependent volume of filtrate and characteristic properties of the cement filtercake (assumptions included).

Where  $dV/dt$  is the time-dependent volume of filtrate,  $K_z$  the permeability of the filtercake,  $A$  the surface area of the filtercake,  $dp$  the differential pressure,  $\eta$  the dynamic viscosity of the filtrate, and  $R_z$  the cake volume settled by the filtrate volume.

Further assuming that the filtercake is not compressible and the flow  $dV/dt$  is constant at a time  $t$  across the height of the filtercake, **Equation 4** can be integrated to **Equation 5**:

$$V = \sqrt{\frac{2 \cdot K \cdot A^2 \cdot \Delta p}{\eta \cdot R}} \cdot \sqrt{t}$$

**Equation 5** Relationship between volume of filtrate and characteristic properties of the cement filtercake.

Where  $V$  is the volume of filtrate,  $K$  the permeability of the filtercake,  $A$  the surface area of the filtercake,  $\Delta p$  the constant differential pressure,  $t$  the time,  $\eta$  the dynamic viscosity of the filtrate, and  $R$  the cake volume settled by the filtrate volume.

Thus, at a constant time, the fluid loss volume of cement slurries will be a function of the filtrate viscosity and the permeability of the cement filtercake (considering the differential pressure, the filtrate area, and the cake volume settled after release of a filtrate volume unit to be constant).

### 2.3.2.2 Working mechanism of the CaAMPS<sup>®</sup>-co-NNDMA fluid loss additive

In this study, an anionic copolymer of 2-acrylamido-2-methylpropane sulfonic acid (AMPS<sup>®</sup>) and *N,N*-dimethyl acrylamide (CaAMPS<sup>®</sup>-co-NNDMA; see **Figure 10**) was used as fluid loss additive.

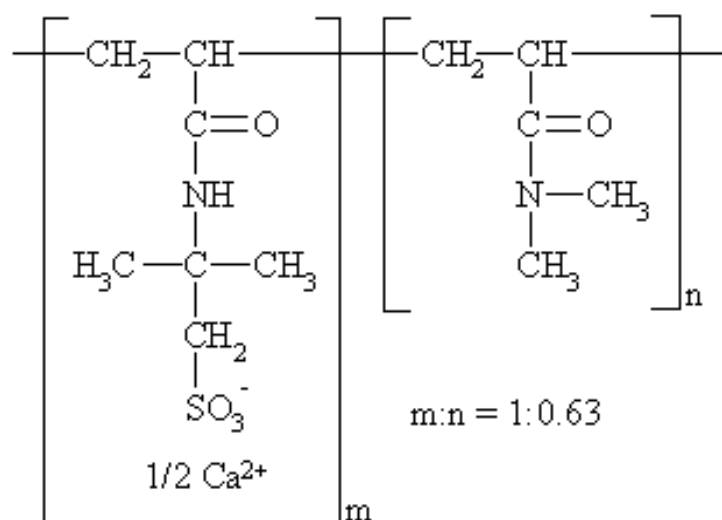


**Figure 10** Chemical structure of CaAMPS<sup>®</sup>-co-NNDMA fluid loss additive.

According to *Desbrières*, two phenomena explain the working mechanism of this polymer: First, an increase of the viscosity of the interstitial water and second, the decrease of the filtercake permeability [60]. When the latter was calculated for different dosages of CaAMPS<sup>®</sup>-*co*-NNDMA, the results revealed that this anionic polymer provides fluid loss control of the cement slurry primarily by reducing the permeability of the filtercake. Here, the volume of filtrate measured and its viscosity as well as the reduced filtercake volume were inserted into the simplified filtration equation developed by *Desbrières* (**Equation 5**). It showed that the permeability of the filtercake decreased by a factor 1,000 while, in contrast, the viscosity of the interstitial water increased only by a factor 5.

Furthermore, it was revealed that these anionic polymers have to adsorb in high quantity onto positively charged cement surfaces to be effective (for an illustration of the adsorptive working mechanism, see **Figure 11**) [62]. Since modern cementing systems contain a large variety of cement additives, mutual interaction of these polymers may influence their effectiveness. Thus, to ensure zonal isolation under harsh borehole conditions, additive incompatibilities have to be avoided.

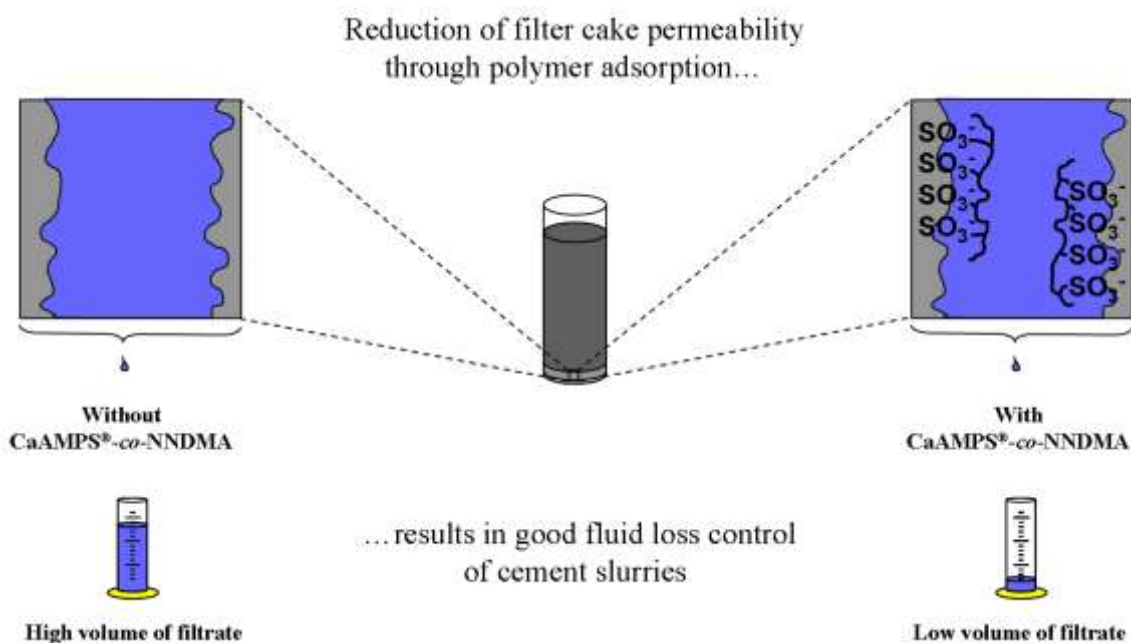


**Figure 11** Schematic illustration of the adsorptive working mechanism of CaAMPS<sup>®</sup>-*co*-NNDMA.

### 2.3.2.3 Incompatibility of polycondensate-based dispersants with CaAMPS<sup>®</sup>-*co*-NNDMA

Dispersants are commonly added to the cement slurry to ensure its pumpability over several kilometers [4]. However, highly anionic dispersants such as acetone formaldehyde sulfite (AFS) polycondensates occupy the surfaces of cement hydrates and prevent adsorption of CaAMPS<sup>®</sup>-*co*-NNDMA [62]. Indeed, because of their higher anionic charge density, AFS molecules show a stronger affinity to the positively charged adsorption sites and even can displace the already adsorbed FLA polymer from the cement surface. Subsequently, this leads to strong dispersion of the cement slurry but simultaneously instigates excessive water loss from the slurry. The phenomenon of competitive adsorption between these two admixtures can be solved either by reduction of the anionic charge density of the AFS molecules [63] or by incorporation of stronger anchor groups into the FLA [64]. Suitable anchor groups are those which strongly chelate insufficiently coordinated calcium atoms present on the surface of cement hydrates. In accordance with this theory, a terpolymer of 2-acrylamido-2-methylpropane sulfonic acid, *N,N*-dimethyl acrylamide and a very small content of maleic anhydride (CaAMPS<sup>®</sup>-*co*-NNDMA-*co*-MA) adsorbs and provides low fluid loss of the cement slurry, even in the presence of AFS dispersant.

### 2.3.3 Microbial biopolymers

Since the mid-1960s, microbial biopolymers have been used in construction applications in ever-increasing quantities. These extracellular polysaccharides are produced by microorganisms through fermentation of low-cost energy sources such as molasses. The industrial process typically yields a viscous broth which is 5 to 7 % active in high molecular-weight gum [9]. The biopolymer is precipitated from the broth by addition of isopropanol, dried, and carefully milled to a specific particle size. When dissolved in water, these polymers develop significant viscosity. Here, however, the main characteristic and advantage is the type of the resulting viscosity: While starch- and cellulose-based biopolymers usually increase only the plastic viscosity (PV) of their aqueous solutions, these microbial biopolymers increase the yield point (YP) and show, in contrast, a low PV. The resultant viscosity profile is referred to as shear-thinning [65]. Additionally, microbial biopolymers are used as free water control agents in oil well cement slurries.

### 2.3.3.1 Microbial biopolymers as free water control agents

The phenomenon known as free water developed on the top surface of a cement slurry can pose a serious problem for zonal isolation, particularly in deviated wellbores. When cement slurry is placed between the annulus, the incorporated mixing water is squeezed out of the lower portion of the slurry by the weight of the cement particles and accommodated in the higher, less stressed layers. As the water capacity of the upper layer is limited, a layer of water may form at the top of the slurry. Thus, cement particles suspended in the slurry segregate and are separated from the mixing water resulting in an inhomogeneous system. Free water control agents such as microbial biopolymers are commonly added to the slurry to prevent this undesired effect. Resulting from the shear-thinning rheology imposed, these polysaccharides increase the yield point of the cement slurry and, consequently, the settling of cement particles is greatly reduced. In this study, welan gum and diutan gum were used as free water control agents.

### 2.3.3.2 Welan gum biopolymer

The usefulness of welan gum in construction applications was first documented in patents describing cement compositions with low-viscosity welan [66]. Later on, further reports were made for the use of welan gum in grouts [67]. This microbial polysaccharide is produced from D-glucose by the bacterial species *Alcaligenes* ATCC 31555 [68]. Welan gum contains repeating units with randomly distributed L-mannosyl and L-rhamnosyl terminal groups substituted on C3 of every (1→4)-linked glucose unit (see **Figure 12**) [69].

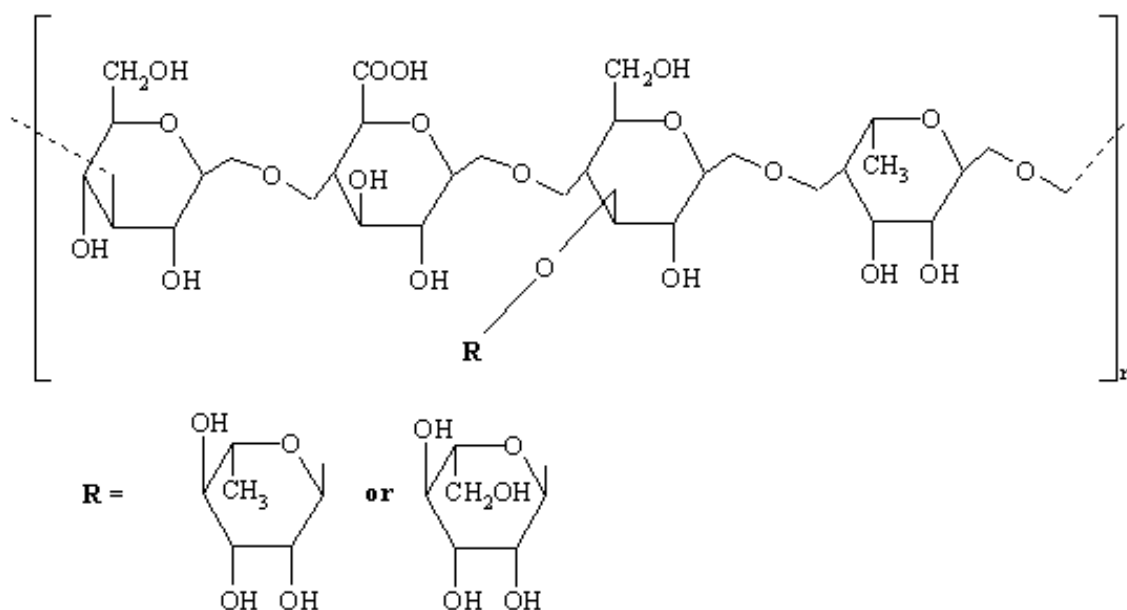


**Figure 12** Chemical structure of welan gum free water agent.

In aqueous solution, this molecule forms a double helix where the side chains fold back on the main chain to form hydrogen bonds with the carboxylate groups. This steric shielding effect provides stability of the double helix against high  $\text{Ca}^{2+}$  concentrations existing in cement pore solution [70] [71]. The welan molecule is rather stiff, whereby it becomes relatively insensitive to temperature and pH variation [72]. These properties make it ideal for applications in concrete, mortars, cement grouts, and high-temperature drilling.

## 2.3.3.3 Diutan gum biopolymer

The free water control agent diutan gum is produced through aerobic fermentation by bacteria of the genus *Sphingomonas* sp. ATCC 53159 [73]. It consists of a repeat unit with L-rhamnose, D-glucose, D-glucuronic acid, D-glucose backbone and a two-sugar L-rhamnose side chain attached to the (1→4) linked glucose residue (see **Figure 13**).

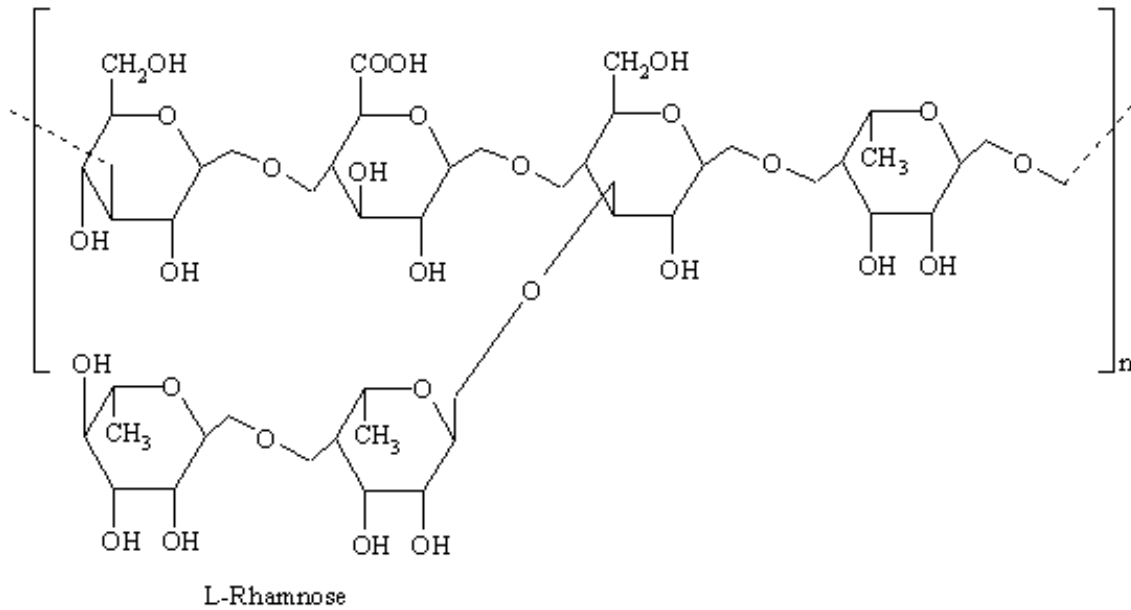


**Figure 13** Chemical structure of diutan gum free water control agent.

As with welan gum, the use of diutan gum leads to an increase in the pseudo-plastic behavior of the cement slurry and ensures high resistance to sedimentation and bleeding. Resulting from its higher molecular weight, diutan gum yields higher viscosities and better temperature stability at lower polymer concentrations, compared to welan gum [74].

### **2.3.4 Cement retarders**

Under harsh borehole conditions such as high temperature, pressure and salinity, cement retarders, such as lignosulfonates, allow accurate control of the setting kinetics of cement. On the one hand, premature setting of the cement slurry during the pumping procedure has to be avoided, since the well can be blocked completely. On the other hand, once the cement slurry is in place, its hydration-induced hardening process should ensure a short waiting on cement (WOC) time to minimize costs resulting from delays.

#### **2.3.4.1 Potential working mechanism of cement retarders**

Currently, five different mechanisms have been proposed to explain the action of retarders in cement:

##### **I Calcium complexation**

The retarder removes calcium from solution and prevents C-S-H formation either by forming insoluble precipitates or by chelating calcium ions [75].

##### **II Nucleation poisoning**

The additive inhibits the formation of nucleates by agglomerates of calcium ions. This behavior blocks the growth of C-S-H and  $\text{Ca(OH)}_2$  crystals [76].

##### **III Surface adsorption**

The admixture adsorbs onto the partially hydrated mineral surfaces and hinders their further reactions with water [77].

##### **IV Layer formation**

The retarder forms a semi-permeable membrane on the cement grain which decelerates the migration of water to the mineral surface. Eventually, the osmosis driven flow of water creates higher pressure inside the protective coating and the layer bursts, allowing hydration to continue at a normal rate [78].

### V Dissolution - precipitation

When organic phosphonic acid is used as a retarder, this additive enhances the dissolution of calcium by extraction. This reaction is followed by precipitation of a layered calcium phosphonate that binds to the surface of the cement grain. Thus, organic phosphonic acids inhibit cement hydration by acting as a diffusion barrier to water as well as a nucleation inhibitor [79].

#### 2.3.4.2 Use of lignosulfonates in oil well cementing

Lignosulfonates are obtained as waste liquor during the production process of papermaking from wood. The pulp provides about 20 to 30 % of lignin [13]. Lignosulfonate contains a complex mixture of sulfonation products of lignin, decomposition products of cellulose and lignin, various carbohydrates (reducing sugars), and free sulfurous acid and sulfates. The composition of lignosulfonates can vary widely depending on the successive process of neutralization, precipitation, and fermentation which the by-product undergoes, as well as on the type and age of wood used as raw material. Both the type and concentration of sugars contained in the untreated sulfite liquor or in commercial admixtures depend on the source and degree of fermentation. Oxidation of sugar during the pulp digestion process leads to the presence of sugar acids such as xylonic, galactonic or gluconic acids in commercial lignosulfonates. Calcium and sodium salts of lignosulfonates (see **Figure 14**) are generally used as (I) cement plasticizers and (II) cement retarders.

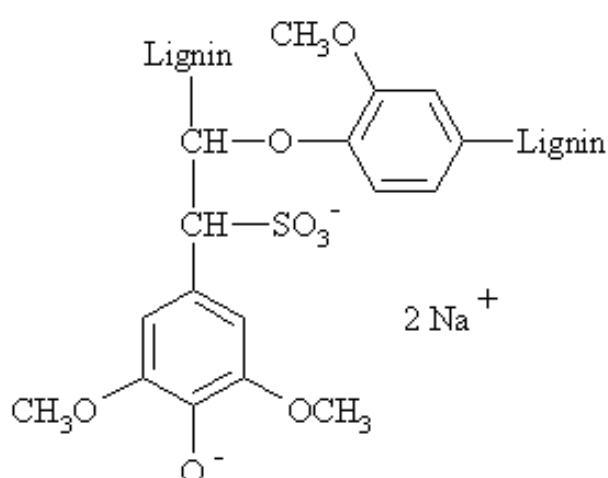


**Figure 14** Chemical structure of sodium lignosulfonate.

### I Use of lignosulfonate as cement plasticizer

Lignosulfonates are the most common concrete plasticizer, their primary function being dispersion of the cement particles and improvement of slurry flowability. Typical average molecular weights range from 20,000 to 100,000 Da, with 80,000 Da being an optimum for concrete plastification [9]. Lignosulfonates are used in concrete either to increase its flowability at a given w/c ratio, or to reduce the w/c ratio of concrete without reducing its flowability. The effectiveness of water-reducing admixtures is expressed as percentage reduction in w/c ratio of untreated concrete. In general, the water reduction achieved with lignosulfonates ranges between 5 and 15 %. However, by increasing the sulfonic groups incorporated into the polymer backbone, a water reducing ratio of 20 % was achieved [80]. This is almost as high as the water reduction provided by a more powerful group of dispersants known as superplasticizers which consists of synthetic polymers. As a consequence, lignosulfonates are mainly used for less demanding applications such as ready-mix concrete. In contrast, these polymers are the most common retarders for oil well cementing.

### II Use of lignosulfonate as cement retarder

Although lignosulfonates have been used as cement retarders for many years, the exact working mechanism is not yet fully understood. However, it was shown that this polymer predominately affects the hydration kinetics of  $C_3S$  and lengthens the osmosis driven dormant/induction period of cement hydration [54] [81]. Upon contact with water, the  $C_3S$  phase will form C-S-H phases which possess a negative surface charge. Oppositely charged  $Ca^{2+}$  ions which are present in abundant quantities in the cement pore solution will immediately form an “electrical double layer” on the surface of this C-S-H phase. It has been postulated that anionic lignosulfonate molecules adsorb through their sulfonate and hydroxyl groups onto this “*Stern layer*” (see **chapter 2.3.1**) and, consequently, incorporate into the C-S-H gel. This interaction causes a change in the morphology of the C-S-H gel leading to a less water-permeable layer. Thus, further hydration is slowed down by this waterproofing effect [82].

### 3 GOAL OF THIS THESIS

In oil well cementing, poly(*N,N*-dimethyl acrylamide-*co*-Ca 2-acrylamido-2-methylpropane sulfonate) (CaAMPS<sup>®</sup>-*co*-NNDMA) is a synthetic copolymer routinely used as cement fluid loss additive. Applicators of CaAMPS<sup>®</sup>-*co*-NNDMA are very familiar with the detrimental effect of high temperature on fluid loss control of cement slurries. Therefore, substantially higher dosages of this costly admixture are often required to achieve a fluid loss which is comparable with that at room temperature.

In the laboratory, the effectiveness of this cement admixture is commonly determined through high-temperature, high-pressure filtration tests of cement slurries. Here, a very careful test protocol has to be applied, as experiments with cement slurries at high temperature are very hard to conduct in the absence of a cement retarder. Under such conditions, the beginning of the setting and hardening of cement can alter the test results. Since, the temperature-dependent change in the performance of CaAMPS<sup>®</sup>-*co*-NNDMA is not well understood, it was the first objective of this study to investigate this effect. For this purpose, the impact of high temperature (100 °C) on the adsorption behavior and hence the effectiveness of CaAMPS<sup>®</sup>-*co*-NNDMA under carefully controlled experimental conditions was tested. In this context, the effect of additional carboxylate anchor groups incorporated into this fluid loss additive also was studied.

In addition to high temperature, polymer incompatibility constitutes a major problem in the use of CaAMPS<sup>®</sup>-*co*-NNDMA as fluid loss additive. In multi-admixture systems which are commonly used in oil well cementing, the efficiency of CaAMPS<sup>®</sup>-*co*-NNDMA often is diminished. In lack of other solutions, slurry formulators avoid the combination of CaAMPS<sup>®</sup>-*co*-NNDMA with certain other admixtures, or they compensate the negative effects of polymer incompatibility with higher, more costly dosages of CaAMPS<sup>®</sup>-*co*-NNDMA. Therefore, the second objective of this work was to determine the effectiveness of CaAMPS<sup>®</sup>-*co*-NNDMA in the presence of certain other cement additives at 80 °C.

First, the robustness of CaAMPS<sup>®</sup>-*co*-NNDMA in salt cement slurries was tested. Here, the adsorption behavior of this fluid loss additive on the surface of cement was investigated in the presence of 100 g/L sodium chloride.

Second, tests were conducted to shed light on factors which cause competitive adsorption and hence polymer incompatibility in the binary additive system consisting of CaAMPS<sup>®</sup>-*co*-NNDMA and a microbial biopolymer (namely, welan gum and diutan gum, respectively).

Last, the interaction between CaAMPS<sup>®</sup>-*co*-NNDMA and the sodium lignosulfonate retarder was analyzed. In the course of the investigation, the working mechanism of this lignosulfonate was studied as well as the efficiency of both additives when used in combination.

Taken together, the main objective of this thesis was to study the physico-chemical interactions which influence the adsorption behavior and the resulting performance of CaAMPS<sup>®</sup>-*co*-NNDMA under varying conditions. The observations and results of this study may help the industry to develop more effective and hence more economic admixture systems for oil well cementing.

## 4 EXPERIMENTAL

### 4.1 Materials

#### 4.1.1 Oil well cement

An API Class G oil well cement (“black label” from Dyckerhoff AG, Wiesbaden, Germany) corresponding to *American Petroleum Institute* (API) Specification 10A was used (see **TABLE 1**; [14]). Its clinker composition was determined through powder XRD technique (XRD pattern of the cement sample see **Figure 15**) using *Rietveld* refinement.

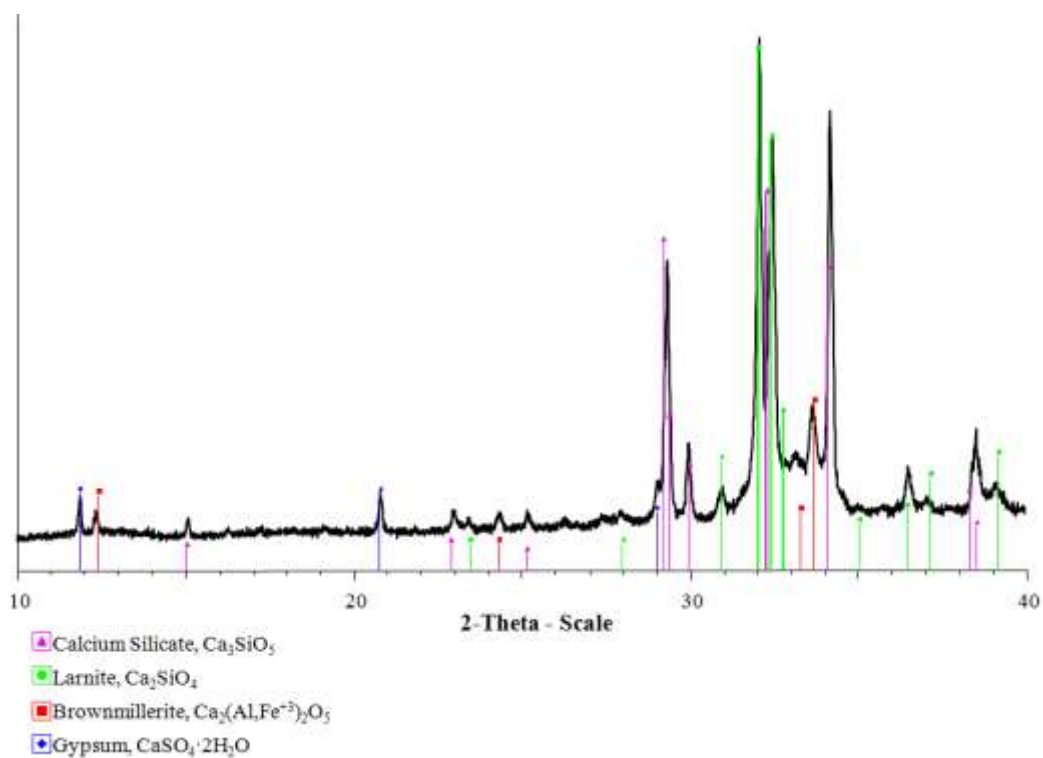


**Figure 15** XRD pattern of the API Class G oil well cement sample used in the study.

The amounts of gypsum ( $\text{CaSO}_4 \cdot 2\text{H}_2\text{O}$ ) and hemi-hydrate ( $\text{CaSO}_4 \cdot 1/2\text{H}_2\text{O}$ ) present in the cement sample were measured by thermogravimetry. Free lime ( $\text{CaO}$ ) was quantified using the extraction method established by *Franke* (see **TABLE 2**).

TABLE 2

Phase composition (Q XRD, *Rietveld*) of the API Class G oil well cement sample

C <sub>3</sub> S (wt. %)	C <sub>2</sub> S (wt. %)	C <sub>3</sub> A <sub>c</sub> (wt. %)	C <sub>4</sub> AF (wt. %)	Free CaO (wt. %)	CaSO <sub>4</sub> ·2H <sub>2</sub> O (wt. %)	CaSO <sub>4</sub> ·1/2 H <sub>2</sub> O (wt. %)	CaSO <sub>4</sub> (wt. %)
59.6	22.8	1.2	13.0	<0.3	2.7	0.0	0.7

C<sub>3</sub>S: tricalcium silicate (Ca<sub>3</sub>(SiO<sub>4</sub>)O); C<sub>2</sub>S: dicalcium silicate (Ca<sub>2</sub>SiO<sub>4</sub>); C<sub>3</sub>A<sub>c</sub>: cubic modification of tricalcium aluminate (Ca<sub>9</sub>Al<sub>6</sub>O<sub>18</sub>); C<sub>4</sub>AF: tetra calcium aluminate ferrite (Ca<sub>4</sub>Al<sub>2</sub>Fe<sub>2</sub>O<sub>10</sub>).

According to the method described by *Blaine*, its specific surface area was found at 3,058 cm<sup>2</sup>/g. The specific density of this sample was 3.18 kg/L, as measured by Helium pycnometry. The particle size distribution of the cement sample was determined employing a laser-based particle size analyzer (see **Figure 16**). Its d<sub>50</sub> value was 11 μm.

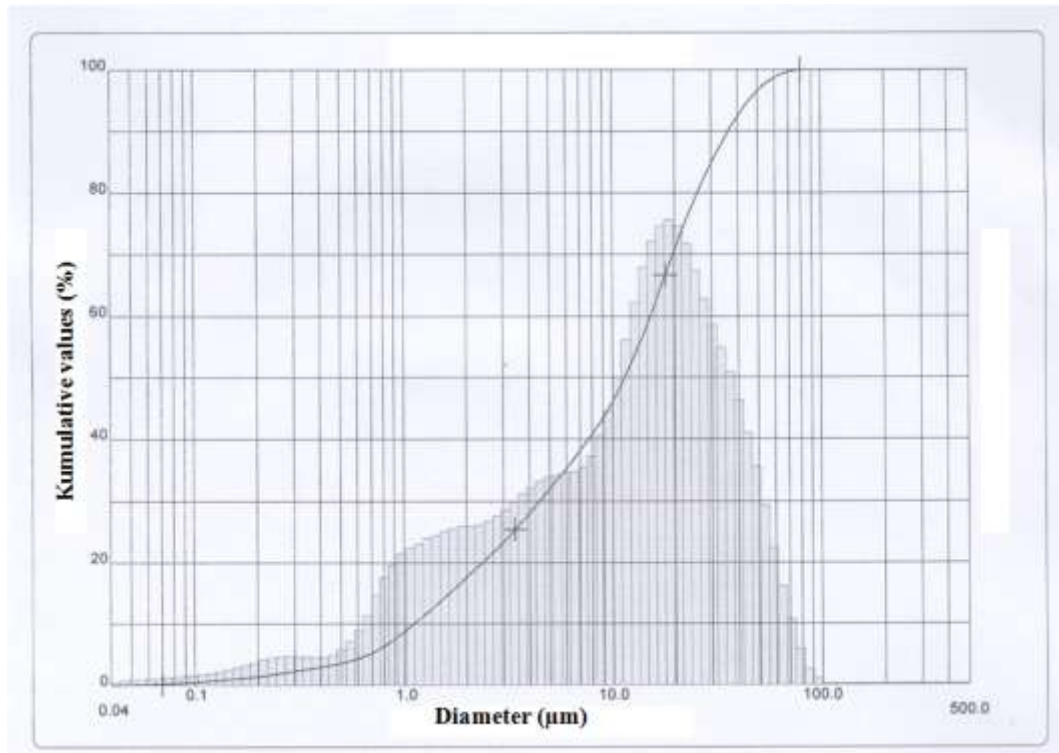


**Figure 16** Particle size distribution of the API Class G cement sample used in the study.

### 4.1.2 Silica

A commercial sample (SSA-1<sup>®</sup> from Halliburton Co., Celle, Germany) containing (wt. %) quartz 97.60, CaO 0.57, MgO 0.18, Al<sub>2</sub>O<sub>3</sub> 0.17, and TiO<sub>2</sub> 0.06 (determined by X-ray fluorescence analysis) was used. The XRD analysis of this silica sample solely showed the X-ray pattern of quartz and hence proves its crystallinity (**Figure 17**).

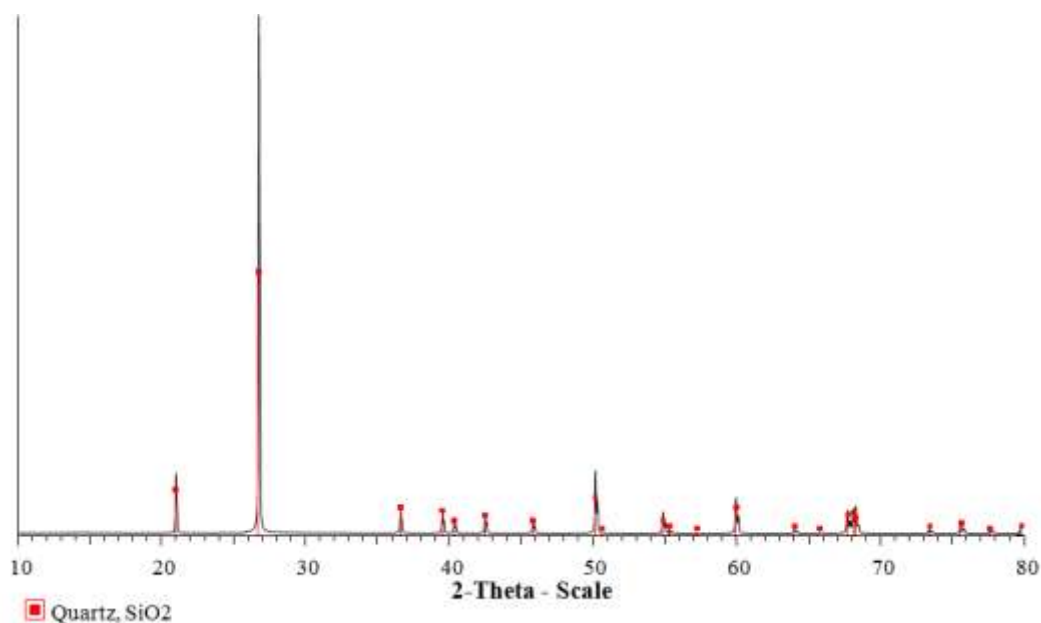


**Figure 17** XRD pattern of the silica sample SSA-1<sup>®</sup> used in the study.

A specific surface area of 1,857 cm<sup>2</sup>/g was determined using the *Blaine* method. Its average particle size ( $d_{50}$  value) was 33  $\mu$ m (see **Figure 18**). Specific density of the silica sample was found at 2.65 kg/L.

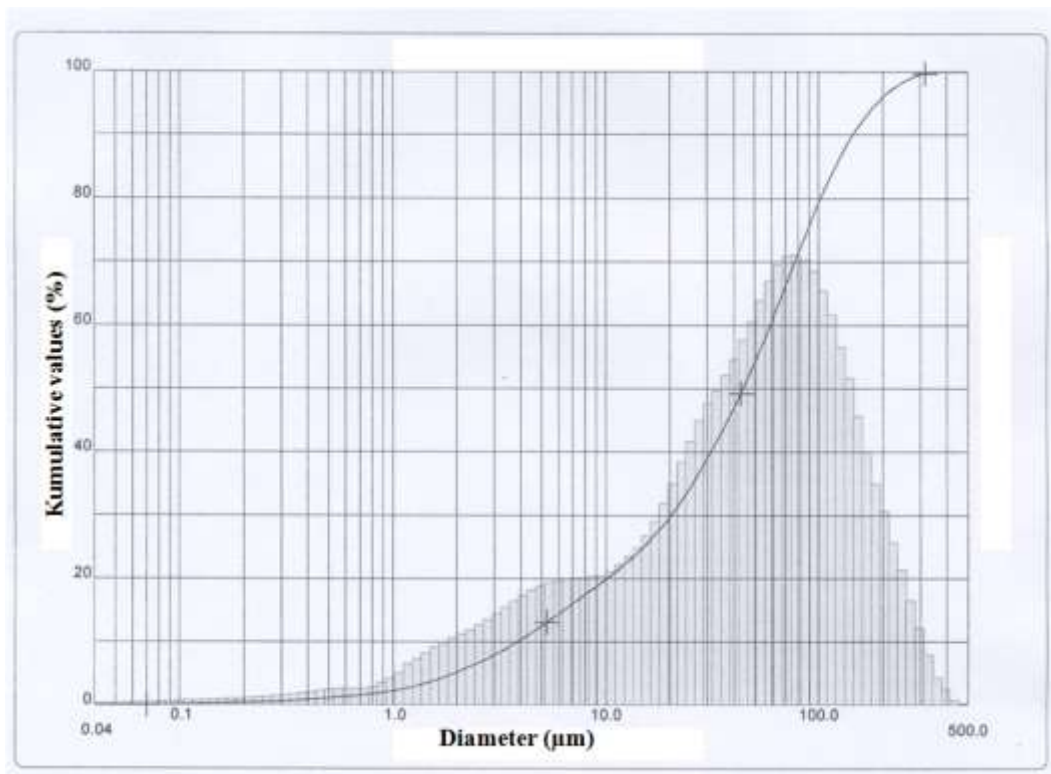


**Figure 18** Particle size distribution of the silica sample SSA-1<sup>®</sup> used in the study.

### 4.1.3 Synthesis of AMPS<sup>®</sup>-based fluid loss polymers

Laboratory grade 2-acrylamido-2-methylpropanesulfonic acid (AMPS<sup>®</sup> monomer 2404 from Lubrizol, Rouen, France) was used as obtained. *N,N*-dimethyl acrylamide (NNDMA) and maleic anhydride (MA) were supplied by Sigma-Aldrich (München, Germany). The AMPS<sup>®</sup>-based fluid loss additives were prepared from these monomers through free-radical polymerization. Sodium persulfate (Sigma-Aldrich, München, Germany) was used as initiator.

The additives were synthesized as follows: 850 mL of deionized water were filled into a 2 L flask equipped with reflux condenser, rotor, and thermometer. Before adding 18.0 g of Ca(OH)<sub>2</sub>, the reactor was purged with N<sub>2</sub> gas for 30 minutes under stirring at 170 rpm. Next, 100.0 g of AMPS<sup>®</sup> were dissolved under continuous stirring and N<sub>2</sub> flux. After adding the respective amounts of MA and NNDMA to the reactor (see **TABLE 3**), the pH value of the mixture was adjusted to ~ 7.0 with Ca(OH)<sub>2</sub>.

**TABLE 3**

**Amounts of monomer used for the synthesis of the AMPS<sup>®</sup>-based fluid loss additives**

Molar ratio of AMPS <sup>®</sup> :NNDMA:MA	Designated	AMPS (g)	NNDMA (g)	MA (g)
1:0.63:0	CaAMPS <sup>®</sup> -co-NNDMA	100.0	30.1	0.0
1:0.63:0.02	terpolymer 1	100.0	30.1	0.9
1:0.63:0.05	terpolymer 2	100.0	30.1	2.2
1:1.00:0.02	terpolymer 3	100.0	47.8	0.9

The reactor was heated to 60 °C and 1.5 g of sodium persulfate were added as powder to initiate the polymerization. The reaction was carried out for 2 h providing an odorless solution with honey-like color and viscosity. For further characterization, the aqueous copolymer solutions were dialyzed and freeze dried.

The size exclusive chromatograms of the synthesized FLAs were comparable (see pages 114/115 in the **Appendix**). As an example, **Figure 19** presents the chromatogram of CaAMPS<sup>®</sup>-*co*-NNDMA. There, the red curve depicts the 90° static light scattering signal, whereas the pink curve presents the dynamic light scattering signal. The refractive index (RI; blue curve) represents the concentration of the molar mass fraction present in the eluant. For the synthesized copolymers, these three signals were detectable after 12 to 20 minutes elution time. The RI signal which appeared after ~ 21 minutes originated from the eluant (0.2 M NaNO<sub>3</sub>).

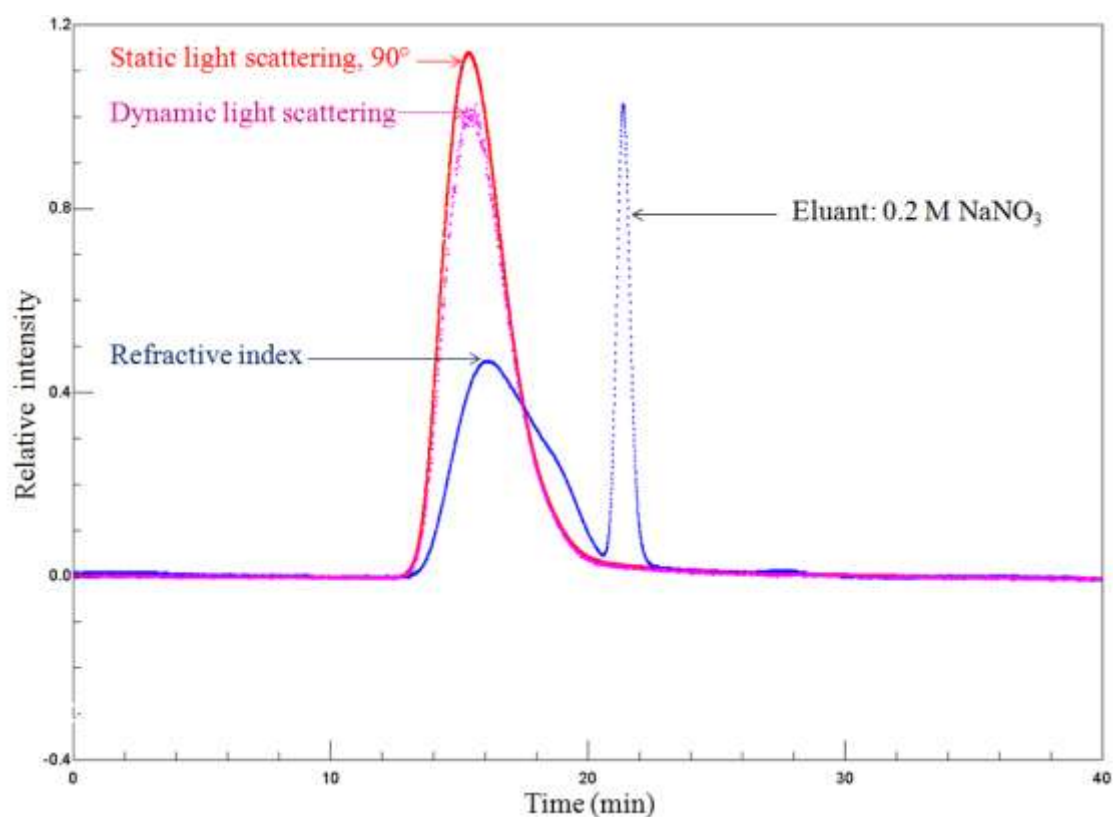


**Figure 19** SEC chromatogram of CaAMPS<sup>®</sup>-*co*-NNDMA (eluant: aqueous 0.2 M NaNO<sub>3</sub>).

The  $^1\text{H-NMR}$  spectrum of CaAMPS<sup>®</sup>-*co*-NNDMA presented in **Figure 20** showed signals at  $\delta = 1.3$  ( $a_1, a_3, b_1$ ), 2.0 ( $a_2$ ), 2.5 ( $b_2$ ) and 3.0 ppm ( $a_4, b_3$ ), respectively

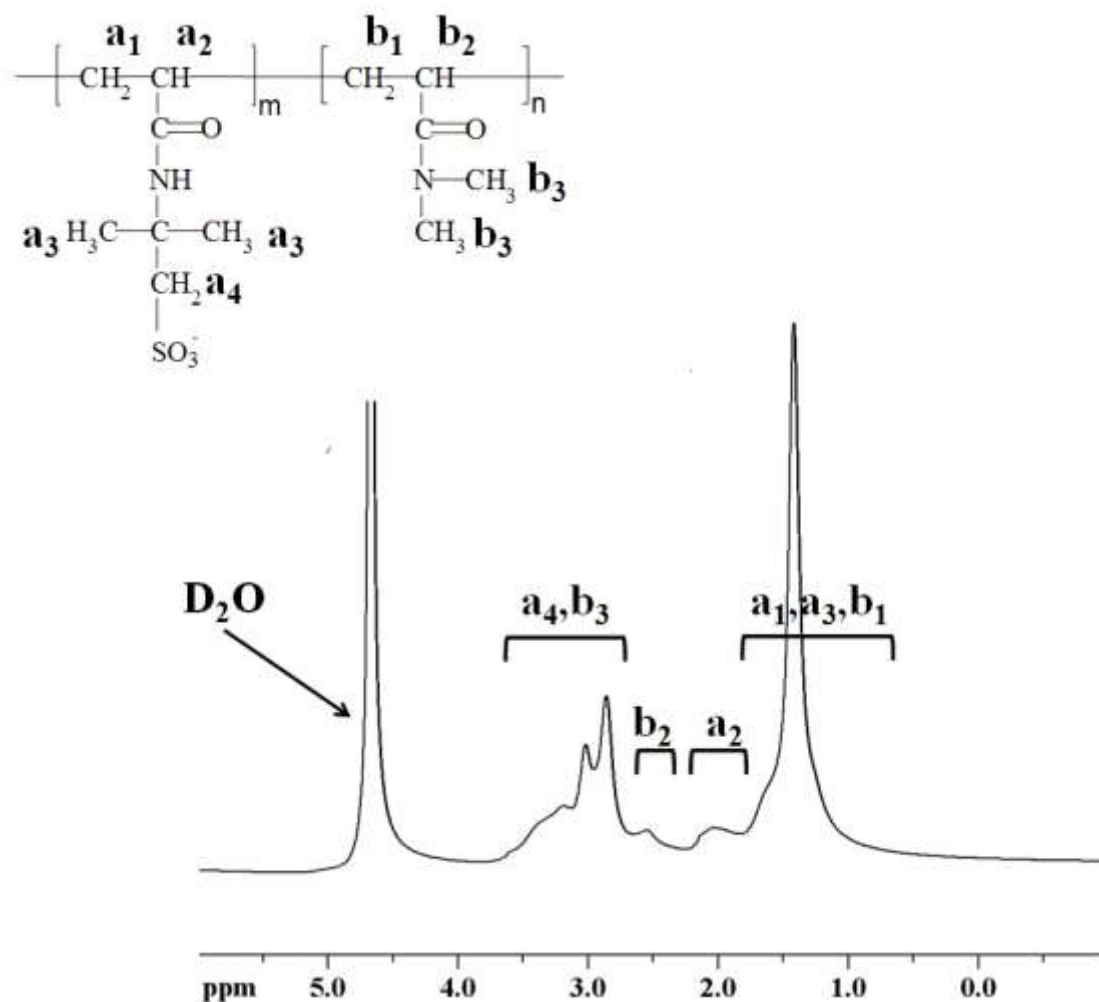


**Figure 20**  $^1\text{H-NMR}$  spectrum of CaAMPS<sup>®</sup>-*co*-NNDMA, measured in  $\text{D}_2\text{O}$ .

**Figure 21** shows that the IR spectrum of CaAMPS<sup>®</sup>-*co*-NNDMA displayed a N-H and O-H stretching band at 3319 cm<sup>-1</sup>, a C=O stretching band at 1612 cm<sup>-1</sup>, a N-H bending band at 1542 cm<sup>-1</sup>, a C-H bending band of geminal dimethyl groups at 1405 cm<sup>-1</sup>, S=O stretching bands at 1177 and 1038 cm<sup>-1</sup>, and a S-O stretching band at 621 cm<sup>-1</sup>.

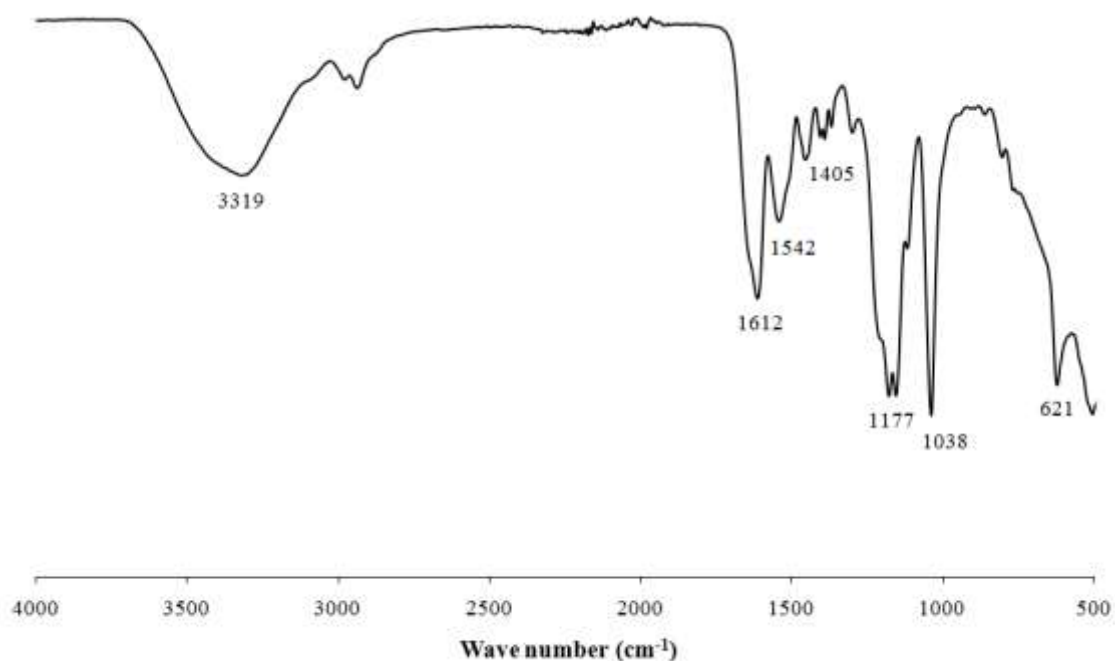


**Figure 21** Powder FT-IR spectrum of CaAMPS<sup>®</sup>-*co*-NNDMA.

For the synthesis of the terpolymers, only 1 to 2 % of maleic anhydride was used. The additional carboxylate functionalities incorporated into the polymer backbone were not detectable via <sup>1</sup>H-NMR or IR spectroscopy, because of their low overall content in the polymer. Thus, the <sup>1</sup>H-NMR and IR spectra of the MA-modified terpolymers were comparable with that of CaAMPS<sup>®</sup>-*co*-NNDMA.

## 4.2 Instruments and procedures

### 4.2.1 Cement characterization

Phase composition of the cement sample was obtained by X-ray powder diffraction using a Bruker axS D8 Advance instrument from Bruker, Karlsruhe, Germany with Bragg-Brentano geometry. Topas 3.0 software was used to quantify the amounts of individual phases present in the sample by following *Rietveld's* method of refinement [83]. The instrument was equipped with a scintillation detector using Cu K $\alpha$  ( $\lambda = 1.5406 \text{ \AA}$ ) radiation with a scanning range between  $5^\circ$  and  $80^\circ 2\theta$ . Specific density of the cement sample was measured on an Ultracycrometer<sup>®</sup> 1000 (Quantachrome Instruments, Boynton Beach, USA). The specific surface area of the sample was determined using a *Blaine* instrument (Toni Technik, Berlin, Germany). The average particle size ( $d_{50}$ ) was obtained from a laser-based particle size analyzer (1064 instrument from Cilas, Marseille, France).

### 4.2.2 Silica characterization

Oxide composition of the silica sample was determined using an X-ray fluorescence spectrometer (Axios from PANalytical, Almelo, Holland). Specific density, specific surface area, and average particle size ( $d_{50}$ ) of the silica sample were measured using the same instruments as described in **chapter 4.2.1** for cement.

### 4.2.3 Polymer characterization

Solids content of the synthesized fluid loss additives was determined using an infrared drying balance (MA35 from Sartorius AG, Göttingen, Germany) which dried the polymer solution for 10 min at  $110^\circ\text{C}$ . The values presented are the average obtained from three separate measurements. Dialysis of the solvated polymers was carried out using membranes with a molecular weight cut off value (MWCO) of 50,000 Da (Spectra/Pro<sup>®</sup> Dialysis Membrane MWCO 50,000 from Spectrum Laboratories, Inc., Rancho Dominguez, USA) at room temperature for 5 days. Employing an ALPHA 1-4 LD plus apparatus (from Martin Christ Gefriertrocknungsanlagen GmbH, Osterode am Harz, Germany), the polymers were freeze dried at a final pressure of 0.1 mbar for 6 hours. Viscosity of the polymer solutions was determined at room temperature with a *Brookfield* viscometer (Model HA from Brookfield

Engineering Labs. Inc, Middleboro, USA) equipped with #7 spindle at 100 rpm. By multiplying the dimensionless reading with the correspondent factor, the viscosity (mPa·s) was obtained. The standard deviation of this method was found to be at  $\pm 1,000$  mPa·s.

Size exclusion chromatography (Waters Alliance 2695 from Waters, Eschborn, Germany) equipped with RI detector 2414 (Waters, Eschborn, Germany) and an 18 angle dynamic light scattering detector (Dawn EOS from Wyatt Technologies, Clinton, USA) was used. The FLAs were separated on a precolumn and two Aquagel-OH 60 columns (Polymer Laboratories, distributed by Varian, Darmstadt, Germany). Molecular weights ( $M_w$  and  $M_n$ ) and radii ( $Rg_z$  and  $Rh_z$ ) of the FLAs were determined using a 0.2 M aqueous  $\text{NaNO}_3$  solution (adjusted to pH 9.0 with NaOH) as an eluant at a flow rate of 1.0 mL/min.  $Rg_z$  was measured at different sulfate concentrations present in the eluant (0 g/L, 6.8 g/L, and 8.3 g/L) by adding the appropriate amounts of  $\text{Na}_2\text{SO}_4$ . Here, the accuracy of this measurement was found to be  $\pm 5$  nm. The value of  $dn/dc$  used to calculate  $M_w$  and  $M_n$  was 0.156 mL/g (value for polyacrylamide) [84].

Infrared spectra were measured with an attenuated total reflectance Fourier transform spectrophotometer (ATR – FTIR) (Vertex 70 from Bruker Optics, Karlsruhe, Germany). Each spectrum was acquired in transmittance mode on a Diamond ATR crystal cell (MPV – Pro from Harrich Scientific Products, Pleasantville, USA) by accumulation of 64 scans with a resolution of  $4\text{ cm}^{-1}$  and a spectral range of  $4000 - 350\text{ cm}^{-1}$ . Moreover, powder samples of the synthesized fluid loss polymers were dissolved in  $\text{D}_2\text{O}$  and analyzed with a JNM-GX 400  $^1\text{H}$ -NMR spectrometer (JEOL GmbH, Eching, Germany) at 300 K.

The specific anionic charge amount of the polymers used in this study was determined in 0.1 M NaOH (pH = 12.6) in presence or absence of calcium ions ( $0.6\text{ g/L Ca}^{2+}$ , added as  $\text{CaCl}_2 \cdot 2\text{H}_2\text{O}$ ), or in cement pore solution at room temperature using a PCD 03 pH apparatus (BTG Müttek GmbH, Herrsching, Germany). Charge titration was carried out according to a literature description employing a 0.001 N solution of laboratory grade poly(diallyl dimethylammonium chloride) from BTG Müttek GmbH, Herrsching, Germany as cationic polyelectrolyte [85]. The values presented in this study are the average obtained from three different measurements. The deviation of this method was found to be  $\pm 5\text{ C/g}$ .

The intrinsic viscosity of the AMPS<sup>®</sup>-based fluid loss additives and biopolymers, respectively, dissolved in cement pore solution was determined at 80 °C using an Ubbelohde capillary viscometer (50110/I from Schott, Mainz, Germany). For this purpose, the flow time of the polymer solution through the capillary was measured. From this, the kinematic viscosity was calculated according to **Equation 6**.

$$\nu = K \cdot (t - \zeta)$$

**Equation 6** Relationship between kinematic viscosity of polymer solutions, characteristics of the capillary viscometer, and flow time.

Where  $\nu$  is the kinematic viscosity,  $K$  the viscometer constant ( $0.1004 \text{ mm}^2/\text{s}^2$ ),  $t$  the flow time of the polymer solution through the capillary, and  $\zeta$  the flow time depending *Hagenbach-Couette* correction term.

Multiplying the kinematic viscosity with the specific density  $\rho$  of the polymer solution gave the value for the dynamic viscosity  $\eta_{dyn}$ . From this, the reduced viscosity was calculated according to **Equation 7**.

$$\eta_{red} = \frac{\eta_{dyn} - \eta_0}{\eta_0 \cdot c}$$

**Equation 7** Relationship between reduced viscosity of polymer solutions, dynamic viscosities, and polymer concentration.

Where  $\eta_{red}$  is the reduced viscosity,  $\eta_{dyn}$  the dynamic viscosity of the polymer solution,  $\eta_0$  the dynamic viscosity of the cement pore solution, and  $c$  the respective concentration of the dissolved polymer.

Finally, the intrinsic viscosity  $\eta_{intr}$  was obtained from the intercept point of  $\eta_{red} = f(c)$  with the y-axis when the polymer concentration  $c$  is extrapolated to 0. Under given conditions, the maximum deviation of this method was found to be  $\pm 0.01 \text{ L/g}$ .

Particle size distribution ( $d_{50}$  value) of  $\text{Na}^+$  lignosulfonate agglomerates was measured in 0.002 M NaOH (pH = 9.0) as a function of the calcium concentration present in the solvent ( $\text{Ca}^{2+}$  added stepwise as 0.1 M aqueous solution of  $\text{CaCl}_2 \cdot 2\text{H}_2\text{O}$ ) using a dynamic light scattering particle size analyzer (LB-550 from Horiba, Irvine, USA).

#### 4.2.4 Cement slurry preparation

Cement slurries were prepared in accordance with the procedures set forth in *Recommended Practice for Testing Well Cements*, API Recommended Practice 10B, issued by the *American Petroleum Institute* [59]. The slurries were mixed at a water-to-cement (w/c) ratio of 0.44 and 0.70, respectively, using a blade-type laboratory blender manufactured by Waring Products, Inc. (Torrington, USA). Prior to cement addition, the synthesized FLA solutions were dissolved in deionized water. In contrast, powdered additives were dry blended with the cement which was added within 15 s to the water placed in a Waring blender cup and mixed for 35 s at 12,000 rpm. To ensure homogeneous consistency, all slurries were stirred in an atmospheric consistometer (model 1250 from Chandler Engineering, Tulsa, USA) for 20 min at 27 °C, 80 °C, and 95 °C, respectively.

#### 4.2.5 Compressive strength analysis

The strength of a hardening cement sample can be estimated ultrasonically [86]. The ultrasonic cement analyzer (model 4262 Twin Cell UCA from Chandler Engineering, Tulsa, USA) measures the travel time of ultrasonic energy through a cement sample as it cures under specific temperature and pressure conditions. The sonic strength is correlated to the transit time (reciprocal of ultrasonic velocity) using an empirical relationship initially established from mechanical compressive strength and transit time data for various slurry systems [7]. Immediately after mixing in the Waring blender, the respective slurry was poured into a cell of the UCA and heated up to 80 °C under a differential pressure of 200 bar (heating rate 1.3 °C/min).

#### 4.2.6 Rheology measurement

For rheological measurements of cement slurries, a Couette-type coaxial cylinder rotational viscometer, FANN 35SA (Fann Instruments Company, Houston, USA) equipped with R1 rotor sleeve (rotor radius: 18.415 mm), B1 bob (bob radius: 17.245 mm, bob height: 3.80 cm) and F1 torsion spring was used. The values of the viscometer reading are recorded for 6 speeds of the rotor (3, 6, 100, 200, 300, 600 rpm). The value of shear stress  $\tau$  (Pa) is calculated by including the torsion spring factor (N cm/degree), the shear stress constant for the effective bob surface ( $\text{cm}^{-3}$ ), and the shear rate constant ( $\text{s}^{-1}/\text{rpm}$ ) [87]. The values of yield point (YP) and plastic viscosity (PV) were obtained according to **Equation 2** (see **chapter 2.2.3**) which describes the behavior of a *Bingham* fluid.

#### 4.2.7 Fluid loss test

Static fluid loss was measured at 27 °C, 80 °C, and 100 °C, respectively, using a 500 mL high temperature high pressure (HTHP) stainless steel filter press cell manufactured by OFI Testing Equipment Inc. (Houston, USA). After pouring the homogenized slurry obtained from the atmospheric consistometer into the HTHP cell, a heating jacket (OFI Testing Equipment Inc., Houston, USA) was used to adjust the test temperature. Then, a differential pressure of 70 bar  $\text{N}_2$  was applied at the top of the cell. Filtration proceeded through a 22.6  $\text{cm}^2$  (3.5  $\text{in}^2$ ) mesh metal sieve placed at the bottom of the cell. For measurements at 100 °C, a steel condenser was used to convert the partially gaseous filtrate into its liquid state. The fluid volume collected within 30 min ( $V_{30}$ ) was doubled as described by API RP 10B and regarded as API fluid loss of the corresponding slurry [59]. When dehydration of the cement slurry occurred before the test was ended, API fluid loss was calculated according to **Equation 8**.

$$\text{API fluid loss} = 2 \cdot V_t \cdot \sqrt{\frac{30}{t}}$$

**Equation 8** Relationship between API fluid loss and time-dependent volume of filtrate.

Where  $V_t$  is the filtrate volume collected until dehydration of the cement slurry that occurred at the time  $t$ .

The values reported for the respective API fluid loss test represents the average obtained from three separate measurements. The maximum deviation of the fluid loss value was  $\pm 10$  mL/30 min.

#### 4.2.8 Analysis of slurry thickening time

Prior to conducting the filtration tests at 100 °C, liquidity of the cement slurry over the entire test period of ~ 70 min had to be ensured by probing its thickening time on an HTHP (high temperature, high pressure) consistometer (model 8240 from Chandler Engineering, Tulsa, USA). This instrument is capable of measuring the consistency (viscosity) of cement pastes under conditions of high temperature (up to 315 °C) and high pressure (up to 2,750 bar). Slurry viscosity was measured in Bearden Units of Consistency ( $B_c$ ), a dimensionless unit obtained from the torque of a paddle rotating in the hydrating cement slurry, with no direct conversion factor to common units for viscosity. In this test, setting and solidification of cement is evidenced by an increase of slurry viscosity from  $< 20 B_c$  for the liquid paste to a value of 70  $B_c$  and higher. At this point, the curing cell has to be depressurized, cooled and dismantled immediately to avoid destruction of the equipment. A value of 70  $B_c$  is generally considered to be the maximum pumpable consistency [8].

In this study, the test protocol as follows was applied: The cement slurry containing 0.5 % bwoc CaAMPS<sup>®</sup>-*co*-NNDMA or CaAMPS<sup>®</sup>-*co*-NNDMA-*co*-MA was mixed in the Waring blender and immediately transferred into the cell of the HTHP consistometer. There, it was heated in a ramp-mode to 100 °C and pressurized with 70 bar (heating rate 1.5 °C/min; pressure rate 2.3 bar/min). Under those conditions, thickening times of 90 min were obtained, i.e., the slurries remained very liquid ( $< 20 B_c$ ) for 80 min and reached 70  $B_c$  after a total curing time of 90 min. This time span was deemed to be sufficient to allow safe operation of the HTHP filtration tests at 100 °C. Additionally, it ensured that low fluid loss values obtained at 100 °C were not originating from premature setting and hardening of the cement paste in the HTHP filtration cell.

Furthermore, employing the HTHP consistometer, the effectiveness of sodium lignosulfonate as cement retarder was tested at 80 °C and 400 bar (heating rate 1.2 °C/min; pressure rate 8.9 bar/min).

#### 4.2.9 Analysis of cement pore solution

Pore solutions of cement slurries prepared without polymer addition were produced by HTHP filtration at 27 °C, 80 °C and 100 °C, respectively. Under the latter conditions, a condenser was used to prevent evaporation of water which would result in higher than actual ion contents. The concentration of cations present in the pore solutions was determined by atomic absorption spectroscopy (AAS) (1100 B instrument from Perkin Elmer, Waltham, USA). The content of anions was measured using ion chromatography (ICS-2000 apparatus from Dionex, Idstein, Germany). Here, the alkaline cement filtrate was adjusted to pH 7.0 by adding 0.1 M HCl.

#### 4.2.10 Measurement of free water content

Stability of the cement paste (separation of so-called “bleeding” or free water) was determined at 80 °C. For this purpose, the slurry was placed in a 250 mL glass cylinder ( $\varnothing$  2.8 cm). The volume of water which separates at the top of the cement slurry after 2 h was declared free water content [8].

#### 4.2.11 Silica slurry preparation

Silica slurries were prepared following the same procedure described for the preparation of cement slurries, with the distinction that as mixing water, cement pore solutions obtained at 27 °C and 100 °C, respectively, were used instead of deionized water.

#### 4.2.12 Adsorption of polymers

Adsorbed amounts of the AMPS<sup>®</sup>-based fluid loss additives, biopolymers and lignosulfonate-based retarder were determined from the filtrate collected in the fluid loss test. Generally, the depletion method was applied, i.e., it was assumed that the decrease in the polymer concentration before and after contact with cement and silica, respectively, solely resulted from the adsorption on the mineral surface. Achievement of adsorption equilibrium was confirmed by zeta potential values which were constant at the time of collecting the filtrate for adsorption measurement. The adsorbed amount was calculated from the difference in the equilibrium concentrations of the polymers present in the liquid phase before and after adsorption (depletion method). When the respective admixture was the sole polymer present

in the cement filtrate, a High TOC II apparatus (Elementar, Hanau, Germany) equipped with a CO<sub>2</sub> detector was used to quantify polymer adsorption. For TOC analysis, the alkaline cement filtrate containing the unadsorbed polymers was adjusted to pH 1.0 by adding 0.1 M HCl.

In a binary additive system, the concentration of the AMPS<sup>®</sup>-based FLA was determined by TN analysis (High TOC II from Elementar, Hanau, Germany; equipped with NO<sub>x</sub> detector). The adsorbed amount of the biopolymer and lignosulfonate-based retarder, respectively, was calculated by subtracting the concentration of the FLA from the sum of adsorbed additives measured by TOC analysis. For this TOC analysis, the alkaline cement filtrate containing the unadsorbed polymers was adjusted to neutral pH by adding 0.01 M phosphoric acid. Here, the maximum deviation of the adsorption measurement was found to be  $\pm 0.1$  mg polymer/g cement and silica, respectively.

#### **4.2.13 Adsorption of sulfate ions onto the silica surface**

Adsorption of sulfate anions on silica was quantified from the filtrate collected in the fluid loss test. The adsorbed amount was calculated from the difference in the concentrations of the anions which were present in the pore solution before and after contact with silica. Sulfate concentration was measured by ion chromatography (ICS-2000 from Dionex, Idstein, Germany). Here, the alkaline filtrate was adjusted to pH 7.0 by adding 0.1 M HCl. The accuracy of the measurement was found to be  $\pm 0.1$  mg sulfate/g silica.

#### **4.2.14 Adsorption of chloride ions onto the cement surface**

Adsorption of chloride anions onto the cement surface was determined from the filtrate which was collected in the fluid loss test. The adsorbed amount was calculated from the difference in the concentrations of the anions present in the pore solution before and after contact with cement. Chloride concentration was measured by ion chromatography (ICS-2000 from Dionex, Idstein, Germany). Here, the alkaline cement filtrate was adjusted to pH 7.0 by adding 0.1 M H<sub>2</sub>SO<sub>4</sub>. The accuracy of this method was found to be  $\pm 0.1$  mg chloride/g cement.

**4.2.15 Zeta potential measurement**

Zeta potential of cement slurries was measured at room temperature on an electro acoustic spectrometer (DT-1200 from Dispersion Technology, Inc., Bedford Hills, USA) [51]. Since zeta potential was determined as a function of time (here 30 min), the cement slurry was poured immediately after mixing into the cup of the spectrometer and measured without homogenization in the atmospheric consistometer. The accuracy of this method was  $\pm 1$  mV.

**4.2.16 Environmental scanning electron microscopy (ESEM)**

The surface of cement slurries was analyzed by an environmental scanning electron microscope (XL 30 ESEM FEG from FEI Company, Eindhoven, The Netherlands) at 1.0 mbar. Energy dispersive X-ray spectroscopy (New XL-30 from EDAX, Mahwah, USA) was used for chemical characterization of the cement slurry containing 0.2 % bwoc Na<sup>+</sup> lignosulfonate at an acceleration voltage of 10,000 V.

## 5 RESULTS AND DISCUSSION

The first part of this study deals with the impact of temperature on cement hydration. Namely, the composition and morphology of hydrates formed by Class G oil well cement at 27 °C and 100 °C were compared.

Next, AMPS<sup>®</sup>-based fluid loss additives (FLAs) were synthesized by aqueous free radical copolymerization technique and characterized regarding their molecular structure and characteristic properties, e.g., their specific anionic charge amount. Then, the physico-chemical effects of high temperature on the performance of these polymers were investigated. Here, the adsorption behavior of these fluid loss additives on cement and silica, another component of cement slurries, was determined at 27 °C. These data were compared with the results obtained from experiments conducted at 100 °C.

The subsequent section focuses on the performance of CaAMPS<sup>®</sup>-*co*-NNDMA fluid loss additive in salt cement slurries. To develop a mechanistic model of the interaction between the copolymer and chloride, the amount of this polymer adsorbed on the cement surface and its resulting effectiveness were measured in absence and presence of sodium chloride at 80 °C.

Next, compatibility of CaAMPS<sup>®</sup>-*co*-NNDMA with the free water control agents welan gum and diutan gum, respectively, was determined. The efficiency of both polymers was tested in cement slurries which were mixed at high water-to-cement ratios.

The last part of this thesis investigates the mutual influence between CaAMPS<sup>®</sup>-*co*-NNDMA and the retarder sodium lignosulfonate regarding their effectiveness in cement slurries.

## 5.1 Cement hydration at ambient and elevated temperature

The first goal of this study was to investigate temperature induced effects on the hydration of API Class G oil well cement. For this purpose, the development of compressive strength of cement slurries which were cured at 27 °C and 100 °C, respectively, was monitored employing an ultrasonic cement analyzer. Composition and morphology of the resulting cement hydrates were identified using X-ray diffraction (XRD) analysis and environmental scanning electron microscopy (ESEM). Another objective was to clarify whether alpha dicalcium silicate hydrate ( $\alpha$ -C<sub>2</sub>SH) was formed through the hydration of C<sub>3</sub>S at elevated temperature. Its presence in the hardened cement sample would imply the use of silica to avoid strength retrogression for the tests conducted at 100 °C (see **chapter 2.2.2.6**).

### 5.1.1 Impact of temperature on cement hydration and the resulting hydrates

The development of compressive strength in cement slurries mixed at a water-to-cement (w/c) ratio of 0.44 and cured for 24 hours was monitored at two different temperatures using an ultrasonic cement analyzer (see **Figure 22**).

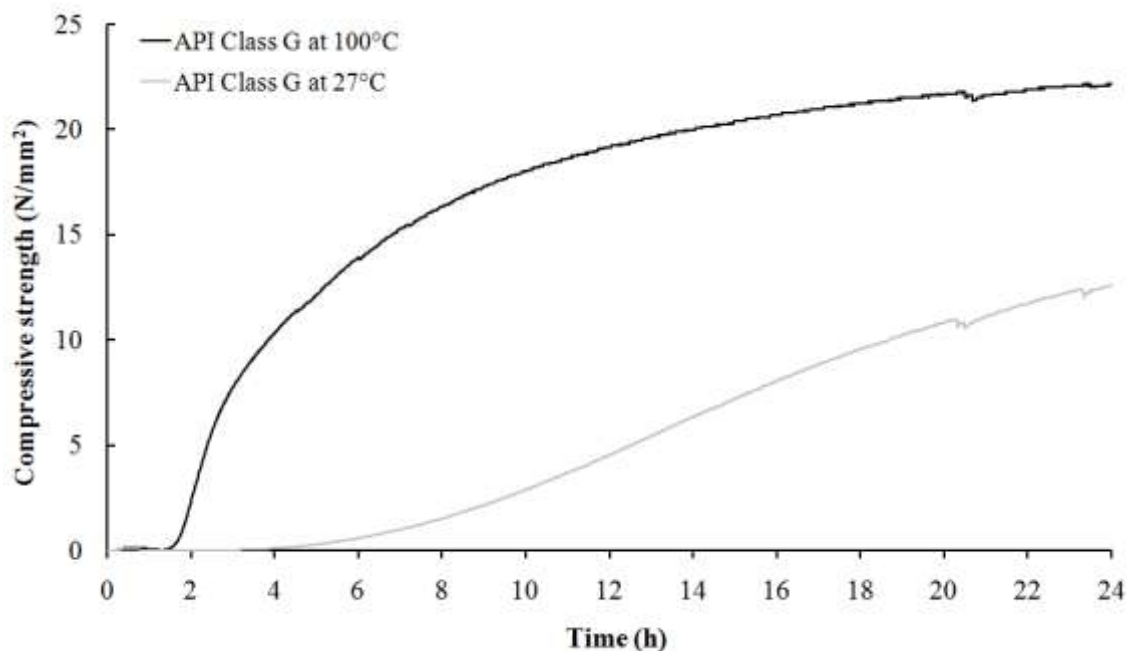


**Figure 22** Development of compressive strength of neat API Class G oil well cement sample cured at 27 °C and 100 °C, respectively (w/c 0.44).

This cement sample reached a compressive strength of  $3.4 \text{ N/mm}^2$  (500 psi) after 12 hours at  $27^\circ\text{C}$  (the time span a hardening cement slurry requires to attain this particular compressive strength is commonly used to estimate the respective waiting on cement time; see **chapter 2.1**). When cured at  $100^\circ\text{C}$ , the cement reached the same strength after only 2 hours. Thus, it becomes obvious that an increase in curing temperature considerably accelerates cement hydration. The final strength of the cement sample remained independent from temperature at  $22.1 \text{ N/mm}^2$  (3,200 psi). This compressive strength was reached after 65 hours when the cement sample was cured at  $27^\circ\text{C}$ , and after only 24 hours at a curing temperature of  $100^\circ\text{C}$ .

The XRD patterns of the hydration products are illustrated in **Figure 23** for a curing temperature of  $27^\circ\text{C}$ , and in **Figure 24** for a curing temperature of  $100^\circ\text{C}$ .

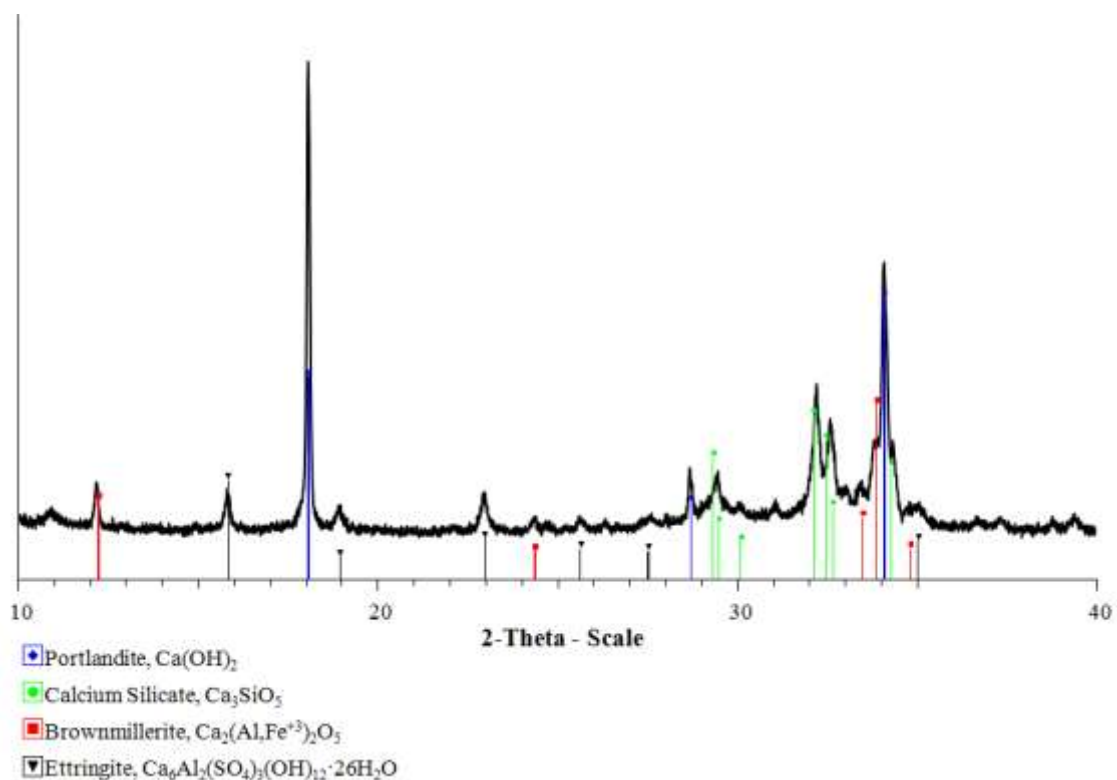


**Figure 23** XRD pattern of neat API Class G oil well cement slurry, cured for 12 hours at  $27^\circ\text{C}$  (w/c 0.44).

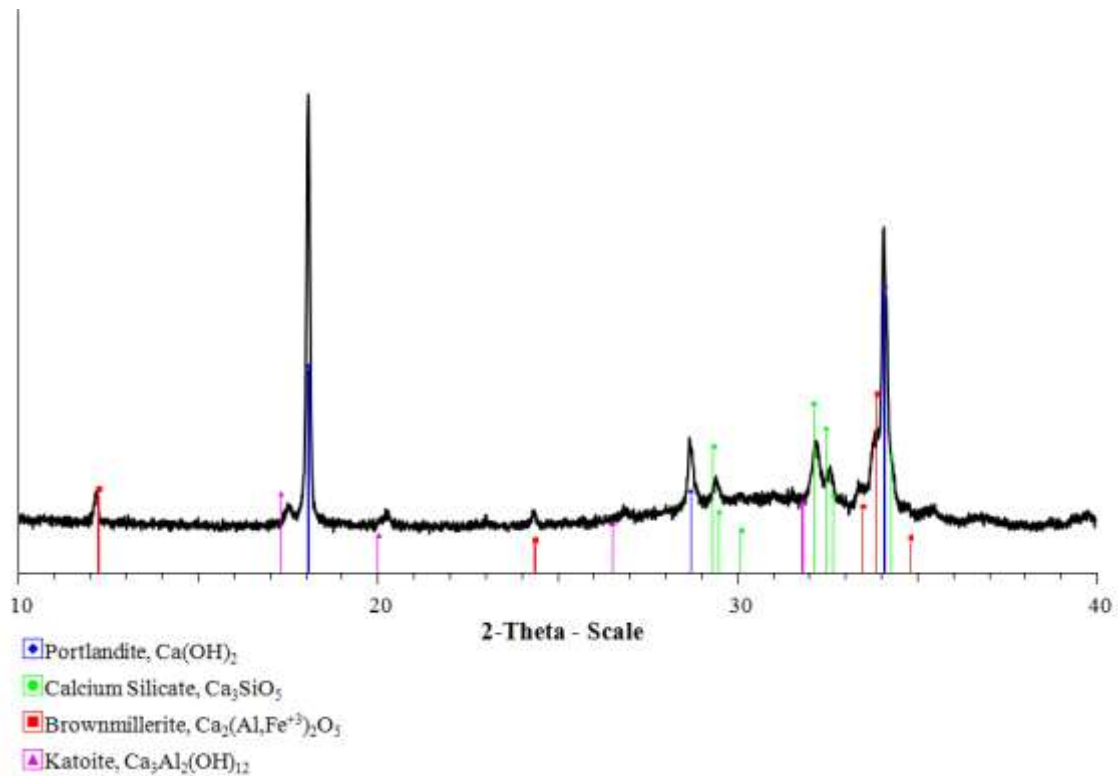


**Figure 24** XRD pattern of neat API Class G oil well cement slurry, cured for 2 hours at 100 °C (w/c 0.44).

At low temperature, the main crystalline hydrates were portlandite and unreacted tricalcium silicate. Calcium aluminate trisulfate (ettringite), an important cement hydrate phase formed instantaneously upon contact of cement with water, was clearly detectable after 12 hours of hydration.

After curing at 100 °C, the cement sample also contained mainly portlandite and unreacted tricalcium silicate. Here, however, no ettringite was detected. At approximately 75 °C, this hydration product transforms to 14-water calcium monosulfoaluminate (monosulfate also named monosulfoaluminate). At higher temperature, the 14-water monosulfate structure breaks up and a relatively small amount of 10-water monosulfate is formed [88]. However, under the conditions studied here, no  $\alpha$ -C<sub>2</sub>SH was found in the hydrating cement.

ESEM micrographs were used to confirm the results obtained from XRD analysis. At low temperature, the hydrating cement produced portlandite which forms hexagonal crystals and ettringite which has a needlelike morphology (see **Figure 25**).

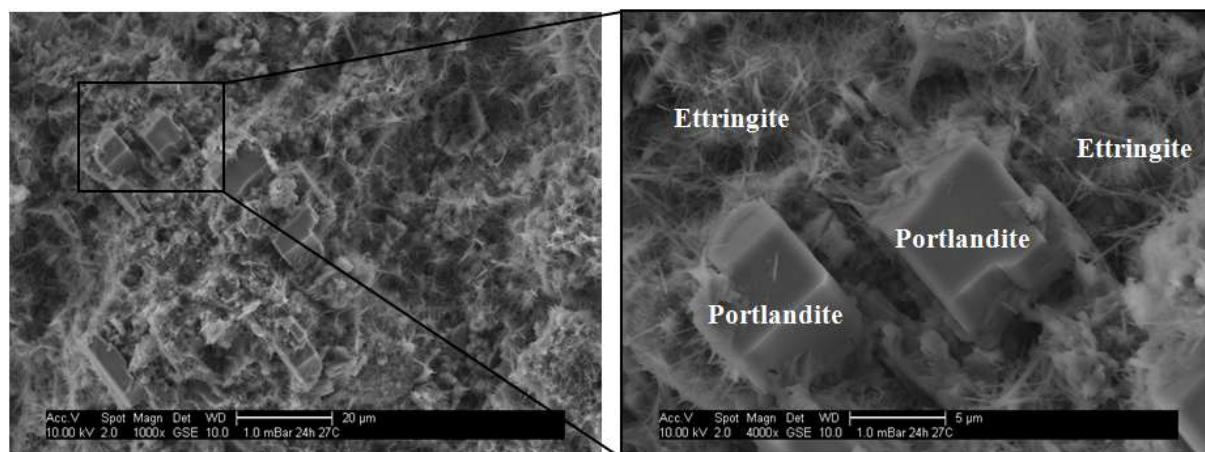


**Figure 25** ESEM micrograph of neat API Class G oil well cement slurry cured for 12 hours at 27°C (w/c 0.44).

In the cement slurry which was cured at 100°C, mainly portlandite and C-S-H phases were found. As expected from XRD measurements, no ettringite was observed in this sample (see **Figure 26**).

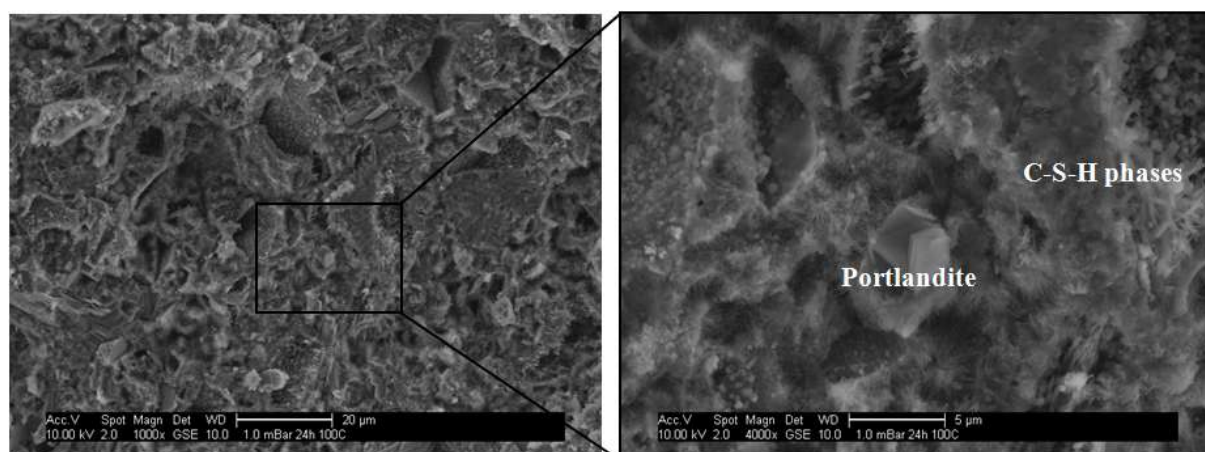


**Figure 26** ESEM micrograph of neat API Class G oil well cement slurry cured for 2 hours at 100 °C (w/c 0.44).

### 5.1.2 Conclusions

The compressive strength development of API Class G oil well cement is considerably accelerated by a temperature increase from 27 °C to 100 °C. The final strength of the hardened cement sample was found to be independent from the curing temperature. X-ray diffraction analysis and environmental scanning electron microscopy proved that the hydration product ettringite is not formed at 100°C. Also, the high temperature hydrate of tricalcium silicate, alpha dicalcium silicate hydrate ( $\alpha$ -C<sub>2</sub>SH), was not found. Thus, for tests conducted at 100 °C it was not necessary to add silica to the slurry in order to prevent strength retrogression. Silica would have provided additional mineral surfaces which, beside the surfaces of cement and its hydrates, could adsorb polyelectrolytes. Thus, for cement additives with an adsorptive working mechanism such as AMPS<sup>®</sup>-based fluid loss additives, it would have been much more complicated to draw accurate conclusions regarding their effectiveness in the presence of silica.

## 5.2 Impact of high temperature on the adsorption behavior and effectiveness of AMPS<sup>®</sup>-based fluid loss additives

A major goal of this study was to investigate the effect of high temperature (100 °C) on the adsorption behavior and effectiveness of AMPS<sup>®</sup>-based FLAs under carefully controlled experimental conditions. Namely, the fluid loss performances of CaAMPS<sup>®</sup>-*co*-NNDMA and CaAMPS<sup>®</sup>-*co*-NNDMA-*co*-MA terpolymers were compared at 27 °C, 80 °C, and 100 °C, respectively, to develop an idea of the robustness of these additives at different temperatures. To understand the mechanism underlying their effectiveness, adsorption of the FLAs on cement and silica as well as their intrinsic viscosity in cement pore solution were determined. Additionally, to test the hypothesis that sulfate anions may influence the conformation and hence the adsorption of these FLAs, the radius of gyration of each AMPS<sup>®</sup>-based copolymer was measured at different sulfate concentrations. Finally, the calcium binding capability of CaAMPS<sup>®</sup>-*co*-NNDMA and CaAMPS<sup>®</sup>-*co*-NNDMA-*co*-MA terpolymers was compared and the data were utilized to explain the adsorption behavior of these admixtures.

### 5.2.1 Synthesis and characterization of the AMPS<sup>®</sup>-based fluid loss additives

First, the calcium salt of 2-acrylamido-2-methylpropanesulfonic acid-*co*-*N,N*-dimethyl acrylamide was synthesized by aqueous free-radical copolymerization according to a process described in detail in the literature [89] [90]. This copolymer was designated CaAMPS<sup>®</sup>-*co*-NNDMA. The molar ratio between the AMPS<sup>®</sup> and NNDMA monomers was 1:0.63, and Na<sub>2</sub>S<sub>2</sub>O<sub>8</sub> was used as an initiator (see **Figure 27**). The characteristic properties of this polymer are summarized in **TABLE 4**.

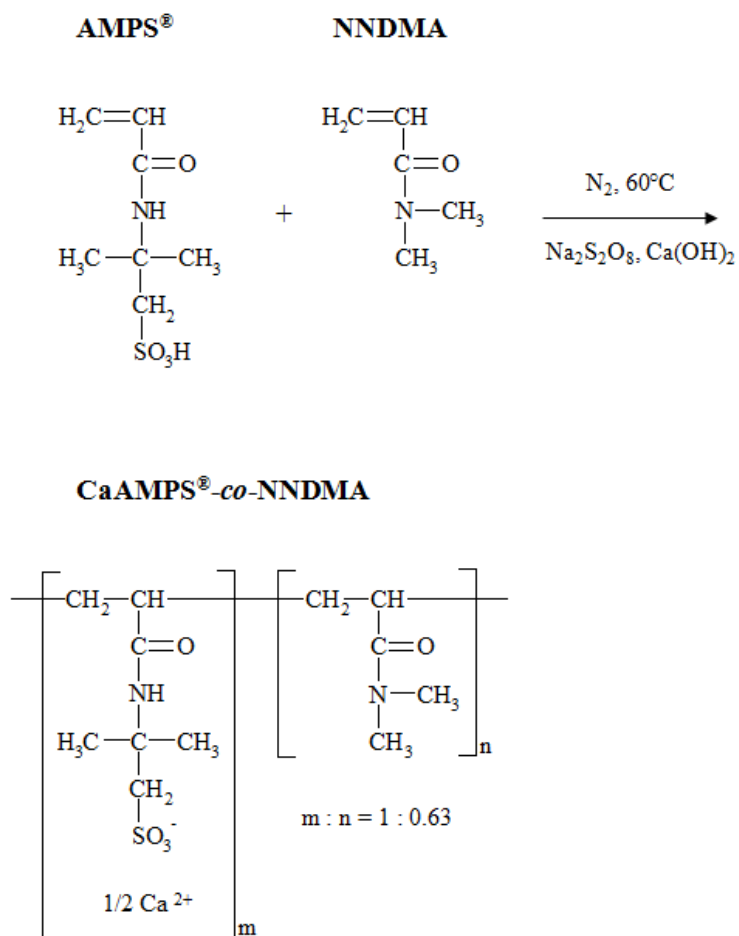


**Figure 27** Synthesis and chemical structure of the fluid loss additive CaAMPS<sup>®</sup>-co-NNDMA.

Next, from AMPS<sup>®</sup>, NNDMA and maleic anhydride (MA), three CaAMPS<sup>®</sup>-co-NNDMA-co-MA-based terpolymers were prepared following the same synthesis method (see **Figure 28**). The molar ratios between the AMPS<sup>®</sup>, NNDMA and MA monomers were 1:0.63:0.02 (terpolymer 1), 1:0.63:0.05 (terpolymer 2) and 1:1.00:0.02 (terpolymer 3), respectively. The characteristic properties of these fluid loss polymers are summarized in **TABLE 4**.

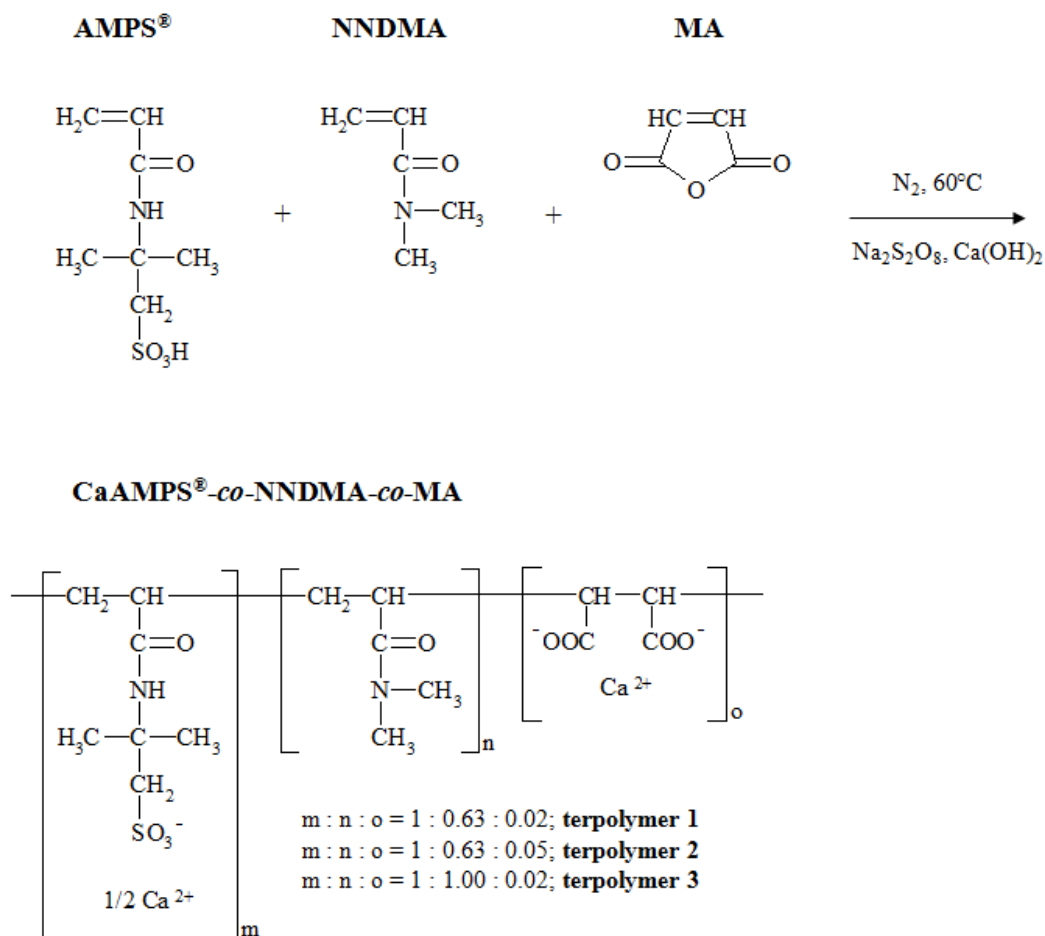


**Figure 28** Synthesis route for the CaAMPS<sup>®</sup>-*co*-NNDMA-*co*-MA-based terpolymers.

The unmodified AMPS<sup>®</sup>-based copolymer exhibited a specific anionic charge amount of 370 C/g (see **TABLE 4**). Through the incorporation of additional carboxylate groups, the specific anionic charge amount of the terpolymers 1 and 2 increased to 380 C/g (molar ratio of AMPS<sup>®</sup>:NNDMA = 1:0.63). As for terpolymer 3 the molar ratio of the uncharged monomer NNDMA was 1 instead of 0.63, its specific anionic charge amount decreased from 370 C/g to 340 C/g.

**TABLE 4**

**Molar ratios of monomers, specific anionic charge amount, solids content, *Brookfield* viscosity, molecular weights, polydispersity index, radii ( $Rg_z$ ,  $Rh_z$ ) and *Burchard* parameter of the synthesized polymers**

Molar ratio of AMPS <sup>®</sup> :NNDMA:MA	Designated	Anionic charge amount, $\varepsilon$ (C/g)	Solids content (%)	<i>Brookfield</i> viscosity (mPa·s)	Molecular weight		Poly- dispersity index $M_w/M_n$	Radius of gyration, $Rg_z$ (nm)	Hydro- dynamic radius, $Rh_z$ (nm)	<i>Burchard</i> parameter, $\rho$
					$M_w$ (g/mol)	$M_n$ (g/mol)				
1:0.63:0	CaAMPS <sup>®</sup> - co-NNDMA	370	18	10,000	$2.0 \cdot 10^6$	$1.2 \cdot 10^6$	1.7	64	7	8.7
1:0.63:0.02	terpolymer 1	380	16	7,000	$1.8 \cdot 10^6$	$1.0 \cdot 10^6$	1.8	58	7	8.3
1:0.63:0.05	terpolymer 2	380	15	6,000	$1.8 \cdot 10^6$	$1.1 \cdot 10^6$	1.7	53	7	7.6
1:1.00:0.02	terpolymer 3	340	18	30,000	$1.8 \cdot 10^6$	$1.1 \cdot 10^6$	1.7	57	7	8.1

All synthesized polymers showed a comparable solids content of approximately 17 wt. %. However, with a *Brookfield* viscosity of approximately 30,000 mPa·s, terpolymer 3 (AMPS<sup>®</sup>:NNDMA:MA = 1:1.00:0.02) was much more viscous, compared to the other synthesized polymers (~ 10,000 mPa·s). Its higher content of *N,N*-dimethyl acrylamide resulted in a stiffer structure and therefore instigated a higher viscosity of the polymer solution.

SEC measurements confirmed that all synthesized polymers possessed comparable molecular weights ( $M_w = \sim 2 \cdot 10^6$  Da;  $M_n = \sim 1 \cdot 10^6$  Da) and hydrodynamic radii  $Rh_z$  (7 nm). The *Burchard* parameter  $\rho$ , calculated from the quotient of the gyration radius,  $Rg_z$  and the hydrodynamic radius,  $Rh_z$ , allows to assess the conformation of the dissolved polymer (see **Appendix**; [91]). For all polymers, this parameter exceeded 2.2 (value for stiff chains). Thus, a relatively stretched conformation was assumed for these fluid loss additives.

Their radius of gyration  $Rg_z$ , however, decreases with increasing amounts of maleic acid anhydride, namely from 64 nm for CaAMPS<sup>®</sup>-*co*-NNDMA to 53 nm for terpolymer 2 (AMPS<sup>®</sup>:NNDMA:MA = 1:0.63:0.05). The following considerations were made to explain this result: The *Q-e* scheme which was introduced by *Alfrey* and *Price* in 1947 can be considered as an empirical approach to placing monomer reactivity on a quantitative basis [92]. Monomer reactivity is separated into the parameter *Q*, which describes the resonance factor present in the monomer, and the parameter *e*, which describes the polar factor. As the *e* values of AMPS<sup>®</sup> and NNDMA are opposite in sign, it can be concluded that these monomers show an alternating arrangement along the polymer backbone. Because the *Q* and *e* values of MA and AMPS<sup>®</sup> are completely different (see **Appendix**; [93]), MA will preferentially undergo homopolymerization and form blocks within CaAMPS<sup>®</sup>-*co*-NNDMA-*co*-MA terpolymer [92].

Apparently, counter ions present in the solvent decrease the intramolecular repulsion caused by the carboxylate groups possessing the same charge more effectively than for the sulfonate functions of CaAMPS<sup>®</sup>-*co*-NNDMA. Thus, the resulting shielding effect is stronger for the MA-modified terpolymers, causing a somewhat more coiled structure and hence a reduced radius of gyration. The following investigations were conducted to clarify whether this change in the conformation of the MA-modified polymers affects their adsorption behavior at high temperature.

### 5.2.2 Temperature-dependent interaction of FLAs with cement

Since the working mechanism of the synthesized fluid loss polymers is adsorptive, the relationship between API fluid loss and the amount of the polymers adsorbed on cement was determined at 27 °C and 100 °C, respectively (see **Figure 29** and **Figure 30**). The adsorbed amount of CaAMPS<sup>®</sup>-*co*-NNDMA was reduced by 15 % as a result of high temperature (4.6 mg polymer/g cement at 27 °C vs. 3.9 mg polymer/g cement at 100 °C; see **Figure 29**). Owing to this reduced FLA adsorption, the API fluid loss of the cement slurry increased from 40 mL/30 min at 27 °C to 120 mL/30 min at 100 °C. Additional tests showed that this negative effect of high temperature on adsorption and therefore fluid loss control could only be overcome by higher FLA dosages. To obtain a similar API fluid loss at 100 °C as observed at 27 °C (~ 40 mL), a dosage as high as 0.8 % by weight of cement (bwoc) of CaAMPS<sup>®</sup>-*co*-NNDMA was required.

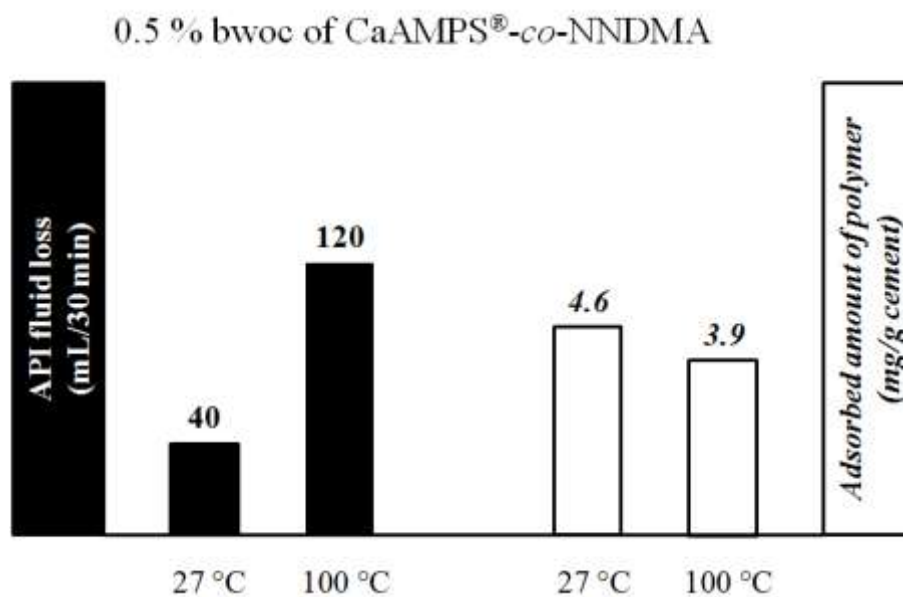


**Figure 29** Relationship between API fluid loss (black bars) and adsorbed amount of CaAMPS<sup>®</sup>-*co*-NNDMA (white bars), determined in cement slurries at 27 °C and 100 °C, respectively (w/c 0.44).

When terpolymer 1 (AMPS<sup>®</sup>:NNDMA:MA = 1:0.63:0.02) was employed, the increase in API fluid loss occurring at high temperature was only 2/3 of the one observed for the unmodified copolymer (from 38 mL/30 min at 27 °C to 80 mL/30 min at 100 °C; see **Figure 30**). The reason is that the adsorbed amount of this CaAMPS<sup>®</sup>-*co*-NNDMA-*co*-MA-based FLA was nearly unaffected by temperature (4.7 mg/g at 27 °C vs. 4.5 mg/g at 100 °C). Terpolymer 1 showed improved performance with temperature, compared to the unmodified polymer. To explain this effect, the following considerations and experiments were made.

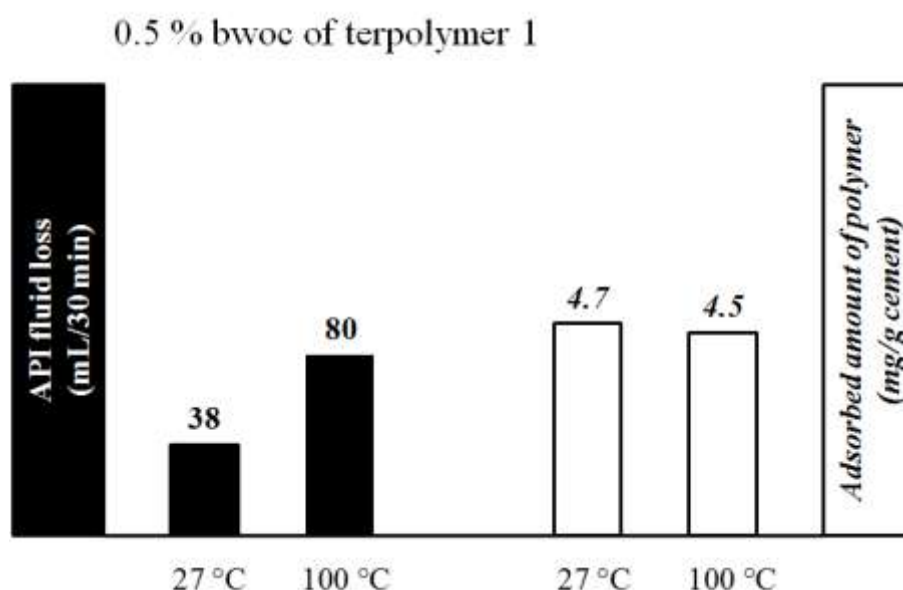


**Figure 30** Relationship between API fluid loss (black bars) and adsorbed amount of terpolymer 1 (AMPS<sup>®</sup>:NNDMA:MA = 1:0.63:0.02) (white bars), determined in cement slurries at 27 °C and 100 °C, respectively (w/c 0.44).

Through incorporation of only ~ 1.3 mol% of maleic anhydride, the CaAMPS<sup>®</sup>-*co*-NNDMA-*co*-MA polymer backbone possesses segments holding additional carboxylate functionalities. In previous work relating to cement dispersants, -COO<sup>-</sup> groups have been found to be stronger anchor groups on cement surfaces than the sulfonate functionalities present in CaAMPS<sup>®</sup>-*co*-NNDMA [58] [94]. To confirm, the specific anionic charge amount of CaAMPS<sup>®</sup>-*co*-NNDMA and terpolymer 1, respectively, was determined in alkaline solution (pH = 12.6) in presence and absence of 0.6 g/L calcium ions using polyelectrolyte titration (this calcium concentration was found in the pore solution obtained from neat cement slurries after 20 min of homogenization). The results presented in **TABLE 5** show that in a Ca<sup>2+</sup> loaded solution,

incorporation of such minor quantity of maleic anhydride into the copolymer had a surprisingly strong effect on the specific anionic charge amount.

TABLE 5

**Specific anionic charge amounts of CaAMPS<sup>®</sup>-*co*-NNDMA and terpolymer 1 (AMPS<sup>®</sup>:NNDMA:MA = 1:0.63:0.02), respectively, measured in 0.1 M NaOH (pH = 12.6) in presence and absence of 0.6 g/L Ca<sup>2+</sup> (polymer concentration: 0.02 g/L)**

Polymer	Specific anionic charge amount (C/g)		Reduction of anionic charge after Ca <sup>2+</sup> addition
	Water @ pH 12.6	Water @ pH 12.6 plus 0.6 g/L Ca <sup>2+</sup>	
CaAMPS <sup>®</sup> - <i>co</i> -NNDMA	368	352	4 %
terpolymer 1	402	275	31 %

After addition of Ca<sup>2+</sup> ions, the specific anionic charge amount of the terpolymer containing MA decreased by 31 % vs. only 4 % for CaAMPS<sup>®</sup>-*co*-NNDMA. Apparently, the carboxylate functionalities of CaAMPS<sup>®</sup>-*co*-NNDMA-*co*-MA possess a considerably stronger calcium binding capability than CaAMPS<sup>®</sup>-*co*-NNDMA. Consequently, the terpolymer exhibits a higher affinity to positively charged mineral surfaces which causes the adsorbed amount of terpolymer 1 to be less dependent on temperature. Through this mechanism, CaAMPS<sup>®</sup>-*co*-NNDMA-*co*-MA provides good fluid loss control of the cement slurry, even at high temperature.

However, when the molar ratio of MA monomer was increased from initially 0.02 to 0.05 (terpolymer 2), the adsorbed amount and hence the effectiveness of the resulting FLA slightly decreased at 100°C (see **Figure 31**).

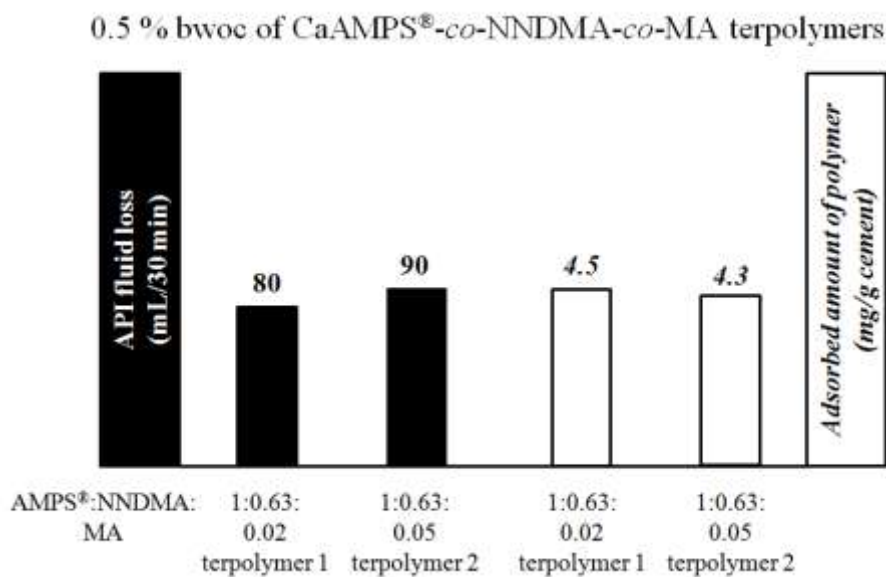


**Figure 31** Relationship between API fluid loss (black bars) and adsorbed amount of CaAMPS<sup>®</sup>-*co*-NNDMA-*co*-MA terpolymers prepared with different molar ratios of maleic anhydride (white bars), determined in cement slurries at 100 °C (w/c 0.44).

The reason behind this unexpected result is that the adsorption behavior of AMPS<sup>®</sup>-based polymers is also influenced by their conformation in solution [95]. As stated in **chapter 5.2.1**, the structure of the MA-modified terpolymers coils, depending on the content of maleic anhydride incorporated into their polymer backbone. Obviously, a coiled polymer will have to unfold in order to develop the maximum number of contact points per unit of surface area. Apparently, a higher content of maleic anhydride used for polymer preparation enforces such coiling effects on the conformation of the terpolymer and hence decreases its tendency to adsorb on the cement surface. Additionally, a coiled polymer will generally exercise a reduced plugging effect compared to a fully stretched polymer which can constrict the pores of the filtercake more effectively, because of its larger steric size.

Polymer adsorption was confirmed by zeta potential measurements. The neat cement slurry possessed a zeta potential of approximately -6 mV. When the FLA was added at a dosage of 0.5 % bwoc to the cement slurry, the zeta potentials decreased to values of -20 mV for CaAMPS<sup>®</sup>-*co*-NNDMA and -21 mV for the CaAMPS<sup>®</sup>-*co*-NNDMA-*co*-MA terpolymers. This decrease can be explained by the loading of negative charges onto the cement surface caused by adsorption of these polymers.

### 5.2.3 Dynamic viscosity of HTHP filtrates at elevated temperature

As shown in **Figure 30**, the adsorbed amount of terpolymer 1 (molar ratios of AMPS<sup>®</sup>:NNDMA:MA = 1:0.63:0.02) on cement is quite independent of the test temperature (~ 4.6 mg polymer/g cement at 27 °C and 100 °C, respectively). Nevertheless, the resulting API fluid loss increased from 38 mL/30 min at 27 °C to 80 mL/30 min at 100 °C. The following investigations were conducted to explain this unexpected effect.

According to *Desbrières*, the volume of filtrate obtained from HTHP filtration tests mainly depends on the dynamic viscosity of the filtrate and the permeability of the filtercake, which in turn is highly influenced by the adsorption of FLAs (see page 22, **Equation 5**; [60]). The relationship between the API fluid loss of cement slurries containing terpolymer 1 and the dynamic viscosity of the resulting filtrates was determined at 27 °C and 80 °C, respectively (see **Figure 32**; a temperature of 80 °C instead of 100 °C was selected because at temperatures > 80 °C, evaporation of the solvent would lead to artificially increased polymer concentrations of the solution and hence to false viscosity measurements).

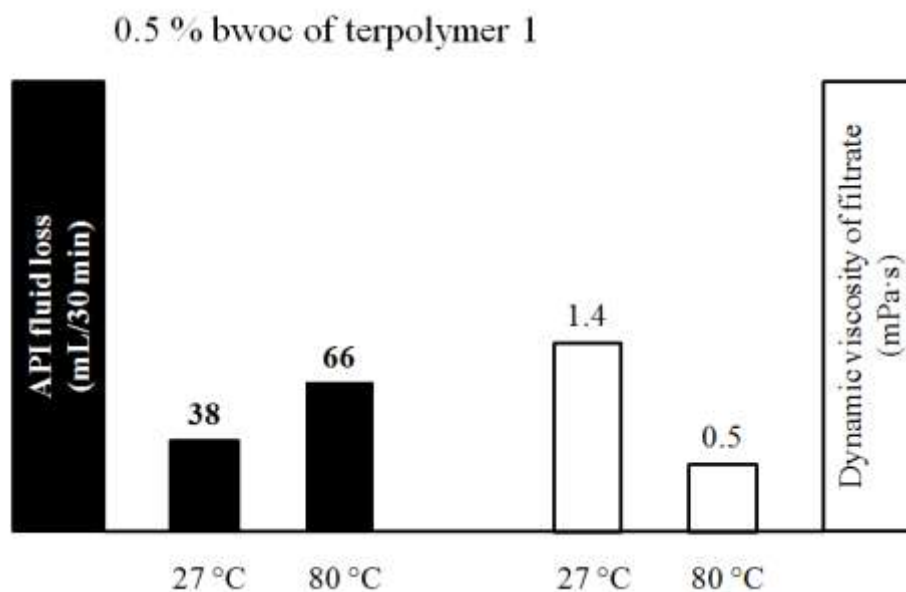


**Figure 32** Relationship between API fluid loss (black bars) and dynamic viscosity of the resulting HTHP filtrate (white bars), determined in cement slurries at 27 °C and 80 °C, respectively (w/c 0.44).

In spite of a constant adsorbed amount of the FLA on cement (4.6 mg/g for both temperatures), the effectiveness of this terpolymer decreased with increasing temperature (38 mL/30 min at 27 °C vs 66 mL/30 min at 80 °C). Obviously, the reason behind this detrimental effect is a dramatic loss of filtrate viscosity from 1.4 mPa·s at 27 °C to 0.5 mPa·s at 80 °C. In CaAMPS<sup>®</sup>-*co*-NNDMA-*co*-MA terpolymers, *N,N*-dimethyl acrylamide is responsible for the stiffness of the polymer backbone. Resulting from the interaction of more rigid polymer chains, a higher NNDMA content present in the respective FLA should lead to higher dynamic viscosity of the polymer solution. Thus, the question arises whether this effect results in lower HTHP filtrates, and whether a higher NNDMA content incorporated into the macromolecule leads to increased FLA effectiveness, even at high temperature.

#### 5.2.4 Dynamic viscosity of HTHP filtrates containing stiffer terpolymers

The dynamic viscosity of two CaAMPS<sup>®</sup>-*co*-NNDMA-*co*-MA polymers (terpolymer 1 and terpolymer 3) solved in cement pore solution was measured at 80 °C (see **TABLE 6**). The main difference between these terpolymers is the molar ratio of NNDMA used for their preparation (see **chapter 5.2.1**). For aqueous solutions containing 11.36 g/L of terpolymer 1 (molar ratio of AMPS<sup>®</sup>:NNDMA = 1:0.63) a dynamic viscosity of 3.0 mPa·s was measured. This polymer concentration correlates to a FLA dosage of 0.5 % bwoc. When terpolymer 3 (molar ratio of AMPS<sup>®</sup>:NNDMA = 1:1) is dissolved in cement pore solution to give a concentration of 11.36 g/L, the dynamic viscosity increases to a value of 6.9 mPa·s. As expected, the content of NNDMA incorporated into the polymer stiffens its solved conformation and strongly influences the viscosity of the polymer solution.

**TABLE 6**

**Dynamic viscosity of CaAMPS<sup>®</sup>-*co*-NNDMA-*co*-MA FLAs solved in cement pore solution, measured at 80 °C (polymer concentration: 11.36 g/L)**

Molar ratio of AMPS <sup>®</sup> :NNDMA:MA	Designated	Dynamic viscosity (mPa·s)
1:0.63:0.02	terpolymer 1	3.0
1:1.00:0.02	terpolymer 3	6.9

Next, the rheology of cement slurries containing the two CaAMPS<sup>®</sup>-*co*-NNDMA-*co*-MA FLAs was determined at 80 °C. As summarized in **TABLE 7**, cement rheology increased with NNDMA content of the respective fluid loss additive. It becomes clear that the use of terpolymer 3 provided high viscosity to the cement system.

**TABLE 7**

**Rheology (shear stress) of cement slurries containing 0.5 % bwoc of CaAMPS<sup>®</sup>-*co*-NNDMA-*co*-MA terpolymers, measured at 80 °C (w/c 0.44)**

Polymer	Shear stress (Pa) at different shear rates (s <sup>-1</sup> )						Plastic Viscosity, $\mu_p$ (mPa·s)	Yield Point, $\tau_0$ (Pa)
	1022	511	340	170	10.2	5.1		
terpolymer 1	85	57	42	25	4	3	57	3
terpolymer 3	131	87	68	46	13	13	84	13

**Figure 33** illustrates the results obtained from HTHP filtration tests of cement slurries containing 0.5 % bwoc of the CaAMPS<sup>®</sup>-*co*-NNDMA-*co*-MA FLAs, conducted at 80 °C. As can be seen there, both terpolymers adsorbed in equally high amount onto the cement surface (4.6 mg/g cement). Unexpectedly, however, the corresponding API fluid loss values were nearly unaffected by the higher NNDMA content present in terpolymer 3 (66 mL/30 min for terpolymer 1 vs. 72 mL/30 min for terpolymer 3). At 80 °C, the dynamic viscosity of the filtrate containing this FLA remained at 0.5 mPa·s, as seen before for terpolymer 1 (see **Figure 32**). Under given conditions, the synthesized CaAMPS<sup>®</sup>-*co*-NNDMA-*co*-MA fluid loss additives showed an adsorption rate of ~90 % on cement hydrates. Thus, the concentration of solved polymers present in the filtrate was not high enough to increase the viscosity of the solution and hence to improve FLA effectiveness. As the molar ratios of the monomers used for the preparation of CaAMPS<sup>®</sup>-*co*-NNDMA and terpolymer 1 differ least from each other (AMPS<sup>®</sup>:NNDMA = 1:0.63 for CaAMPS<sup>®</sup>-*co*-NNDMA and 1:0.063:0.02 for terpolymer 1, respectively) the following experiments concentrated on these two polymers.

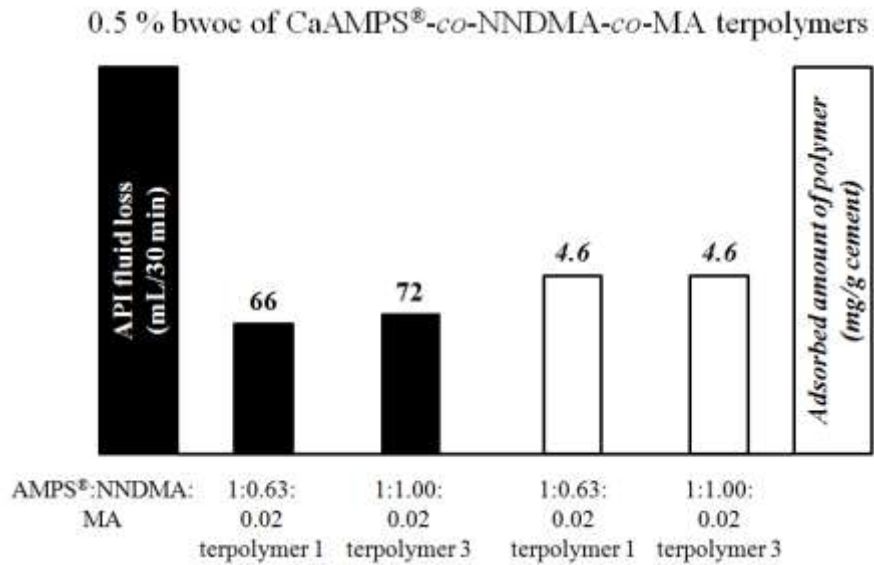


**Figure 33** Relationship between API fluid loss (black bars) and adsorbed amount of CaAMPS<sup>®</sup>-*co*-NNDMA-*co*-MA terpolymers (white bars), determined in cement slurries at 80 °C (w/c 0.44).

### 5.2.5 Effect of temperature on the sulfate content of cement pore solutions

To understand the reasons behind the reduced performance of CaAMPS<sup>®</sup>-*co*-NNDMA at high temperature even better, the concentration of ions present in the cement pore solution obtained from filtration at 27 °C and 100 °C, respectively, was compared using ion chromatography. *Maitland et al.* reported that calcium aluminate trisulfate (ettringite), becomes unstable at temperatures  $\geq 75$  °C and decomposes into calcium monosulfoaluminate (monosulfate) and gypsum [88]. Consequently, we found that through this reaction, the sulfate concentration present in the cement pore solution collected at 100 °C was significantly higher than that measured at 27 °C (8.3 g/L sulfate vs. 6.8 g/L sulfate). Opposite to this trend, the Ca<sup>2+</sup> concentration remained nearly constant (0.7 g/L at 27 °C vs. 0.6 g/L at 100 °C). Resulting from their high anionic charge density, sulfate anions may also adsorb onto the surface of cement hydrates. Competition between sulfate and CaAMPS<sup>®</sup>-*co*-NNDMA for limited adsorption sites may occur. Therefore, it can be speculated that a higher sulfate concentration may also contribute to the reduced effectiveness of CaAMPS<sup>®</sup>-*co*-NNDMA at high temperature. To test this hypothesis, adsorption of CaAMPS<sup>®</sup>-*co*-NNDMA and of sulfate on silica was determined. These data were compared with the results obtained from adsorption measurements of terpolymer 1 and sulfate on silica.

The high sulfate content ( $\sim 3$  to  $4$  wt. %  $\text{CaSO}_4 \cdot n\text{H}_2\text{O}$ ) of API oil well cement makes an analysis of adsorbed sulfate on cement surfaces practically impossible. Therefore, to quantify sulfate and FLA adsorption on positively charged mineral surfaces, the adsorbent was changed from reactive cement to inert silica. In highly alkaline suspensions ( $\text{pH} > 12$ ), silica is negatively charged which stems from deprotonated silanol groups present on its surface [96]. This was confirmed for the silica sample used here by measurement of the zeta potential in  $0.1$  M NaOH (see **Figure 34**).

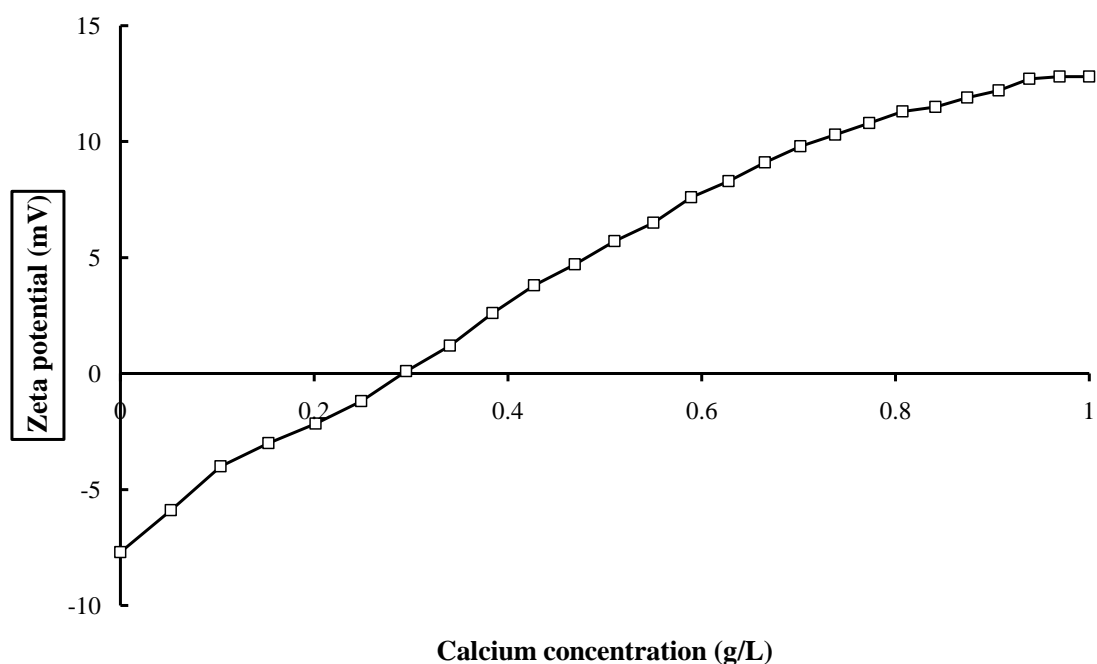


**Figure 34** Development of zeta potential for silica sample SSA-1<sup>®</sup> at a pH value of 12.6 as a function of the calcium concentration present in the solvent (water to silica ratio = 0.44).

At a water to silica ratio of 0.44, a value for the zeta potential of  $-8$  mV was found. Addition of minor amounts of calcium ions (added as  $\text{CaCl}_2 \cdot 2\text{H}_2\text{O}$ ), however, caused a reversal in the sign of the surface charge to highly positive values ( $\sim +8$  mV at a dosage of  $0.6$  g/L  $\text{Ca}^{2+}$ ). This change in surface charge is a consequence of the adsorption of  $\text{Ca}^{2+}$  ions onto the negatively charged silica surface [97]. This way, it could be demonstrated that silica can provide positively charged adsorption sites for anionic FLA polymers in a similar way than cement and is therefore a suitable substitute for the following experiments.

### 5.2.6 Sulfate-dependent adsorption of FLAs on silica

Adsorption of sulfate and the FLAs on silica was determined at 100 °C using cement pore solutions collected at different temperatures. The difference in their sulfate concentration was 6.8 g/L at 27 °C and 8.3 g/L at 100 °C. Independent of this fact, the adsorbed amount of CaAMPS<sup>®</sup>-*co*-NNDMA remained at 0.6 mg polymer/g silica for both experiments (see **Figure 35**). At the same time, a constant value of 0.1 mg adsorbed sulfate/g silica was measured. Thus, in spite of an increase of the sulfate concentration of the cement pore solution, the adsorption equilibrium did not alter towards higher sulfate and lower FLA adsorption. Therefore, competitive adsorption between this polymer and sulfate anions can be excluded as a mechanism behind the reduced effectiveness of this FLA polymer at high temperature. This instigates that increased kinetic energy of the polymer molecules dissolved in water at 100 °C decreases the adsorbed amount and hence is the reason for the reduced performance of CaAMPS<sup>®</sup>-*co*-NNDMA at high temperature.

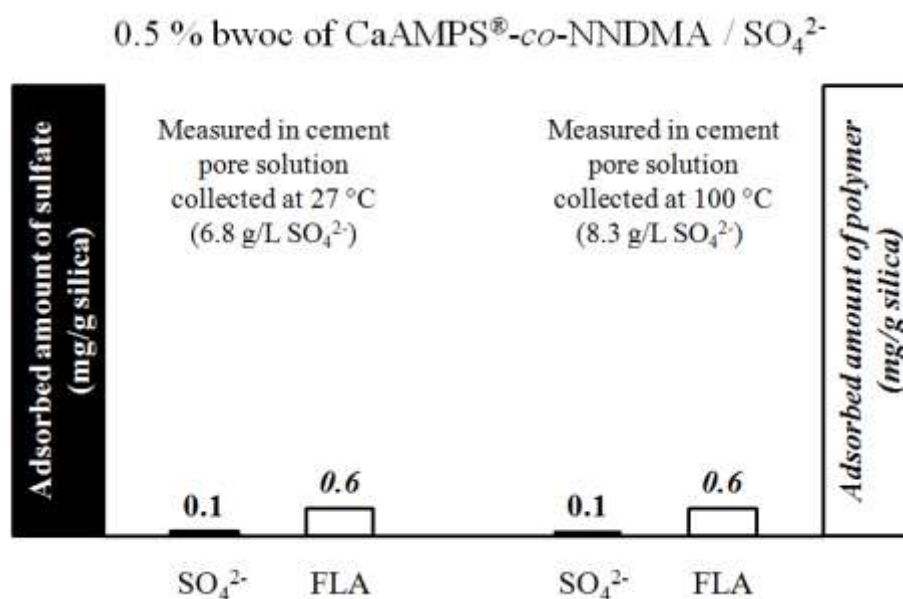


**Figure 35** Adsorbed amounts of sulfate (black bars) and CaAMPS<sup>®</sup>-*co*-NNDMA (white bars) on silica as a function of the sulfate concentration present in the mixing water, determined at 100 °C (water to silica ratio = 0.44).

The adsorbed amount of terpolymer 1 (molar ratios of AMPS<sup>®</sup>:NNDMA:MA = 1:0.63:0.02) on silica was also independent of the sulfate concentration. However, the adsorption of 4.7 mg polymer/g silica of this polymer clearly exceeded the adsorbed amount of 0.6 mg polymer/g silica for CaAMPS<sup>®</sup>-*co*-NNDMA; see **Figure 36**. Owing to the incorporation of homopolymer blocks holding carboxylate anchor groups, this terpolymer exhibits a strong affinity to the positively charged silica surface, even at 100 °C. It can be speculated that for this modified terpolymer and under these conditions, the *Gibbs* free energy of adsorption  $\Delta G_{ads}^0$  is higher than its kinetic energy. The result is improved performance of this CaAMPS<sup>®</sup>-*co*-NNDMA-*co*-MA terpolymer at high temperature.

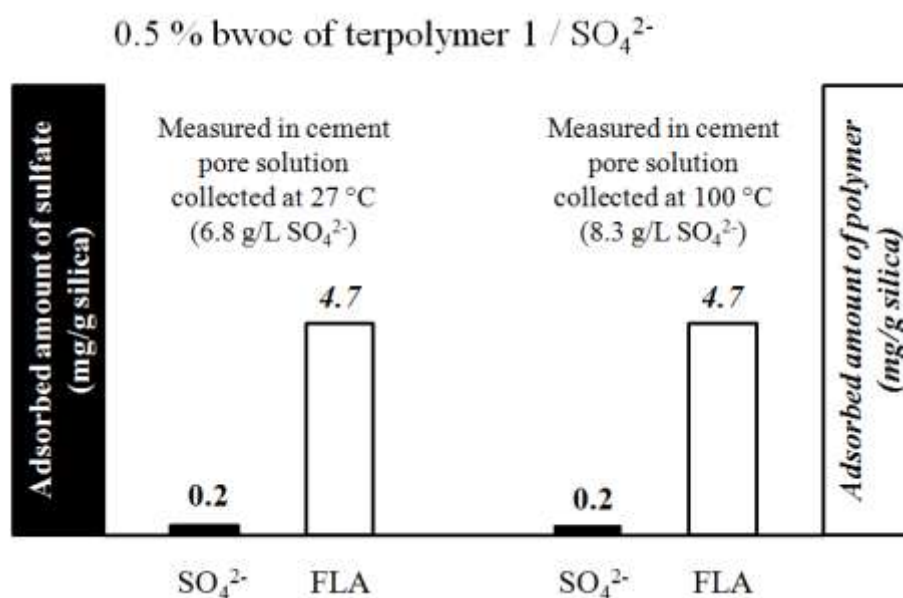


**Figure 36** Adsorbed amounts of sulfate (black bars) and terpolymer 1 (molar ratios of AMPS<sup>®</sup>:NNDMA:MA = 1:0.63:0.02; white bars) on silica as a function of the sulfate concentration present in the mixing water, determined at 100 °C (water to silica ratio = 0.44).

### 5.2.7 Conformation of solvled FLA polymers

Another factor which may influence the adsorption of AMPS<sup>®</sup>-based fluid loss additives onto mineral surfaces is the molecular conformation of the solvled polymer. For example, it has been demonstrated that sulfate ions present in the cement pore solution cause shrinkage and coiling of polycarboxylate-type dispersants commonly used in concrete [98]. There, the consequence is lower adsorption and hence reduced dispersing power. To investigate the effect of sulfate ions on the conformation of solvled FLA polymers, the intrinsic viscosity of CaAMPS<sup>®</sup>-*co*-NNDMA and terpolymer 1 (molar ratios of AMPS<sup>®</sup>:NNDMA:MA = 1:0.63:0.02), respectively, was determined at 80 °C in cement pore solutions collected by filtration at 27 °C and 100 °C, respectively. At temperatures higher than 80 °C, evaporation of the solvent would lead to artificially increased polymer concentrations of the solution and hence to false intrinsic viscosities.

The results exhibited in **TABLE 8** demonstrate that for both polymers, a higher SO<sub>4</sub><sup>2-</sup> concentration reduced the intrinsic viscosity (CaAMPS<sup>®</sup>-*co*-NNDMA: from 0.36 L/g at 6.8 g/L sulfate to 0.33 L/g at 8.3 g/L sulfate; terpolymer 1: from 0.34 L/g at 6.8 g/L sulfate to 0.30 L/g at 8.3 g/L sulfate). These data suggest that an elevated sulfate concentration causes some coiling effect on the solvled macromolecules.

**TABLE 8**

**Intrinsic viscosity of CaAMPS<sup>®</sup>-*co*-NNDMA and terpolymer 1 (molar ratios of AMPS<sup>®</sup>:NNDMA:MA = 1:0.63:0.02), respectively, determined at different sulfate concentrations present in cement pore solutions and 80 °C (w/c 0.44)**

Polymer	Intrinsic viscosity (L/g)	
	6.8 g/L SO <sub>4</sub> <sup>2-</sup> <sup>a</sup>	8.3 g/L SO <sub>4</sub> <sup>2-</sup> <sup>b</sup>
CaAMPS <sup>®</sup> - <i>co</i> -NNDMA	0.36	0.33
terpolymer 1	0.34	0.30

<sup>a</sup> measured in cement pore solution collected at 27 °C

<sup>b</sup> measured in cement pore solution collected at 100 °C

To confirm this effect, the radius of gyration of these polymers was determined at increasing sulfate concentrations (see **TABLE 9**). It was found that for both polymers,  $Rg_z$  decreased with increasing sulfate concentration. For example,  $Rg_z$  of CaAMPS<sup>®</sup>-*co*-NNDMA exhibited a decrease from 64 nm in sulfate-free environment to 53 nm in the presence of 8.3 g/L  $SO_4^{2-}$ . Similarly, the radius of gyration of terpolymer 1 decreased from 58 nm in the absence of sulfate to 41 nm at 8.3 g/L sulfate. Thus, it becomes evident that both macromolecules undergo similar shrinkage in the presence of sulfate.

**TABLE 9**

**Radius of gyration of CaAMPS<sup>®</sup>-*co*-NNDMA and terpolymer 1 (molar ratios of AMPS<sup>®</sup>:NNDMA:MA = 1:0.63:0.02), respectively, determined at different sulfate concentrations present in the eluant (0.2 M NaNO<sub>3</sub>)**

Polymer	Radius of gyration, $Rg_z$ (nm)		
	0 g/L $SO_4^{2-}$	6.8 g/L $SO_4^{2-}$	8.3 g/L $SO_4^{2-}$
CaAMPS <sup>®</sup> - <i>co</i> -NNDMA	64	62	53
terpolymer 1	58	54	41

As a coiled polymer has to unfold to develop the maximum number of contact points per unit of surface area, a fluid loss additive in coiled conformation, consequently, has lower tendency to adsorb on the cement surface than a stretched molecule which exists in a sulfate-free solution [95]. Thus, the coiling effect observed instigates a slightly reduced performance for both FLA polymers.

### 5.2.8 Conclusions

Temperature deteriorated the effectiveness of CaAMPS<sup>®</sup>-*co*-NNDMA as fluid loss additive through reduced polymer adsorption. This detrimental effect was mainly caused by poor calcium binding capability of the sulfonate anchor groups which coordinate with calcium atoms present on the mineral surface. As the kinetic energy of CaAMPS<sup>®</sup>-*co*-NNDMA is increased by high temperature, adsorption of this copolymer becomes less favorable. The sulfate concentration present in the cement pore solution also increases at high temperature, resulting from thermal degradation of ettringite. A higher sulfate concentration leads to shrinkage of the solved fluid loss additive and decreases the amount of polymer adsorbed on the mineral surface. Competitive adsorption between sulfate and the polymer did not significantly impact the adsorption behavior of the FLA. This was in contrast to dispersant molecules based on polycarboxylate chemistry where numerous cases are documented describing a strong effect of sulfate on the adsorption of those admixtures [98] [99].

Slightly modified CaAMPS<sup>®</sup>-*co*-NNDMA-*co*-MA FLAs contain few homopolymer blocks holding vicinal carboxylate functionalities which present much stronger anchor groups than sulfonates. The result is high and stable adsorption, independent of temperature and sulfate concentration. Consequently, their fluid loss performance is little affected by those two parameters. Obviously, the blocks of carboxylate functionalities are the key for their improved performance. Modifications of these terpolymers regarding the molar ratio of the MA and NNDMA monomers used for their preparation, however, did not further improve the effectiveness of these CaAMPS<sup>®</sup>-*co*-NNDMA-*co*-MA FLAs.

### 5.3 Effectiveness of AMPS<sup>®</sup>-based FLAs in salt cement slurries

When salt formations are cemented, salt cement slurries are commonly used to prevent well bore washout resulting from osmotic dissolution of salt into the slurry. There, sodium chloride is added to the cement paste up to its saturation level of 36 % by weight of water (bwow) [7]. In this chapter, the impact of a high concentration of solved NaCl (100 g/L) on the effectiveness of AMPS<sup>®</sup>-based fluid loss additives was clarified. For this purpose, static filtration tests of cement slurries containing CaAMPS<sup>®</sup>-*co*-NNDMA and terpolymer 1 (molar ratios of AMPS<sup>®</sup>:NNDMA:MA = 1:0.63:0.02), respectively, were conducted in presence and absence of sodium chloride. Additionally, the adsorbed amount of these fluid loss additives and chloride ions, respectively, on the cement surface was measured.

#### 5.3.1 Effectiveness of CaAMPS<sup>®</sup>-*co*-NNDMA in salt cement slurries

The relationship between the adsorbed amount and the resulting effectiveness of CaAMPS<sup>®</sup>-*co*-NNDMA in cement slurries prepared with fresh water and in presence of 10 % NaCl bwow was determined for different polymer dosages at 80 °C (see **TABLE 10**). In fresh water slurries, the adsorbed amount of the fluid loss additive increased with increasing polymer dosages from 4.2 mg/g cement at 0.5 % bwoc CaAMPS<sup>®</sup>-*co*-NNDMA to 8.2 mg/g cement at 0.9 % bwoc FLA. Thus, the corresponding API fluid loss values decreased from 90 mL/30 min to 36 mL/30 min.

When 10 % bwow NaCl were added to the cement slurry, however, for all tested dosages, the adsorbed amount of CaAMPS<sup>®</sup>-*co*-NNDMA decreased by approximately 21 %. Consequently, fluid loss control of the respective slurries became very poor. Here, CaAMPS<sup>®</sup>-*co*-NNDMA could not achieve acceptable fluid loss control, even at dosages as high as 0.9 % bwoc. Obviously, this polymer possesses only limited salt tolerance.

TABLE 10

**API fluid loss and adsorbed amount of CaAMPS<sup>®</sup>-*co*-NNDMA in cement slurries prepared with fresh water and in presence of 100 g/L NaCl, respectively, measured for different polymer dosages at 80 °C (w/c 0.44)**

Polymer dosage (% bwoc)	Dosage of NaCl (% bwow)	API fluid loss (mL/30 min)	Adsorbed amount of polymer (mg/g cement)
0.5	0	90	4.2
0.5	10	418	0.9
0.7	0	53	6.2
0.7	10	439	1.3
0.9	0	36	8.2
0.9	10	350	3.5

As shown in **chapter 5.2.7**, a high concentration of sulfate ions present in the solvent changes the conformation of the solvated CaAMPS<sup>®</sup>-*co*-NNDMA which in turn influences its adsorption behavior onto the cement surface. To clarify whether chloride ions also cause this effect, the intrinsic viscosity of this AMPS<sup>®</sup>-based FLA dissolved in cement pore solution was measured in presence and absence of 10 % NaCl bwow at 80 °C. Here, the intrinsic viscosity remained independent of the NaCl concentration present in the solvent at approximately 0.36 L/g. Therefore, it can be concluded that the low tendency to adsorb on cement, as observed for CaAMPS<sup>®</sup>-*co*-NNDMA in salt cement systems, does not result from a conformational change of the polymer.

As chloride ions possess a significant anionic charge density, the question arises whether these anions can also adsorb on cement and compete with anionic FLA molecules for limited adsorption sites present on the mineral surface. Therefore, the amount of chloride ions adsorbed on the cement surface was measured in slurries at 10 % NaCl bwow. The adsorption was also determined for CaAMPS<sup>®</sup>-*co*-NNDMA in cement slurries containing 0.5 % bwoc of FLA (see **Figure 37**; left). These data were compared with the results obtained from adsorption measurements of a binary additive system (10 % NaCl and 0.5 % FLA) (see **Figure 37**; right).

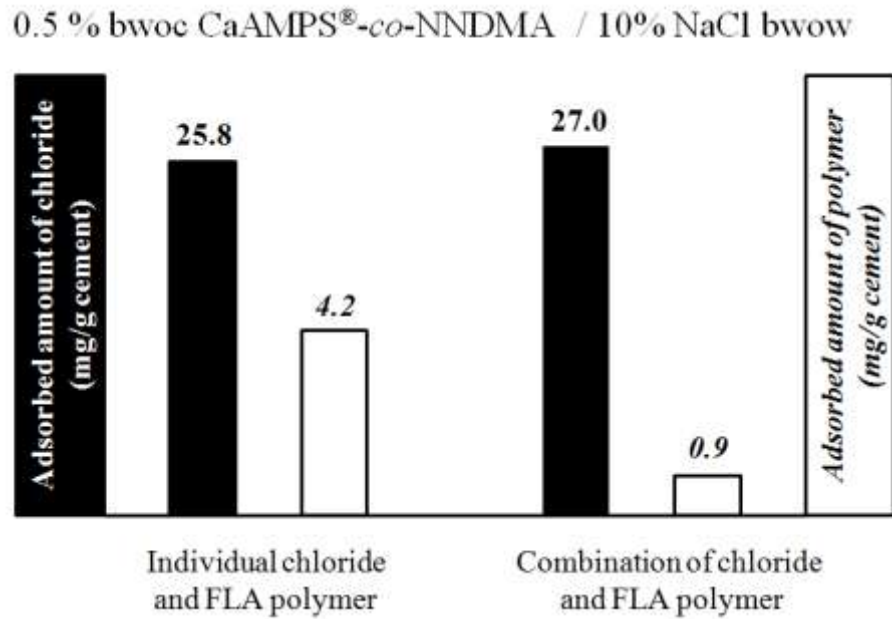


**Figure 37** Amounts of chloride ions (black bars) and FLA polymer (white bars), respectively, adsorbed on cement, as determined for individual (10 % NaCl and 0.5 % FLA, respectively) and combined system (10 % NaCl + 0.5 % FLA) at 80 °C (w/c 0.44).

The adsorption of chloride ions on cement was not influenced by the presence of the AMPS<sup>®</sup>-based fluid loss additive (25.8 mg adsorbed Cl<sup>-</sup>/g cement in absence of the FLA vs. 27.0 mg adsorbed Cl<sup>-</sup>/g cement in the presence of 0.5 % bwoc of CaAMPS<sup>®</sup>-*co*-NNDMA). In contrast, the adsorbed amount of CaAMPS<sup>®</sup>-*co*-NNDMA decreased dramatically from 4.2 mg/g cement in the chloride-free fresh water slurry to 0.9 mg/g cement in the salt cement slurry. Obviously, competitive adsorption between CaAMPS<sup>®</sup>-*co*-NNDMA and chloride ions leads to the displacement of already adsorbed FLA molecules from the mineral surface. This detrimental effect causes the reduced salt tolerance of CaAMPS<sup>®</sup>-*co*-NNDMA.

### 5.3.2 Effectiveness of CaAMPS<sup>®</sup>-*co*-NNDMA-*co*-MA in salt cement slurries

The carboxylate anchor groups of terpolymer 1 (molar ratios of AMPS<sup>®</sup>:NNDMA:MA = 1:0.63:0.02) instigate an increased calcium chelating ability compared to the sulfonate functionalities provided by CaAMPS<sup>®</sup>-*co*-NNDMA (see **chapter 5.2.2**). Thus, in case of competitive adsorption between chloride anions and AMPS<sup>®</sup>-based fluid loss polymers, terpolymer 1 should be less easily displaced from the cement surface. The resulting FLA effectiveness of this polymer should hence be better than that for CaAMPS<sup>®</sup>-*co*-NNDMA, even in salt cement slurries. To verify this hypothesis, the adsorbed amount of the MA-modified terpolymer and the respective API fluid loss were determined in the presence of 10 % NaCl bwoc at different polymer dosages at 80 °C (**TABLE 11**).

**TABLE 11**

**API fluid loss and adsorbed amount of CaAMPS<sup>®</sup>-*co*-NNDMA and terpolymer 1 (molar ratios of AMPS<sup>®</sup>:NNDMA:MA = 1:0.63:0.02), respectively, in salt cement slurries at different polymer dosages and 80 °C (w/c 0.44; 100 g/L NaCl)**

Polymer	Polymer dosage (% bwoc)	API fluid loss (mL/30 min)	Adsorbed amount of polymer (mg/g cement)
CaAMPS <sup>®</sup> - <i>co</i> -NNDMA	0.5	418	0.9
terpolymer 1	0.5	402	2.6
CaAMPS <sup>®</sup> - <i>co</i> -NNDMA	0.7	439	1.3
terpolymer 1	0.7	140	3.7
CaAMPS <sup>®</sup> - <i>co</i> -NNDMA	0.9	350	3.5
terpolymer 1	0.9	44	7.1

In salt cement slurries, the amount of terpolymer 1 adsorbed on cement was up to 2 times the amount of CaAMPS<sup>®</sup>-*co*-NNDMA (e.g., 7.1 mg adsorbed CaAMPS<sup>®</sup>-*co*-NNDMA-*co*-MA/g cement at a dosage of 0.9 % bwoc vs. 3.5 mg adsorbed CaAMPS<sup>®</sup>-*co*-NNDMA/g cement under the same conditions). Thus, the CaAMPS<sup>®</sup>-*co*-NNDMA-*co*-MA FLA provided enhanced fluid loss control for cement slurries, even in the presence of NaCl (e.g.,

44 mL/30 min for cement slurries containing 0.9 % bwoc of terpolymer 1 vs. 350 mL/30 min for CaAMPS<sup>®</sup>-*co*-NNDMA). These results confirm that competitive interaction occurs between AMPS<sup>®</sup>-based fluid loss additives and chloride anions for limited adsorption sites on cement.

### 5.3.3 Conclusions

Effectiveness of CaAMPS<sup>®</sup>-*co*-NNDMA was shown to be very poor in salt cement slurries. Here, the chloride anions provide stronger adsorption ability to the cement surface than the polymer. Therefore, competitive adsorption between chloride ions and anionic FLA molecules for a limited number of adsorption sites on the cement hydrates resulted in displacement (desorption) of the polymer.

Through incorporation of additional carboxylate anchor groups into the polymer backbone, the adsorbed amount of the terpolymer CaAMPS<sup>®</sup>-*co*-NNDMA-*co*-MA could be increased compared to that of the copolymer. Thus, FLA effectiveness and salt stability of this terpolymer significantly exceeded that of CaAMPS<sup>®</sup>-*co*-NNDMA. This result clearly proves the existence of competitive interaction between chloride anions and the FLA polymer for limited adsorption sites of the cement surface.

## 5.4 Interaction between CaAMPS<sup>®</sup>-*co*-NNDMA and biopolymers

Free water developed at the top of a cement column can pose a serious problem for zonal isolation [8]. Free water control agents such as welan gum and diutan gum are commonly added to the slurry to prevent this undesired effect. The goal of this investigation was to clarify the interaction between CaAMPS<sup>®</sup>-*co*-NNDMA and such microbial biopolymers with respect to the performance of each admixture in oil well cement. Thus, fluid loss, rheology and free water content of cement slurries containing the AMPS<sup>®</sup>-based FLA as well as welan gum and diutan gum, respectively, were measured at 80 °C. To understand the mechanism of interaction, adsorption of CaAMPS<sup>®</sup>-*co*-NNDMA and of the free water control agents on cement was measured when used as single additive and as combinations of both admixtures. Additionally, to estimate their tendency to adsorb onto the cement surface, the calcium binding capability of the AMPS<sup>®</sup>-based copolymer and of the biopolymers, respectively, was determined.

### 5.4.1 Interaction of CaAMPS<sup>®</sup>-*co*-NNDMA with cement

The relationship between HTHP fluid loss and the amount of CaAMPS<sup>®</sup>-*co*-NNDMA adsorbed on cement was determined at different w/c ratios (0.44 and 0.70, respectively) at 80 °C. As can be seen in **Figure 38**, the adsorbed amount of the FLA increased with the w/c ratio (4.2 mg FLA/g cement at w/c 0.44 vs. 4.8 mg FLA/g cement at w/c 0.70). Nevertheless, the resulting fluid loss control of the slurry remained almost constant (100 mL/30 min at w/c 0.44 vs. 112 mL/30 min at w/c 0.70). At higher w/c ratios, additional mixing water is present in the cement slurry. Thus, more capillary pores are formed in the matrix of the hydrating cement [13]. To achieve a comparable reduction of filtercake permeability through FLA adsorption, a higher adsorbed amount of CaAMPS<sup>®</sup>-*co*-NNDMA is necessary.

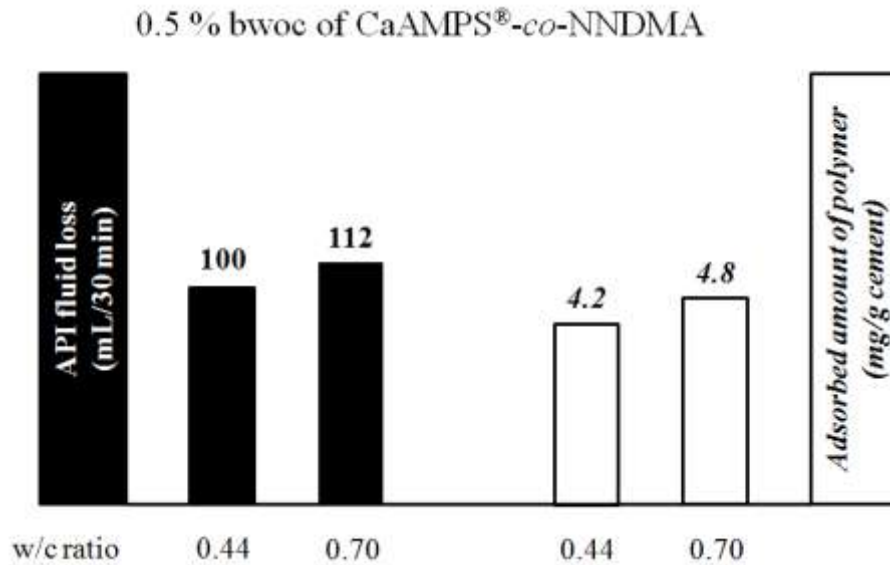


**Figure 38** API fluid loss (black bars) of API Class G oil well cement slurries and adsorbed amounts of CaAMPS<sup>®</sup>-*co*-NNDMA (white bars) as a function of w/c ratio, measured at 80 °C.

Rheological data of cement slurries prepared with 0.5 % bwoc CaAMPS<sup>®</sup>-*co*-NNDMA presented in **TABLE 12** demonstrated that at a w/c ratio of 0.70, the cement slurry possessed practically no yield point (YP), leading to sedimentation and development of free water. Therefore, such slurries required stabilization by microbial biopolymers for free water control.

**TABLE 12**

**Rheology (shear stress) and free water content of cement slurries containing 0.5 % bwoc of CaAMPS<sup>®</sup>-*co*-NNDMA, measured at different w/c ratios and at 80 °C**

w/c ratio	Free water content (mL)	Shear stress (Pa) at different shear rates (s <sup>-1</sup> )						Plastic viscosity, $\mu$ (mPa·s)	Yield point, $\tau_0$ (Pa)
		1022	511	340	170	10.2	5.1		
0.44	0	109	75	57	38	7	6	67	6.1
0.70	3	16	10	7	4	1	0	12	0.2

## 5.4.2 Interaction of microbial biopolymers with cement

### 5.4.2.1 Interaction of welan gum with cement

First, the adsorption of welan gum on cement was quantified by TOC analysis (see **Figure 39**; left). There, it becomes obvious that most of the welan gum added adsorbed on cement (~ 90 % adsorption at a dosage of 0.06 % bwoc), indicating a very strong interaction with this mineral surface, in spite of the low specific anionic charge amount found for this biopolymer (- 121 C/g, as measured in cement pore solution at 27 °C).

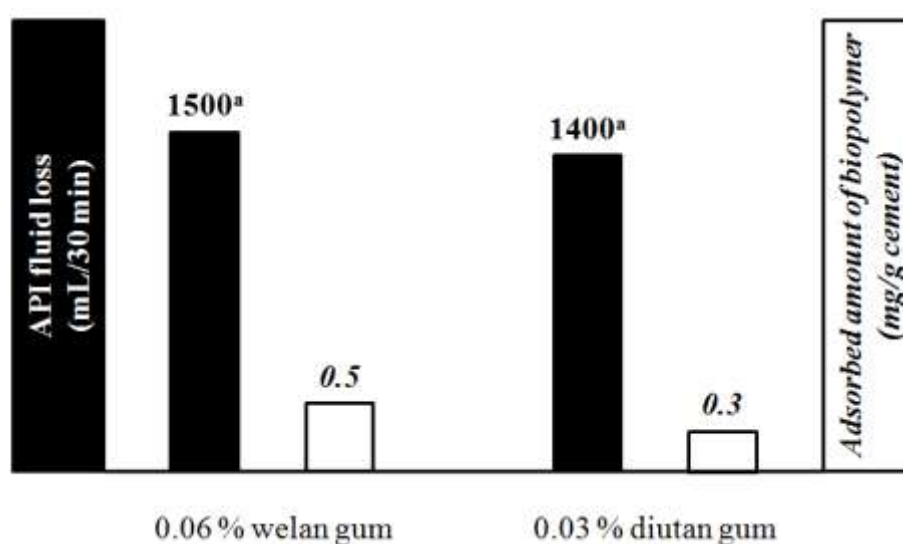


**Figure 39** API fluid loss (black bar) of API Class G oil well cement slurries and adsorbed amounts of the biopolymers welan gum and diutan gum, respectively (white bar), measured at 80 °C (w/c 0.70).

<sup>a</sup> Dehydration of cement slurry within less than 30 min.

Adsorption of anionic welan gum was confirmed by zeta potential measurements. The zeta potential of the cement slurry (- 6 mV) became more negative when 0.06 % bwoc of welan gum were added (- 10 mV). This way, it was demonstrated that the higher negative charge of the cement particles is caused by adsorption of this anionic polysaccharide. However, under the conditions tested, addition of this biopolymer did not provide any fluid loss control to the cement slurry (calculated API fluid loss of ~1500 mL/30 min at 0.06 % bwoc welan gum). This result confirms that welan gum solely acts as viscosity modifier and free water control agent.

#### 5.4.2.2 Interaction of diutan gum with cement

As determined by TOC analysis, the interaction of diutan gum with cement is very strong and comparable with that of welan gum (~ 90 % adsorption at a dosage of 0.03 % bwoc diutan gum). Polymer adsorption was confirmed by zeta potential measurements. Neat cement slurry provided a zeta potential of ~ - 6 mV. When diutan gum at 0.03 % bwoc dosage was added, the zeta potential decreased to a value of - 9 mV. The reason for this effect is the loading of negative charges onto the cement surface caused by adsorption of this anionic biopolymer. Like welan gum, diutan gum solely acts as viscosity modifier and free water control agent. Thus, this polymer did not provide any fluid loss control to the cement slurry (calculated API fluid loss of ~ 1400 mL/30 min at 0.03 % bwoc diutan gum; see **Figure 39**; right).

### 5.4.3 Binary systems containing CaAMPS<sup>®</sup>-*co*-NNDMA and a free water control agent

#### 5.4.3.1 Combination of CaAMPS<sup>®</sup>-*co*-NNDMA with welan gum

First, effectiveness of welan gum was tested with respect to free water control of cement slurries containing 0.5 % bwoc of the FLA at a w/c ratio of 0.70. From the results presented in **TABLE 13** it becomes obvious that a dosage of 0.06 % bwoc, welan gum was sufficient to prevent any free water formation.

**TABLE 13**

**Rheology (shear stress) and free water content of cement slurries containing 0.5 % bwoc of CaAMPS<sup>®</sup>-*co*-NNDMA and welan gum, measured at 80 °C (w/c 0.70)**

Welan gum dosage (wt. %)	Free water content (mL)	Shear stress (Pa) at different shear rates (s <sup>-1</sup> )						Plastic viscosity, $\mu$ (mPa·s)	Yield point, $\tau_0$ (Pa)
		1022	511	340	170	10.2	5.1		
0	3	16	10	7	4	1	0	12	0.2
0.06	0	35	21	16	10	3	3	27	2.5

The rheological data indicate that the biopolymer stabilizes the cement slurry without destroying its pumpability by imparting excessive viscosity. The effect can be attributed to the shear-thinning type of rheology provided by welan gum. It establishes a high yield point (YP) in the cement slurry which prevents sag of solid particles, whereas the plastic viscosity (PV) was only slightly increased.

In a binary additive system containing both CaAMPS<sup>®</sup>-*co*-NNDMA and welan gum, the anionic biopolymer may compete with the FLA for adsorption sites on the cement surface. The strong interaction with cement may hence negatively impact fluid loss performance. To test this hypothesis, the API fluid loss of cement slurries containing both CaAMPS<sup>®</sup>-*co*-NNDMA and welan gum were compared with the adsorbed amount of each admixture (see **Figure 40**).

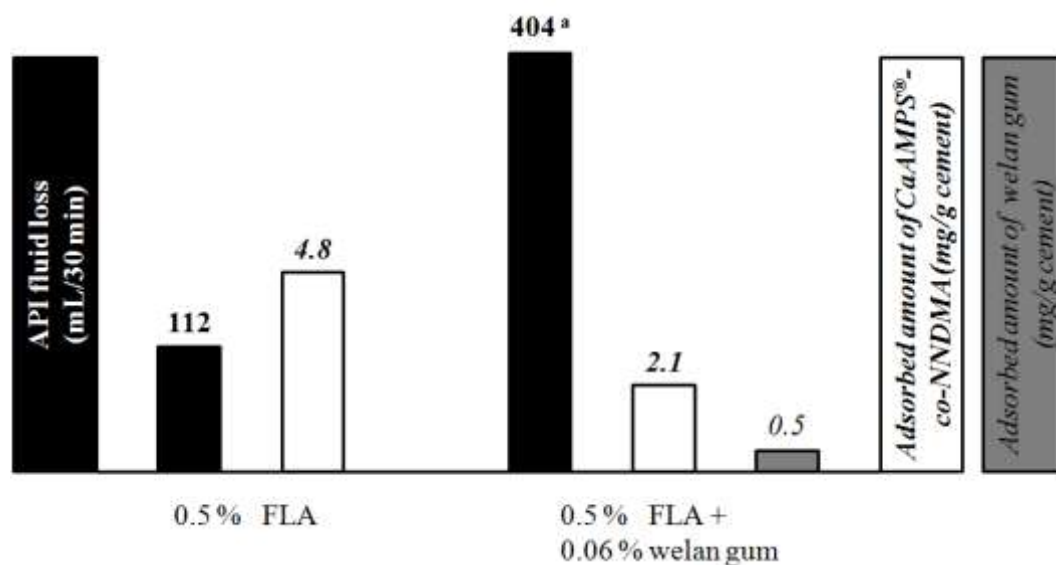


**Figure 40** API fluid loss (black bars) of API Class G oil well cement slurries and adsorbed amount of CaAMPS<sup>®</sup>-*co*-NNDMA (white bars) and welan gum (gray bars), respectively, measured at 80 °C (w/c 0.70).

<sup>a</sup> Dehydration of cement slurry within less than 30 min.

When used as the sole admixture, CaAMPS<sup>®</sup>-*co*-NNDMA adsorbed in high amount (4.8 mg/g cement) and provided good fluid loss control (112 mL/30 min). In the presence of 0.06 % bwoc of welan gum, however, effectiveness of the fluid loss additive decreased substantially, leading to dehydration of the cement slurry within less than 30 min. Indeed, the adsorbed amount of CaAMPS<sup>®</sup>-*co*-NNDMA dropped to 2.1 mg/g cement while welan gum adsorbed in a considerable amount (0.5 mg/g cement; this corresponds to 90 % polymer adsorption). Thus, it becomes clear that welan gum occupies surface sites on cement hydrates which then are no longer available as adsorption sites for the FLA. Consequently, the fluid loss control of cement slurries decreased when both polymers were used in combination (404 mL/30 min).

The carboxylate functionalities of welan gum possess a much more pronounced ability to complex calcium. Therefore, they represent significantly stronger anchor groups for adsorption than the sulfonate groups present in CaAMPS<sup>®</sup>-*co*-NNDMA. This could be confirmed assaying the specific anionic charge amount of CaAMPS<sup>®</sup>-*co*-NNDMA and welan gum, respectively, in alkaline solution with and without 0.6 g/L calcium ions. It was found

that, in the presence of  $\text{Ca}^{2+}$ , the anionic charge of welan gum decreased by 26 % vs. only 4 % for CaAMPS<sup>®</sup>-*co*-NNDMA (see TABLE 14).

TABLE 14

**Specific anionic charge amount of CaAMPS<sup>®</sup>-*co*-NNDMA and welan gum, respectively, measured at pH 12.6 in presence and absence of 0.6 g/L  $\text{Ca}^{2+}$  (polymer concentration: 0.02 g/L)**

Polymer	Specific anionic charge amount (C/g)		Reduction of anionic charge by $\text{Ca}^{2+}$
	Water @ pH 12.6	Water @ pH 12.6 plus 0.6 g/L $\text{Ca}^{2+}$	
CaAMPS <sup>®</sup> - <i>co</i> -NNDMA	368	352	4 %
Welan gum	117	87	26 %

This result shows that calcium ions preferentially chelate the carboxylate functionalities of welan gum compared to the sulfonate groups contained in the FLA polymer. It also confirms that welan gum possesses a much stronger calcium binding capability than the AMPS<sup>®</sup>-based FLA. This property explains the more pronounced interaction of the biopolymer with the surface of cement and hence its high adsorption as well as the reduced ability of the AMPS<sup>®</sup>-based FLA to adsorb on cement in binary additive systems. However, the negative effect of welan gum on FLA performance could be overcome by a much increased dosage of CaAMPS<sup>®</sup>-*co*-NNDMA. While in the absence of welan gum only 0.5 % bwoc of the FLA were required to achieve an API fluid loss of 112 mL/30 min at 80 °C, the FLA dosage necessary to achieve the same fluid loss needs to be increased to 1.1 % bwoc when 0.06 % bwoc welan gum is present. The disadvantage of this increased dosage is higher cost for applicators.

5.4.3.2 Combination of CaAMPS<sup>®</sup>-*co*-NNDMA with diutan gum

First, the effectiveness of diutan gum was monitored at 80 °C through free water and rheological measurements of cement slurries already containing 0.5 % bwoc of CaAMPS<sup>®</sup>-*co*-NNDMA. In absence of the biopolymer, a cement paste prepared at a w/c ratio of 0.70 had practically no yield point, resulting in development of free water (see **TABLE 15**).

**TABLE 15**

**Rheology (shear stress) and free water content of cement slurries containing 0.5 % bwoc of CaAMPS<sup>®</sup>-*co*-NNDMA and increasing dosages of diutan gum, measured at 80 °C (w/c 0.70)**

Diutan gum dosage (wt. %)	Free water content (mL)	Shear stress (Pa) at different shear rates (s <sup>-1</sup> )						Plastic viscosity, $\mu$ (mPa·s)	Yield point, $\tau_0$ (Pa)
		1022	511	340	170	10.2	5.1		
0	3	16	10	7	4	1	0	12	0.2
0.03	0	30	18	14	9	2	2	24	1.7

Here, the addition of only 0.03 % bwoc of diutan gum was sufficient to provide stable cement slurries. To achieve a comparable result with welan gum, the biopolymer dosage had to be doubled. The lower concentration for diutan gum can be explained by the significantly higher molecular weight of this biopolymer (2.9 to 5.2·10<sup>6</sup> g/mol for diutan gum vs. 0.7 to 1.0·10<sup>6</sup> g/mol for welan gum [100]). Additionally, the intrinsic viscosity of these biopolymers, as determined in cement pore solution at 80 °C, indicated a much stiffer conformation for solved diutan gum molecules than for welan gum (0.92 L/g for diutan gum vs. 0.65 L/g for welan gum).

Compatibility of the AMPS<sup>®</sup>-based fluid loss additive with diutan gum was clarified through HTHP filtration tests and adsorption measurements of cement slurries containing 0.5 % bwoc of CaAMPS<sup>®</sup>-*co*-NNDMA and 0.03 % bwoc of diutan gum (see **Figure 41**). When used as the sole admixture, CaAMPS<sup>®</sup>-*co*-NNDMA adsorbed in high amount (4.8 mg/g cement) and provided good fluid loss control (112 mL/30 min). In the presence of 0.03 % bwoc diutan

gum, CaAMPS<sup>®</sup>-*co*-NNDMA molecules were displaced from the cement surface and its adsorbed amount decreased to 3.3 mg/g cement. Consequently, API fluid loss of the cement slurry increased from 112 mL/30 min to 148 mL/30 min in the binary additive system. Nevertheless, these results confirm that compared to welan gum, diutan gum exercises a much minor effect on adsorption and fluid loss performance of CaAMPS<sup>®</sup>-*co*-NNDMA.

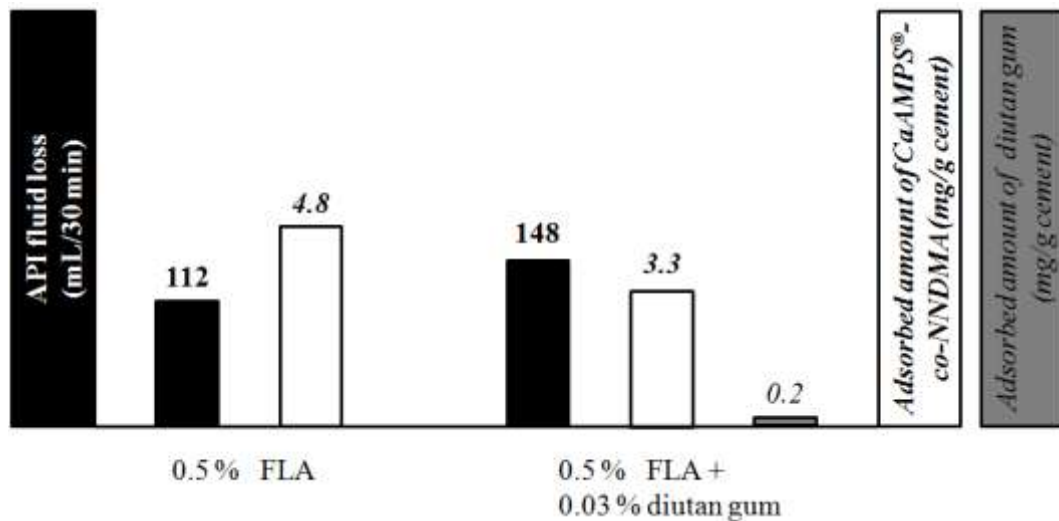


**Figure 41** API fluid loss (black bars) of API Class G oil well cement slurries and adsorbed amounts of CaAMPS<sup>®</sup>-*co*-NNDMA (white bars) and diutan gum (gray bar), respectively, as measured at 80 °C (w/c 0.70).

This result was confirmed by additional tests. For cement slurries prepared with CaAMPS<sup>®</sup>-*co*-NNDMA and 0.03 % bwoc welan gum, competitive adsorption was much stronger than for diutan gum (see **Figure 42**). The FLA adsorbed in lower quantity on cement (2.3 mg adsorbed CaAMPS<sup>®</sup>-*co*-NNDMA/g cement) than in the presence of diutan gum, thus resulting in poor fluid loss control of the slurry (API fluid loss = 419 mL/30min).

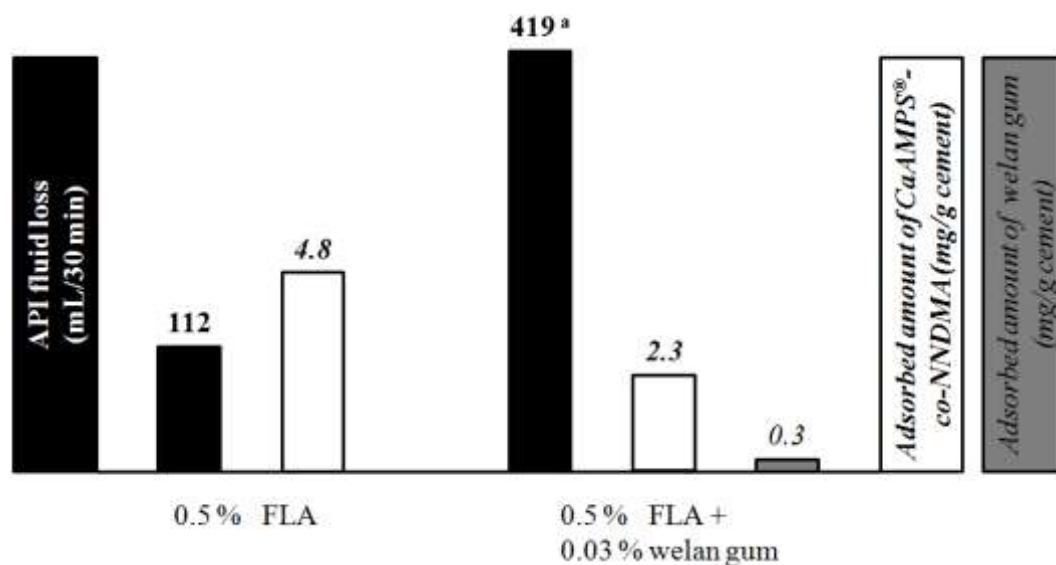


**Figure 42** API fluid loss (black bars) of API Class G oil well cement slurries and adsorbed amounts of CaAMPS<sup>®</sup>-*co*-NNDMA (white bars) and welan gum (gray bar), respectively, as measured at 80 °C (w/c 0.70).

<sup>a</sup> Dehydration of cement slurry within less than 30 min.

#### 5.4.3.3 Calcium binding capability of CaAMPS<sup>®</sup>-*co*-NNDMA and the biogums

To elucidate whether differences in calcium binding capability of diutan gum and the FLA caused the observed effects, the specific anionic charge amount of the AMPS<sup>®</sup>-based fluid loss additive and the biogums was measured at 27 °C in alkaline solution with and without 0.6 g/L calcium ions (see **TABLE 16**). From the results, the calcium binding capability of each polymer was determined. As discussed before, calcium ions can chelate the carboxylate functionalities of the biogums more effectively than the sulfonate groups contained in CaAMPS<sup>®</sup>-*co*-NNDMA. Thus, it was found that in the presence of Ca<sup>2+</sup>, the specific anionic charge amounts of diutan gum and welan gum, respectively, decreased much more pronounced than for the fluid loss additive.

TABLE 16

Specific anionic charge amount of CaAMPS<sup>®</sup>-*co*-NNDMA and the biogums, respectively, measured at pH 12.6 in presence and absence of 0.6 g/L Ca<sup>2+</sup> (polymer concentration: 0.02 g/L)

Polymer	Specific anionic charge amount (C/g)		Reduction of anionic charge by Ca <sup>2+</sup>
	Water @ pH 12.6	Water @ pH 12.6 plus 0.6 g/L Ca <sup>2+</sup>	
CaAMPS <sup>®</sup> - <i>co</i> -NNDMA	368	352	4 %
Diutan gum	148	131	11 %
Welan gum	117	87	26 %

As the anionic charge amount of diutan gum is reduced less through calcium complexation than that of welan gum (11 % for diutan vs. 26 % for welan), it becomes obvious that the latter possesses stronger carboxylate anchor groups. In comparison to welan gum which provides only one randomly distributed L-mannosyl or L-rhamnosyl terminal group, diutan gum possesses longer side chains. Here, the carboxylic acid functions distributed along the molecular backbone are much more effectively shielded. This effect results in weaker carboxylate anchor groups for diutan gum. Thus, in case of a competitive adsorption, occurring between CaAMPS<sup>®</sup>-*co*-NNDMA and this biopolymer, the sulfonate anchor groups of the FLA are strong enough to ensure its adsorption and, consequently, provide fluid loss control of the cement slurry.

#### 5.4.4 Conclusions

In this chapter, it was shown that the carboxylate functionalities of welan gum possess high calcium chelating capability. Therefore, welan gum can successfully reduce adsorption of CaAMPS<sup>®</sup>-*co*-NNDMA, in spite of welan gum possessing a much lower anionic charge amount than the FLA.

In a binary additive system containing CaAMPS<sup>®</sup>-*co*-NNDMA and the free water control agent diutan gum, both admixtures provide good performance in the cement slurry. Here, the strong carboxylate anchor groups of diutan gum are effectively shielded by two L-rhamnose side chains of this biopolymer, thus reducing its calcium binding capability and hence its tendency to adsorb on cement. In case of competitive adsorption between CaAMPS<sup>®</sup>-*co*-NNDMA and diutan gum, the fluid loss polymer which possesses only weak sulfonate anchor groups interacts strong enough with the cement surface to provide good FLA effectiveness. These results clearly confirm that the calcium binding capability of an admixture is a key factor which strongly impacts its adsorption behavior on cement.

### 5.5 Interaction between CaAMPS<sup>®</sup>-*co*-NNDMA and Na<sup>+</sup> lignosulfonate

In oil well cementing, lignosulfonate-based polymers are most commonly used as cement plasticizer and retarder [9]. The present investigation compares the effectiveness of Ca<sup>2+</sup> lignosulfonate (Ca-LS) and Na<sup>+</sup> lignosulfonate (Na-LS) at 80 °C. For this purpose, rheology and compressive strength development of cement slurries containing these polymers were measured. Additionally, in order to characterize the adsorption behavior of Ca-LS and Na-LS, respectively, their capability to chelate calcium ions was determined. With respect to the performance in actual field application, the interaction between CaAMPS<sup>®</sup>-*co*-NNDMA and Na<sup>+</sup> lignosulfonate was investigated. Thus, fluid loss control of cement slurries prepared with CaAMPS<sup>®</sup>-*co*-NNDMA was measured at 80 °C. These data were compared with the results obtained from measurements of cement slurries which contained the binary additive system of CaAMPS<sup>®</sup>-*co*-NNDMA and Na-LS. To understand the mechanism of their interaction, the adsorption behavior of these two polymers on cement was determined in both the single and the binary additive system.

#### 5.5.1 Comparison of Ca-LS and Na-LS as cement plasticizer and retarder

First, the calcium binding capability of Ca<sup>2+</sup> lignosulfonate and Na<sup>+</sup> lignosulfonate was determined through measurements of their specific anionic charge amount in absence and presence of calcium ions (see TABLE 17).

TABLE 17

Specific anionic charge amount of lignosulfonate-based polymers, measured in absence and presence of 0.6 g/L Ca<sup>2+</sup> (polymer concentration: 0.2 g/L)

Polymer	Specific anionic charge amount (C/g)		Reduction of the specific anionic charge amount by Ca <sup>2+</sup>
	Water @ pH 12.6	Water @ pH 12.6 plus 0.6 g/L Ca <sup>2+</sup>	
Ca <sup>2+</sup> lignosulfonate	197	126	36 %
Na <sup>+</sup> lignosulfonate	389	102	74 %

A calcium concentration of 0.6 g/L reduced the specific anionic charge amount of these polymers by 36 % for  $\text{Ca}^{2+}$  lignosulfonate and by 74 % for  $\text{Na}^+$  lignosulfonate. Thus,  $\text{Ca}^{2+}$  lignosulfonate showed a considerably lower capability to chelate calcium ions. This should highly decrease its tendency to adsorb on cement, compared to  $\text{Na}^+$  lignosulfonate. To verify this statement, the rheology of a cement slurry containing Ca-LS as well as the adsorbed amount of this polymer on cement was measured and compared with the results obtained for Na-LS (see **TABLE 18**).

**TABLE 18**

**Rheology (shear stress) of cement slurries containing different dosages of  $\text{Ca}^{2+}$  lignosulfonate and  $\text{Na}^+$  lignosulfonate, respectively, as well as adsorbed amounts of each additive, measured at 80°C (w/c 0.44)**

Dosage (% bwoc)	Polymer	Shear stress (Pa) at different shear rates ( $\text{s}^{-1}$ )						Adsorbed amount (mg/g cement)
		1022	511	340	170	10.2	5.1	
0.0	Neat cement	93	82	75	64	20	17	0
0.2	Ca-LS	69	60	55	49	16	12	1.5
0.2	Na-LS	47	38	34	30	11	9	1.8
0.4	Ca-LS	65	59	54	49	20	17	2.9
0.4	Na-LS	21	9	6	4	2	2	3.6

The rheology of neat cement slurry decreased only slightly when Ca-LS was added to the system and remained constant, even at a dosage as high as 0.4 % bwoc of  $\text{Ca}^{2+}$  lignosulfonate. Resulting from its reduced tendency to chelate calcium ions,  $\text{Ca}^{2+}$  lignosulfonate adsorbed in smaller amounts on the cement surface, compared to Na-LS (e.g., 2.9 mg/g cement for 0.4 % bwoc Ca-LS vs. 3.6 mg/g cement for 0.4 % bwoc Na-LS). Consequently, the resulting electrostatic repulsion between the cement grains was diminished. Thus, it becomes clear that  $\text{Ca}^{2+}$  lignosulfonate loses its effectiveness as cement plasticizer at elevated temperature. In contrast,  $\text{Na}^+$  lignosulfonate strongly increased the fluidity of the respective cement slurry.

This polymer possesses a high tendency to chelate calcium atoms which are immobilized on the cement surface, thus producing a high amount of adsorbed Na-LS. To obtain a comparable rheology for cement slurries containing  $\text{Ca}^{2+}$  lignosulfonate instead of 0.2 % bwoc Na-LS, a polymer dosage as high as 0.6 % bwoc Ca-LS was necessary.

Next, the retarding effect of  $\text{Ca}^{2+}$  lignosulfonate and  $\text{Na}^+$  lignosulfonate, respectively, was compared through ultra sonic measurements of the compressive strength development of cement slurries at 80 °C (see **TABLE 19**).

**TABLE 19**

**Compressive strength development of cement slurries containing  $\text{Ca}^{2+}$  lignosulfonate and  $\text{Na}^+$  lignosulfonate, respectively, measured at 80 °C and 200 bar (w/c 0.44)**

Dosage (% bwoc)	Cement retarder	Time to reach a compressive strength of 3.4 N/mm <sup>2</sup> (hh:mm)
0.2	Ca-LS	08:30
0.2	Na-LS	07:50
0.4	Ca-LS	23:00
0.4	Na-LS	21:30

Under those conditions, the neat cement slurry needed approximately 3 hours to reach a compressive strength of 3.4 N/mm<sup>2</sup> (500 psi). As shown in **TABLE 19**, both lignosulfonate-based retarders were very effective and similarly retarded the hydration of cement (e.g., to ~ 23 hours for 0.4 % bwoc Ca-LS vs. ~ 22 hours for 0.4 % bwoc Na-LS). Nevertheless,  $\text{Ca}^{2+}$  lignosulfonate was shown to be less effective as plasticizer at 80 °C, making the use of additional expensive dispersants necessary to adjust cement rheology. Since that would lead to reduced cost-effectiveness of the formulation, the following investigations were conducted only with  $\text{Na}^+$  lignosulfonate as cement plasticizer and retarder.

### 5.5.2 Interaction of Na<sup>+</sup> lignosulfonate with calcium ions

Upon contact of cement with water, a high concentration of calcium ions is immediately released into the pore solution by dissolving cement clinker phases [13]. As the calcium binding capability of Na-LS is very high (see **chapter 5.5.1**), the question arises whether this polymer may precipitate in a cement slurry. To clarify the calcium-stability of Na<sup>+</sup> lignosulfonate, the concentration of the solvated polymer as a function of the Ca<sup>2+</sup> content was measured at high pH value (see **Figure 43**). The initial Na-LS concentration was 4.6 g/L in a Ca<sup>2+</sup> free solution (corresponding to a polymer dosage of 0.2 % bwoc).

For calcium concentrations of more than 0.4 g/L, the Na-LS concentration decreased dramatically and reached a plateau of approximately 1.5 g/L Na-LS at 0.7 g/L Ca<sup>2+</sup>. This result clearly indicates that Na<sup>+</sup> lignosulfonate precipitates at calcium concentrations generally found in cement pore solutions (here 0.6 g/L Ca<sup>2+</sup>, as measured by AAS analysis).

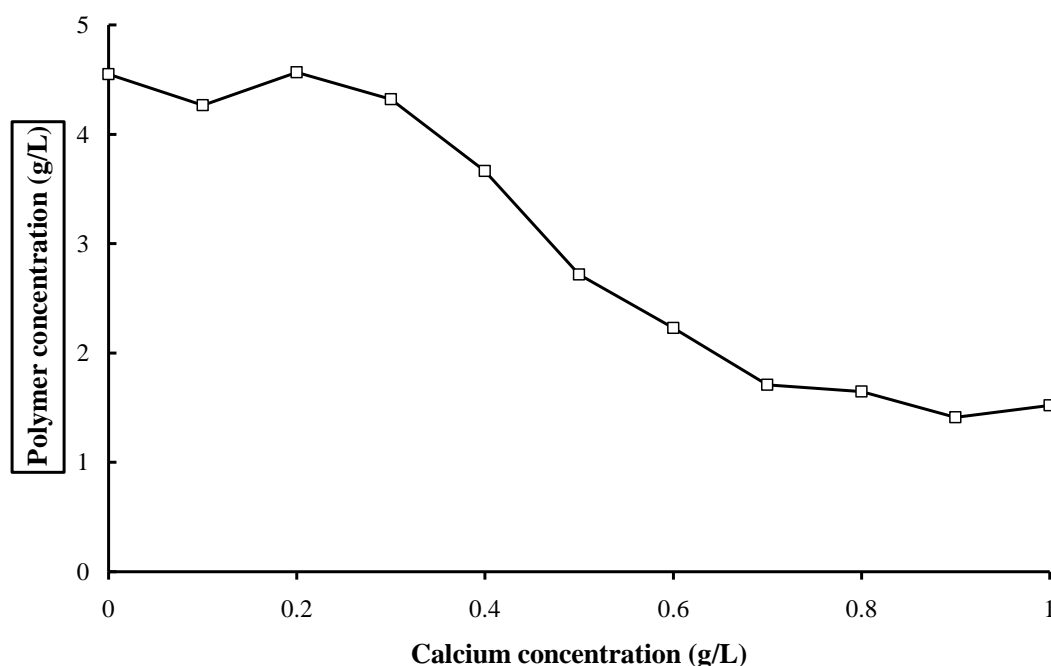


**Figure 43** Concentration of solvated Na<sup>+</sup> lignosulfonate as a function of calcium concentration, measured at 27 °C (pH = 9.0, as adjusted with NaOH; Ca<sup>2+</sup> added as a 0.1 M CaCl<sub>2</sub>·2 H<sub>2</sub>O solution).

To further determine the calcium-stability of Na<sup>+</sup> lignosulfonate, the particle size ( $d_{50}$  value) and the specific anionic charge amount of the polymer as a function of the calcium concentration present in the solvent were measured at 27 °C (see **Figure 44**). It was found that Na-LS formed agglomerates which grew with increasing Ca<sup>2+</sup> concentration until reaching a maximum size of ~ 2.4 μm at 0.5 g/L calcium. In contrast, the specific anionic charge amount of Na<sup>+</sup> lignosulfonate decreased continuously with increasing calcium concentration from - 389 C/g without calcium to - 77 C/g at 1.0 g/L Ca<sup>2+</sup>. This allows the conclusion that in the presence of calcium ions, Na-LS forms negatively charged agglomerates which then precipitate (see **Figure 45**).

The influence of these agglomerates on the effectiveness of Na<sup>+</sup> lignosulfonate as retarder in cement slurries is investigated in the following chapter.

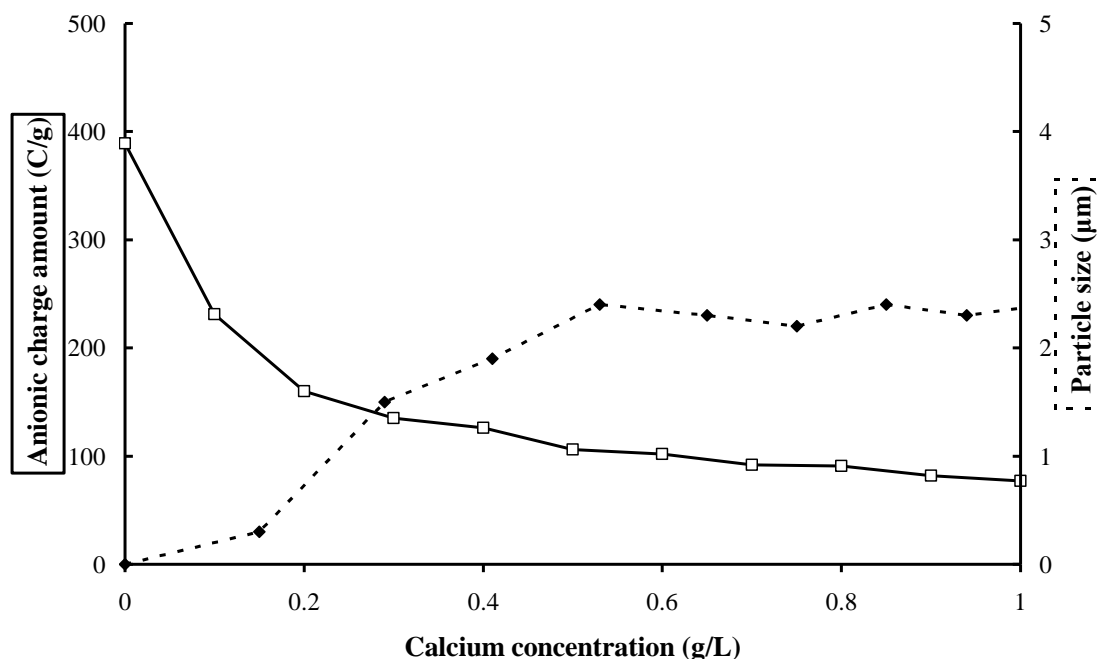


**Figure 44** Specific anionic charge amount and particle size of Na<sup>+</sup> lignosulfonate as a function of the calcium concentration present in the solvent, measured at 27 °C (pH = 9.0, adjusted with NaOH; Ca<sup>2+</sup> added as a 0.1 M CaCl<sub>2</sub>·2 H<sub>2</sub>O solution).

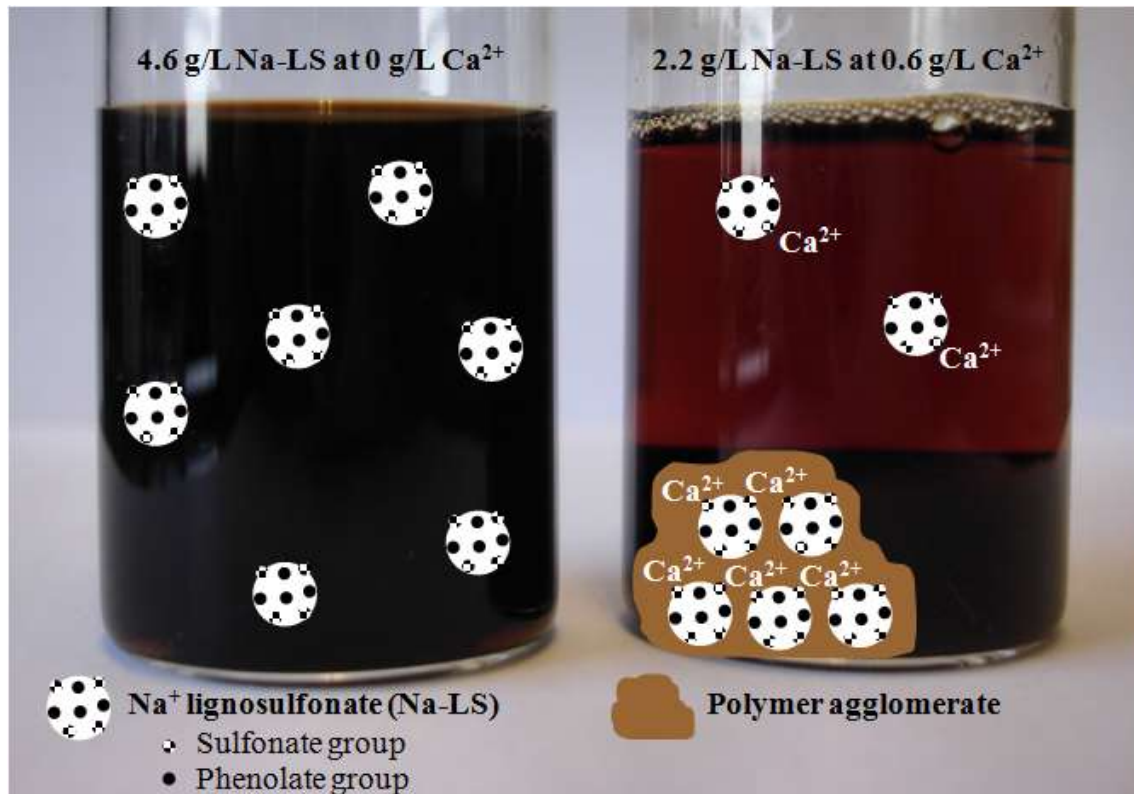


**Figure 45** Illustration of the formation of less soluble negatively charged agglomerates by interaction of  $\text{Na}^+$  lignosulfonate (Na-LS) with  $\text{Ca}^{2+}$  ions.

### 5.5.3 Interaction of $\text{Na}^+$ lignosulfonate with cement

To quantify the retarding effect of  $\text{Na}^+$  lignosulfonate on cement hydration, the compressive strength development of cement slurries containing different dosages of this polymer was determined at 80 °C. Additionally, the amount of Na-LS adsorbed on the cement surface was measured at the same temperature (see **TABLE 20**). With increased dosages of Na-LS, the cement took longer to reach a compressive strength of 3.4 N/mm<sup>2</sup> (from ~ 3 hours without retarder to ~ 35 hours at a dosage of 0.5 % bwoc of Na-LS). The adsorbed amount of  $\text{Na}^+$  lignosulfonate on cement measured as a function of the polymer dosage provided a similar trend. This result suggests an adsorptive working mechanism for  $\text{Na}^+$  lignosulfonate.

TABLE 20

**Compressive strength development of cement slurries containing increasing dosages of Na<sup>+</sup> lignosulfonate and adsorbed amount of this polymer, measured at 80 °C (w/c 0.44)**

Dosage of Na-LS (w% bwoc)	Time to reach a compressive strength of 3.4 N/mm <sup>2</sup> at 200 bar (hh:mm)	Adsorbed amount of Na-LS (mg/g cement)
0.0	02:40	0
0.1	04:20	0.9
0.2	07:50	1.8
0.3	12:40	2.7
0.4	21:30	3.6
0.5	34:50	4.5

Zeta potential and rheological measurements of cement slurries conducted at increasing dosages of Na-LS confirm this concept (see **TABLE 21**). A continuous adsorption of an anionic polymer onto the positive sites of cement grains leads to increasingly negative zeta potential numbers and the resulting electrostatic repulsion of correspondently charged particles provides highly dispersed cement slurries. This behavior is observed here. Obviously, the Na-LS agglomerates are still sufficiently negatively charged to adsorb on cement and disperse it.

TABLE 21

**Zeta potential and rheology (shear stress) of cement slurries containing different dosages of Na<sup>+</sup> lignosulfonate, measured at 27 °C and 80 °C, respectively (w/c 0.44)**

Dosage of Na-LS (% bwoc)	Zeta potential at 27 °C (mV)	Shear stress (Pa) at different shear rates (s <sup>-1</sup> ) and 80 °C					
		1022	511	340	170	10.2	5.1
0.0	- 5	93	82	75	64	20	17
0.1	- 12	63	48	44	39	13	11
0.2	- 15	47	38	34	30	11	9
0.3	- 16	28	17	14	11	6	4
0.4	- 17	21	9	6	4	2	2
0.5	- 17	20	7	5	4	1	1

This hypothesis is supported by an ESEM micrograph of a cement slurry containing 0.2 % bwoc of Na-LS which showed a dense layer covering the cement surface (see **Figure 46**). A high carbon content of 19 %, as measured by energy dispersive X-ray spectroscopy, clearly proved the polymeric nature of this coating. Thus, Na<sup>+</sup> lignosulfonate forms agglomerates which adsorb onto positively charged cement sites and retard cement hydration through physical blocking of early cement hydrates. All reactions concerning the setting of the cement slurry continue as usual after this semi-permeable layer has burst.

The next chapter investigates the interaction of CaAMPS<sup>®</sup>-co-NNDMA fluid loss additive with this lignosulfonate-based retarder regarding their adsorption behavior in the presence of both admixtures.

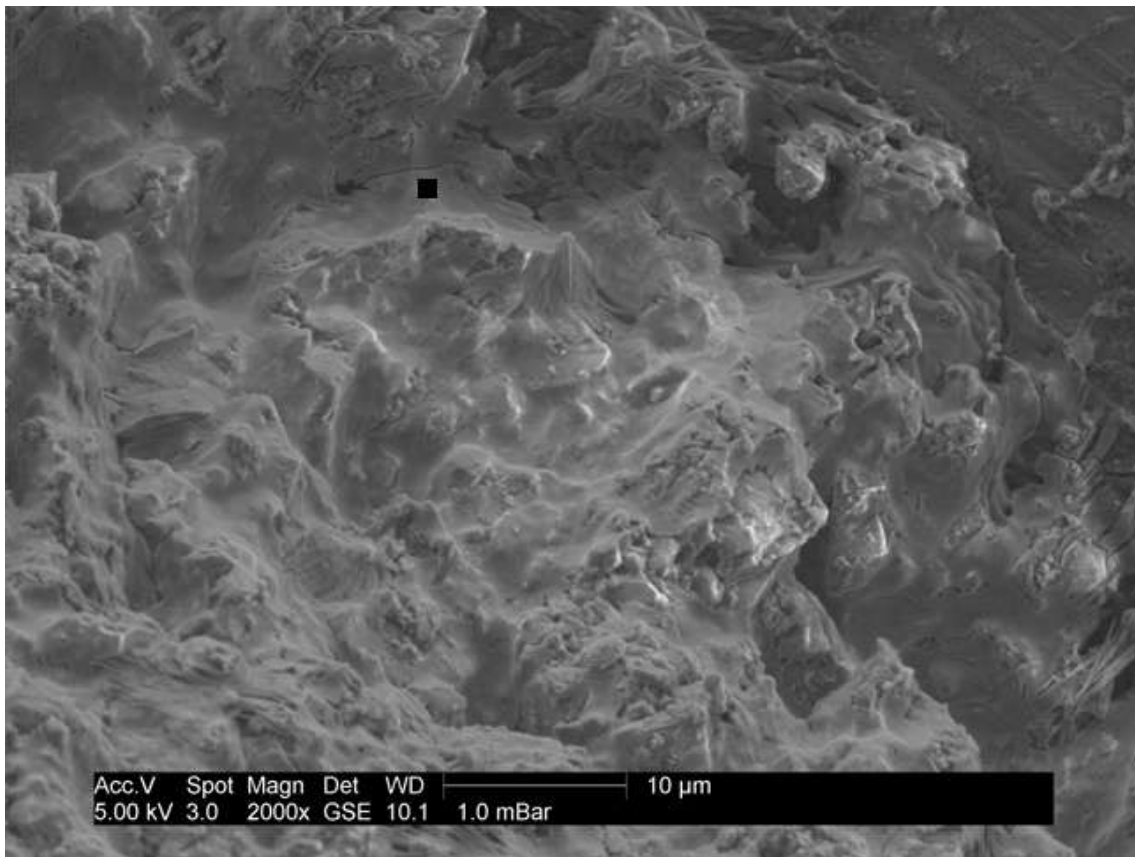


**Figure 46** ESEM micrograph of a Class G oil well cement slurry containing 0.2 % bwoc  $\text{Na}^+$  lignosulfonate, analyzed directly after mixing at room temperature (w/c 0.44). Area for EDX measurement ( $1\mu\text{m} \times 1\mu\text{m}$ ) indicated by black square.

#### 5.5.4 Adsorption behavior and effectiveness of CaAMPS<sup>®</sup>-co-NNDMA

The anionic agglomerates formed by Na<sup>+</sup> lignosulfonate were only slightly charged (- 210 C/g, as measured in cement pore solution) and very voluminous (~ 2 μm; see **chapter 5.5.2**). Thus, it can be concluded that their anionic charge density is very low. In contrast, the fluid loss polymer CaAMPS<sup>®</sup>-co-NNDMA provided a much higher anionic charge amount (- 367 C/g, as measured in cement pore solution) and smaller size ( $Rg_z = 64$  nm; see **TABLE 4**). Thus, when both polymers are present in cement slurries, the much higher anionic charge density of CaAMPS<sup>®</sup>-co-NNDMA should result in preferred adsorption of the FLA on cement.

To verify this statement, zeta potential measurements of cement slurries were conducted at 27 °C. Here, the additive system containing individual 0.5 % bwoc of CaAMPS<sup>®</sup>-co-NNDMA and the binary admixture system containing 0.5 % bwoc FLA and 0.2 % bwoc Na-LS were compared. At a w/c ratio of 0.44, the neat cement slurry showed a zeta potential of - 6 mV. Adsorption of anionic CaAMPS<sup>®</sup>-co-NNDMA onto the cement surface caused the zeta potential to decrease to a value of - 20 mV. Cement slurries containing the fluid loss additive and the lignosulfonate provided the same zeta potential. Thus, it becomes clear that the adsorption of CaAMPS<sup>®</sup>-co-NNDMA on cement is not perturbed by Na<sup>+</sup> lignosulfonate.

For further evidence, the effectiveness of the fluid loss polymer was tested in the binary admixture system. First, however, the fluid loss control of cement slurries prepared only with 0.2 % bwoc Na<sup>+</sup> lignosulfonate was determined at 80 °C. Here, the calculated API fluid loss was 1500 mL/30 min. The voluminous agglomerates formed by Na-LS apparently do not provide any fluid loss control to cement slurries. Next, the relationship between HTHP fluid loss and the amount of CaAMPS<sup>®</sup>-co-NNDMA adsorbed on cement was measured in the absence and presence of 0.2 % bwoc Na<sup>+</sup> lignosulfonate at 80 °C (see **Figure 47**).

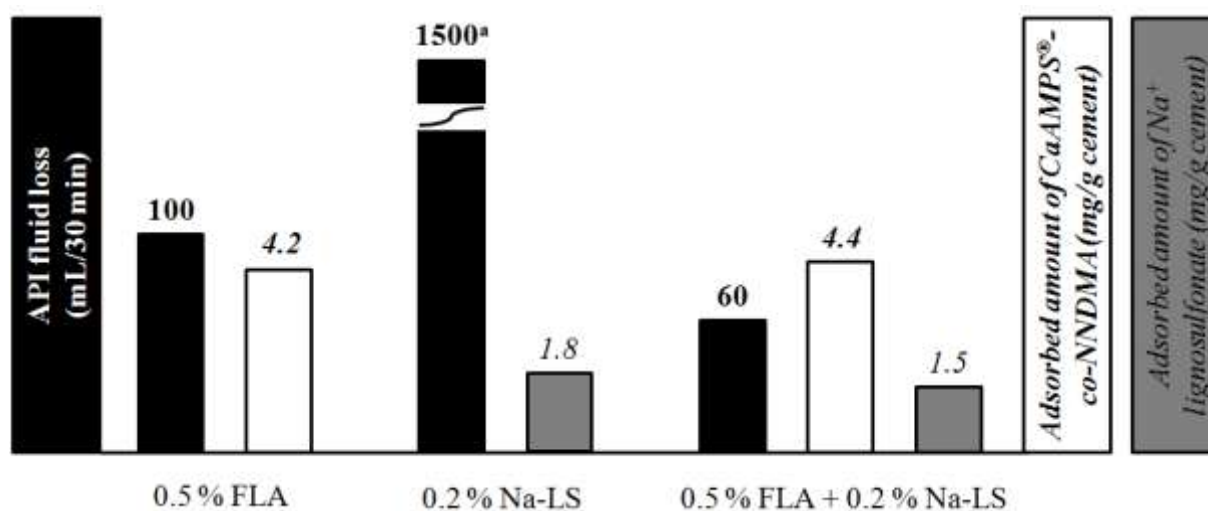


**Figure 47** API fluid loss (black bars) of API Class G oil well cement slurries, adsorbed amount of CaAMPS<sup>®</sup>-*co*-NNDMA (white bars) and adsorbed amount of Na<sup>+</sup> lignosulfonate (gray bar), respectively, measured at 80 °C (w/c 0.44).

<sup>a</sup> Dehydration of cement slurry within less than 30 min.

When 0.5 % bwoc of CaAMPS<sup>®</sup>-*co*-NNDMA were added as the sole admixture to the cement slurry, the adsorbed amount of 4.2 mg FLA/g cement caused an API fluid loss of 100 mL/30 min. In a cement slurry containing this FLA and 0.2 % bwoc of the lignosulfonate, the adsorbed amount of CaAMPS<sup>®</sup>-*co*-NNDMA was only slightly influenced by the presence of Na-LS (4.4 mg/g cement). In contrast, when both polymers were added to the cement slurry, the resulting fluid loss enhanced considerably to 60 mL/30 min. The voluminous agglomerates formed by Na<sup>+</sup> lignosulfonate can physically plug the pores of the filtercake. In the presence of CaAMPS<sup>®</sup>-*co*-NNDMA, this effect leads to a further decrease in filtercake permeability and hence to improved FLA performance.

The next chapter investigates whether this synergistic interaction between CaAMPS<sup>®</sup>-*co*-NNDMA and Na-LS also shows in the efficiency of the retarder.

### 5.5.5 Adsorption behavior and effectiveness of Na<sup>+</sup> lignosulfonate

As shown in **chapter 5.5.3**, Na<sup>+</sup> lignosulfonate retarder has to adsorb onto the cement surface to be effective. The presence of CaAMPS<sup>®</sup>-*co*-NNDMA molecules (see **chapter 5.5.4**) may lead to competitive interaction between both polymers for limited adsorption sites and to displacement of the retarder from the cement surface. To verify this theory, rheology measurements of cement slurries prepared with 0.5 % bwoc of CaAMPS<sup>®</sup>-*co*-NNDMA were conducted at 80 °C in absence and presence of 0.2 % bwoc Na<sup>+</sup> lignosulfonate. Additionally, the adsorbed amount of Na-LS on cement was determined for this binary additive system and compared with the results obtained for a cement slurry containing only Na-LS (see **TABLE 22**).

**TABLE 22**

**Rheology (shear stress) of cement slurries containing 0.5 % bwoc of CaAMPS<sup>®</sup>-*co*-NNDMA in absence and presence of Na<sup>+</sup> lignosulfonate and adsorbed amount of Na-LS on cement, measured at 80 °C (w/c 0.44)**

Dosage of Na-LS (% bwoc)	Adsorbed amount of Na-LS (mg/g cement)	Shear stress (Pa) at different shear rates (s <sup>-1</sup> )					
		1022	511	340	170	10.2	5.1
0.0	0.0	122	91	71	45	16	16
0.2	1.5	92	63	46	28	4	2

The cement slurry prepared with CaAMPS<sup>®</sup>-*co*-NNDMA as the sole additive possessed a relatively high viscosity. Through addition of Na-LS, however, the cement slurry became more dispersed. This effect results from the adsorption of the agglomerates formed by Na<sup>+</sup> lignosulfonate and Ca<sup>2+</sup> ions onto the mineral surface, causing electrostatic repulsion of correspondingly charged cement particles. Here, the adsorbed amount of Na-LS decreased only slightly, from 1.8 mg/g cement in the absence of CaAMPS<sup>®</sup>-*co*-NNDMA (see **TABLE 20**) to 1.5 mg/g cement in the presence of this FLA. Thus, competitive adsorption between CaAMPS<sup>®</sup>-*co*-NNDMA and Na-LS is evidently negligible.

However, the question arises whether these voluminous agglomerates also precipitate onto already adsorbed CaAMPS<sup>®</sup>-*co*-NNDMA. This could influence the stability of the semi-permeable layer formed by the lignosulfonate-based retarder and hence its effectiveness. To answer this question, the thickening times of cement slurries containing different Na-LS dosages were measured in absence and presence of CaAMPS<sup>®</sup>-*co*-NNDMA at 80 °C (see **TABLE 23**). Under the conditions tested here, the neat cement slurry remained pumpable only for a short period of time. With increasing dosages of Na<sup>+</sup> lignosulfonate, however, the thickening time increased from ~ 1 hour without retarder to ~ 6 hours at a dosage of 0.3 % bwoc of Na<sup>+</sup> lignosulfonate.

**TABLE 23**

**Thickening time of API Class G cement slurries containing increased dosages of Na<sup>+</sup> lignosulfonate in absence and presence of CaAMPS<sup>®</sup>-*co*-NNDMA, measured at 400 bar and 80 °C (w/c 0.44)**

Dosage of Na-LS (% bwoc)	Dosage of FLA (% bwoc)	Thickening time (hh:mm)
0.0	0.0	01:00
0.0	0.5	01:10
0.1	0.0	02:00
0.1	0.5	02:00
0.2	0.0	03:30
0.2	0.5	04:30
0.3	0.0	05:40
0.3	0.5	11:50

As the addition of 0.5 % bwoc of FLA only marginally influenced the thickening time of the neat cement slurry, it becomes obvious that CaAMPS<sup>®</sup>-*co*-NNDMA has only a slightly retarding effect. In contrast, the presence of this fluid loss additive strongly enhanced the retarding effect of Na<sup>+</sup> lignosulfonate (~ 3.5 hours of pumpability for a cement slurry containing 0.2 % bwoc of Na<sup>+</sup> lignosulfonate vs. ~ 4.5 hours for a combination of 0.2 % bwoc

of Na-LS and 0.5 % bwoc of FLA). CaAMPS<sup>®</sup>-*co*-NNDMA molecules which have already adsorbed onto the cement surface stabilize the semi-permeable layer formed by the lignosulfonate-based polymer enhancing the effectiveness of this cement retarder. Thus, in the binary admixture system of CaAMPS<sup>®</sup>-*co*-NNDMA and Na<sup>+</sup> lignosulfonate, a synergistic effect regarding the efficiency of both polymers is observed.

### 5.5.6 Conclusions

At calcium concentrations commonly found in cement pore solutions, the cement retarder Na<sup>+</sup> lignosulfonate and Ca<sup>2+</sup> ions form negatively charged agglomerates which adsorb onto the cement surface and build a semi-permeable layer. Through this mechanism, Na<sup>+</sup> lignosulfonate retards cement hydration by slowing the migration of water into the unhydrated cement particle.

In cement slurries containing Na<sup>+</sup> lignosulfonate and CaAMPS<sup>®</sup>-*co*-NNDMA fluid loss additive, a synergistic effect is observed regarding the effectiveness of both polymers. Through combined adsorption of agglomerates formed by Na<sup>+</sup> lignosulfonate and the FLA, the pores of the filtercake are more effectively plugged, in comparison to cement systems containing CaAMPS<sup>®</sup>-*co*-NNDMA as the sole admixture. In a binary additive system composed of CaAMPS<sup>®</sup>-*co*-NNDMA and Na-LS, this effect results into an even lower permeability of the filtercake and hence improved FLA effectiveness.

Na-LS agglomerates also interact with adsorbed FLA molecules which stabilize the polymer layer present on the surface of cement. The result is improved performance of Na<sup>+</sup> lignosulfonate as cement retarder.

This study demonstrates that besides polymer incompatibility which is often shown in literature [94] [101], synergistic interactions between additives also may occur.

## 6 SUMMARY AND OUTLOOK

### 6.1 Summary

The major objective of primary cementing is to provide zonal isolation in oil, gas, and water wells, i.e., to separate water or gas in one zone from oil in other zones. To meet this demand, Portland cement systems for well cementing have to perform under harsh borehole conditions. High pressure, temperature and salinity make it necessary to use various cement admixtures.

Fluid loss additives such as poly(*N,N*-dimethyl acrylamide-*co*-Ca 2-acrylamido-2-methylpropane sulfonate) (CaAMPS<sup>®</sup>-*co*-NNDMA) are often employed to prevent uncontrolled water loss from the cement slurry when it is pumped across porous formations. Reduced fluid loss from the cement slurry ensures a complete cementation of the borehole and, consequently, proper zonal isolation. The synthetic fluid loss polymer CaAMPS<sup>®</sup>-*co*-NNDMA adsorbs onto the cement surface to reduce the permeability of the filtercake and hence achieve fluid loss control of the cement slurry.

Occasionally, salt formations are cemented in oil and gas wells. Here, the use of cement slurries prepared with fresh water would lead to well bore washout resulting from osmotic dissolution of salt into the slurry and hence to the loss of well integrity. Thus, salt cement slurries containing high concentrations of sodium chloride are routinely applied to prevent this detrimental effect. Other important additives are free water control agents such as welan gum and diutan gum. These microbial biopolymers stabilize cementing systems and ensure zonal isolation, even at low slurry densities. Additionally, to ensure an extended pumping time of 4 to 6 hours, cement retarders such as sodium lignosulfonate are added to cement.

This work concentrated on elucidating the various physico-chemical interactions which influence the adsorption behavior CaAMPS<sup>®</sup>-*co*-NNDMA on cement. The first objective of this study was to clarify the temperature tolerance of CaAMPS<sup>®</sup>-*co*-NNDMA. For this purpose, the impact of high temperature (100 °C) on the adsorption behavior and hence the effectiveness of CaAMPS<sup>®</sup>-*co*-NNDMA under carefully controlled experimental conditions was tested.

In addition to high temperature, polymer incompatibility constitutes a major problem in the use of CaAMPS<sup>®</sup>-*co*-NNDMA as fluid loss additive. In multi-admixture systems which are commonly used in oil field applications, the efficiency of CaAMPS<sup>®</sup>-*co*-NNDMA is often diminished. Therefore, the second objective of this work was to determine the effectiveness of CaAMPS<sup>®</sup>-*co*-NNDMA at 80 °C in the presence of a selection of important cement additives. **TABLE 24** summarizes the results of these investigations and suggests ways to improve the performance of CaAMPS<sup>®</sup>-*co*-NNDMA.

TABLE 24

**Summary of the results concluded from this work regarding the effectiveness of AMPS<sup>®</sup>-based fluid loss additives (FLAs) in various cementing systems**

	<b>Impact on FLA performance</b>	<b>Options for improved FLA effectiveness</b>
<b>High temperature</b>	Reduced FLA adsorption due to increased kinetic energy of the dissolved polymer results in poor FLA performance.	Incorporation of stronger anchor groups into the polymer, e.g., carboxylate functionalities.
<b>Salt cement slurry</b>	Cl <sup>-</sup> anions displace adsorbed FLA molecules from cement surface, thus resulting in poor FLA effectiveness.	Incorporation of stronger anchor groups into the polymer, e.g., carboxylate functionalities.
<b>Presence of free water control agents</b>	Competitive adsorption between anionic welan gum leads to diminished FLA adsorption and hence to poor fluid loss control of the cement slurry.	Use of diutan gum which possesses weaker anchor groups because of a shielding effect by its longer side chain groups.
<b>Presence of sodium lignosulfonate</b>	Agglomerates formed by lignosulfonate and Ca <sup>2+</sup> ions interact with the AMPS <sup>®</sup> copolymer and plug the pores of the cement filtercake more effectively, resulting in enhanced fluid loss.	Synergistic effect occurring in this binary additive system, no correction required.

First, the study demonstrates that high temperature negatively impacts the performance of CaAMPS<sup>®</sup>-*co*-NNDMA. Comparison of FLA adsorption on cement at 27 °C, 80 °C and 100 °C, respectively, clarified that the diminished performance of the polymer at higher temperature is mainly caused by the behavior of its sulfonate anchor groups. These functional groups poorly coordinate with calcium atoms which are immobilized on the mineral surface, resulting in reduced adsorption. Additionally, ettringite, a cement hydrate mineral, decomposes at temperatures above 80 °C, thus increasing the sulfate content of the cement slurry. This effect was shown to induce shrinkage and coiling of the FLA, which in turn is also responsible for its reduced adsorption. On the other hand, further experiments revealed that competitive interaction between sulfate ions and the fluid loss additive has no impact on its adsorption behavior.

A slightly modified fluid loss polymer, CaAMPS<sup>®</sup>-*co*-NNDMA-*co*-MA, possesses few homopolymer blocks holding vicinal carboxylate functionalities. These groups provide a significantly higher calcium binding capability than the sulfonate functions of CaAMPS<sup>®</sup>-*co*-NNDMA. Therefore, the carboxylate functionalities cause stronger immobilization of the modified FLA onto the mineral surface. This results in high and stable adsorption of maleic acid-modified CaAMPS<sup>®</sup>-*co*-NNDMA-*co*-MA, which was independent of temperature and sulfate concentration. Consequently, its fluid loss performance was little affected by those two parameters. These results demonstrate that a relatively minor modification in polymer composition and structure can cause surprisingly strong alterations of its properties.

In salt cement slurries, the effectiveness of CaAMPS<sup>®</sup>-*co*-NNDMA was shown to be diminished. Here, chloride anions which possess a much higher anionic charge density than CaAMPS<sup>®</sup>-*co*-NNDMA adsorb on the cement surface. Additionally, these anions are present in high concentration (100 g/L) and therefore occupy the mineral surface to a major extent. Both effects hinder adsorption of the fluid loss polymer.

Further experiments demonstrated that the microbial biopolymer and water control agent welan gum also reduced adsorption of CaAMPS<sup>®</sup>-*co*-NNDMA, because its carboxylate functionalities possess high calcium chelating capability. This resulted in poor fluid loss control of the cement slurry in this binary additive system. In comparison, diutan gum showed reduced calcium binding capability. This result could be attributed to the elongated side chain groups of this biogum. They are capable of shielding the carboxylate functionalities incorporated along the polymer backbone more effectively than the side chain groups of

welan gum. Thus, in the presence of diutan gum, the amount of CaAMPS<sup>®</sup>-*co*-NNDMA adsorbed on cement is sufficiently high to ensure its effectiveness as fluid loss additive.

This part of the study clearly shows that adsorption and hence effectiveness of CaAMPS<sup>®</sup>-*co*-NNDMA may be perturbed by other anionic admixtures which are also present in cementing systems, if they possess a stronger affinity to the cement surface than the AMPS<sup>®</sup>-based copolymer. Through this competitive mechanism, adsorption of CaAMPS<sup>®</sup>-*co*-NNDMA may be reduced and hence its performance as fluid loss additive. Here, the interaction between competing additives depends on their anionic charge density, the quality of their anchor groups relative to the binder surface (calcium chelating ability), the steric position of the anchor group and its amount present in the polymer. Competitive adsorption between additives and resulting admixture incompatibilities can be addressed by fine-tuning the molecular structures of the polymers with respect to their anionic charge density, the quality and steric position of their anchor group. This way, multi-admixture systems with superior performance can be developed.

Beside competitive adsorption resulting into polymer incompatibility, experiments revealed that in binary additive systems synergistic effects may also take place. In this study, the presence of the cement retarder sodium lignosulfonate improved the performance of CaAMPS<sup>®</sup>-*co*-NNDMA as fluid loss agent. It was found that the lignosulfonate forms negatively charged agglomerates with calcium ions present in the cement pore solution. These agglomerates adsorb onto the cement surface and build a semi-permeable layer. Through this mechanism, sodium lignosulfonate retards cement hydration by hindering the migration of water to the non-hydrated cement surface.

Through simultaneous adsorption of the agglomerates formed by lignosulfonate and the fluid loss additive, the pores of the cement filtercake are plugged more effectively, compared to systems containing CaAMPS<sup>®</sup>-*co*-NNDMA as the sole admixture. In the binary additive system containing CaAMPS<sup>®</sup>-*co*-NNDMA and sodium lignosulfonate, this effect resulted into an even lower permeability of the filtercake and hence improved effectiveness of the fluid loss polymer.

This study demonstrates the importance of knowledge on the various physico-chemical interactions which influence the adsorption behavior and performance of cement additives. The results for CaAMPS<sup>®</sup>-*co*-NNDMA fluid loss additive are highly valuable for developing more effective admixture systems for oil well cementing.

## 6.2 Outlook

In this study, the temperature tolerance of CaAMPS<sup>®</sup>-*co*-NNDMA fluid loss polymer was tested at 100 °C. Further increase in temperature (up to 200 °C) would imply the addition of silica to the cementing system in order to prevent strength retrogression. In this binary matrix, the question arises on which mineral surface the fluid loss polymer will adsorb preferably. To study the resulting impact on the performance of this fluid loss polymer at such high temperatures may lead to important new insights and the development of improved polymers.

Furthermore, these test conditions make the use of powerful cement retarders necessary. Lignosulfonate-based cement retarders are added to cement slurries for primary cementing of wells with bottom hole temperatures up to 150 °C. Beyond this temperature, these additives become less effective. To overcome this detrimental effect, synthetic AMPS<sup>®</sup>-based polymers are commonly used as cement retarders. In spite of such severe temperature conditions, these expensive copolymers perform up to 250 °C, making deep wells possible at all. To study the mutual interaction of AMPS<sup>®</sup>-based fluid loss polymers with AMPS<sup>®</sup>-based retarders would be an interesting challenge for further investigations.

Additionally, understanding the reasons behind the reduced temperature-tolerance of lignosulfonate-based polymers could help to develop additives which are better adjusted to high temperature conditions. As lignosulfonate is a low priced material, it would be very cost-effective to modify it in order to increase its temperature tolerance and replace the more expensive AMPS<sup>®</sup> copolymers as cement retarders.

## 7 ZUSAMMENFASSUNG

Bei der Zementierung von Bohrlöchern müssen unterschiedliche Gesteinsformationen und produzierende Horizonte gegeneinander sowie gegen gas- und wasserführende Zonen dauerhaft abgedichtet werden (*zonal isolation*). Die eingesetzten Portland-Zementsysteme müssen hierbei optimal auf die im Bohrloch herrschenden Bedingungen eingestellt werden. Hoher Druck, hohe Temperaturen und hoher Salzgehalt machen den Einsatz von Zusatzmitteln notwendig.

Während des Verpumpens von Zementschlämmen entlang poröser Gesteinsformationen kann eine Art Druckfiltration stattfinden, die eine unvollständige Zementierung des Bohrloches nach sich zieht. *Fluid loss additive* (Wasserretentionsmittel) reduzieren den unkontrollierten Wasserverlust der Zementschlämme und ermöglichen *zonal isolation*. Das Wasserretentionsmittel Poly(*N,N*-dimethylacrylamid-*co*-Ca 2-acrylamido-2-methylpropan sulfonat) (CaAMPS<sup>®</sup>-*co*-NNDMA) erreicht dies durch Adsorption auf der Zementoberfläche, die eine reduzierte Permeabilität des Filterkuchens zur Folge hat.

In Öl- und Gasbohrungen wird gelegentlich auch in Salzfronten zementiert. Die Verwendung einer Zementschlämme, die mit Süßwasser angemischt wurde, führt zu einem starken Konzentrationsgefälle zwischen Schlämme und Formation. Um die osmotische Auflösung der Salzfront zu verhindern, wird Zementschlämme mit hohem Natriumchloridgehalt verwendet. Weitere wichtige Zementzusatzmittel sind *free water control agents* wie Welan gum und Diutan gum. Diese mikrobiellen Biopolymere stabilisieren auch bei niedrigen Schlämmdichten die verwendeten Zementsysteme und gewährleisten dadurch die Integrität des Bohrlochs. Da die meisten Zementationsarbeiten eine Pumpdauer von vier bis sechs Stunden benötigen, werden außerdem Zusatzmittel wie zum Beispiel Natriumlignosulfonat verwendet, welche die Zementhydratation verzögern.

In der vorliegenden Arbeit wurden die physikalisch-chemischen Wechselwirkungen untersucht, die das Adsorptionsverhalten und die daraus resultierende Wirksamkeit von CaAMPS<sup>®</sup>-*co*-NNDMA an Zement beeinflussen. Zusätzlich zur Temperaturtoleranz bei 100 °C wurden Wechselwirkungen mit *free water control agents* und Verzögerern untersucht, da in der Ölbohrindustrie häufig Inkompatibilitäten zwischen gemeinsam eingesetzten Additiven auftreten.

Die Adsorption des Wasserretentionsmittels CaAMPS<sup>®</sup>-*co*-NNDMA wird über Sulfonatgruppen vermittelt, über die das Polymer Calciumionen komplexiert, die an der Zementkornoberfläche immobilisiert sind. Es wurde gezeigt, dass die Wirksamkeit von CaAMPS<sup>®</sup>-*co*-NNDMA aufgrund reduzierter Polymeradsorption an Zement bei hoher Temperatur abnimmt. Dieser Effekt konnte hauptsächlich auf die geringe Calcium-Bindfähigkeit der Sulfonatgruppen des CaAMPS<sup>®</sup>-*co*-NNDMA zurückgeführt werden.

Zusätzlich wurde beobachtet, dass sich die bei hoher Temperatur erhöhte Sulfatkonzentration der Zementporenlösung auf die Wirksamkeit des CaAMPS<sup>®</sup>-*co*-NNDMA auswirkt. Die erhöhte Sulfatkonzentration wird durch die Umwandlung des Hydratationsproduktes Ettringit bei Temperaturen über 80 °C bedingt und führt zu einer Verringerung des Gyrationradius des Polymers, welche dessen Adsorption ebenfalls negativ beeinflusst. Kompetitive Adsorption zwischen Sulfatanionen und Polymermolekülen um die in begrenzter Anzahl vorhandenen Adsorptionsplätze an der Zementkornoberfläche konnte hingegen nicht beobachtet werden.

Das mit zusätzlichen vicinalen Carboxylat-Funktionen modifizierte Polymer CaAMPS<sup>®</sup>-*co*-NNDMA-*co*-MA zeigte hingegen stärkeres Calcium-Bindevermögen im Vergleich zum unmodifizierten Polymer. Unabhängig von Temperatur und Sulfatgehalt der Porenlösung führte dies zu einer stabilen Adsorption von CaAMPS<sup>®</sup>-*co*-NNDMA-*co*-MA an der Zementoberfläche und dadurch zu einer verbesserten Wirksamkeit. Die Ergebnisse dieser Untersuchung zeigen, dass bereits geringfügige Veränderungen der Polymerzusammensetzung einen erstaunlich starken Effekt auf dessen Eigenschaften haben können. Zusätzlich gewährt diese Studie einen Einblick in die Vielfältigkeit der Parameter, die, in einem System so komplex wie hydratisierendem Zement, Einfluss auf das Verhalten von Additiven ausüben.

Zudem wurde gezeigt, dass in salinen Zementschlämmen die Wirksamkeit von CaAMPS<sup>®</sup>-*co*-NNDMA stark erniedrigt ist. Die in hoher Konzentration vorliegenden Chloridionen, die eine sehr viel höhere anionische Ladungsdichte als das Wasserretentionsmittel aufweisen, adsorbieren bevorzugt auf der Zementkornoberfläche und verhindern so die Adsorption des Wasserretentionsmittels CaAMPS<sup>®</sup>-*co*-NNDMA.

Weitere Experimente zu Polymerinkompatibilität zeigten, dass das mikrobielle Polymer Welan gum die adsorbierte Menge des Wasserretentionsmittels reduziert und dessen Wirksamkeit verringert, da seine Carboxylat-Ankergruppen ein hohes Calcium-Bindevermögen aufweisen. In Gegensatz zu Welan gum besitzt das mikrobielle Biopolymer Diutan gum längere Seitengruppen, die dessen Carboxylat-Ankergruppen effektiver

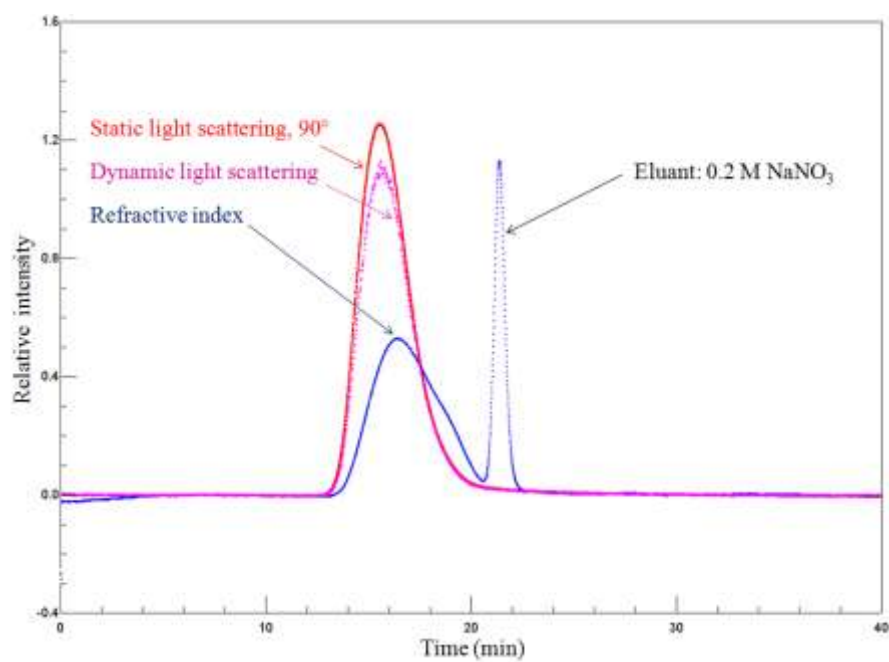
abschirmen. Dadurch wird das Calcium-Bindevermögen von Diutan gum so verringert, dass in Gegenwart dieses *free water control agents* das Wasserretentionsmittel CaAMPS<sup>®</sup>-co-NNDMA in genügend hoher Menge adsorbieren kann, um seine Wirksamkeit aufrecht zu erhalten.

Die Ergebnisse dieser Studie zeigen, dass Adsorption und dadurch Wirksamkeit von CaAMPS<sup>®</sup>-co-NNDMA in Gegenwart von weiteren anionischen Additiven gestört werden kann, wenn diese im Vergleich zu CaAMPS<sup>®</sup>-co-NNDMA eine höhere Affinität zur Zementkornoberfläche aufweisen. Durch kompetitive Adsorption kann die adsorbierte Menge und somit die Effektivität dieses AMPS<sup>®</sup>-basierten Polymers erniedrigt werden. Die kompetitive Wechselwirkung zwischen Polymeren wird durch deren anionische Ladungsdichte, die Qualität ihrer Ankergruppen (Calcium-Bindevermögen) und deren Konzentration beeinflusst. Kompetitive Adsorption zwischen Additiven und resultierende Polymerinkompatibilität kann durch gezielte Modifizierung der Polymerstruktur in Hinblick auf deren anionische Ladungsdichte und die Qualität der Ankergruppen verhindert werden. Dadurch können Multikomponentensysteme aufgebaut werden, die sich durch überragende Wirksamkeit auszeichnen. Das Wissen um die Wirkmechanismen der einzelnen Additive ist hierbei der Schlüssel zur Optimierung der Wirksamkeit des Systems.

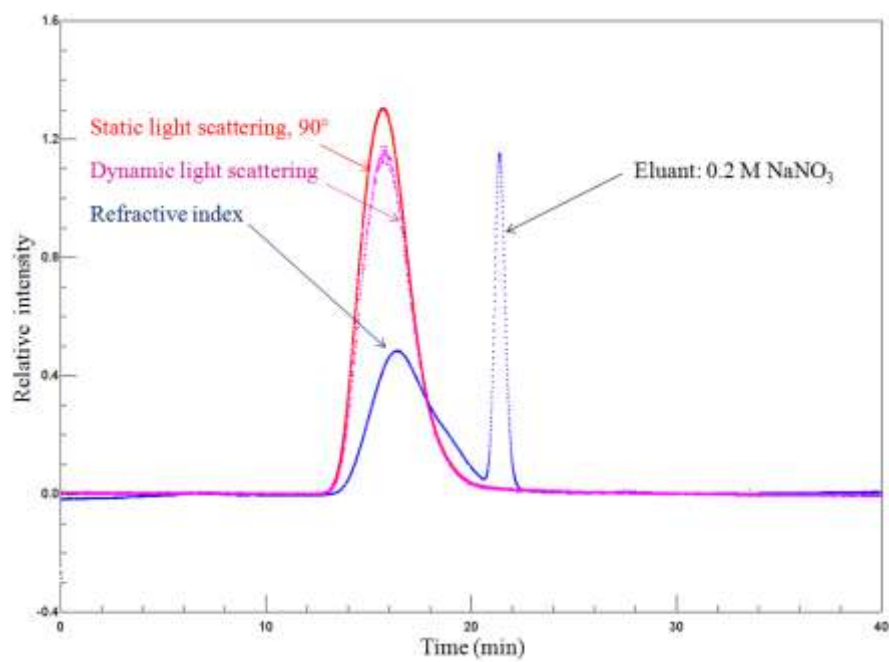
Neben der beschriebenen Polymerinkompatibilität konnten aber auch synergistische Wechselwirkungen von Additiven nachgewiesen werden. In dieser Studie wurde gezeigt, dass sich die Wirksamkeit des Wasserretentionsmittels CaAMPS<sup>®</sup>-co-NNDMA in Gegenwart des Verzögerers Natriumlignosulfonat verbessert. Dieses Lignin-basierte Polymer bildet negativ geladene Agglomerate mit Calciumionen, die in hoher Konzentration in der Zementporenlösung vorhanden sind. Diese adsorbieren auf der Zementkornoberfläche, bilden eine semi-permeable Schicht und verhindern dadurch den Kontakt des noch nicht hydratisierten Zementkorns mit Wasser. Dadurch wird einerseits die Zementhydratation verzögert, andererseits verschließt die gleichzeitige Adsorption von Lignosulfonat-Agglomeraten und *fluid loss polymer* die Poren des Zementfilterkuchens effektiver als in Zementssystemen, die nur CaAMPS<sup>®</sup>-co-NNDMA enthalten. In einem binären Additivsystem bestehend aus Natriumlignosulfonat und dem Wasserretentionsmittel, führt dies zu einer stärkeren Reduktion der Filterkuchenpermeabilität und dadurch zu einer besseren Wirksamkeit des CaAMPS<sup>®</sup>-co-NNDMA.

Die hier beobachteten Zusammenhänge können auch auf andere im Ölfeld verwendete Systeme, wie zum Beispiel Bohrspülungen, übertragen werden.

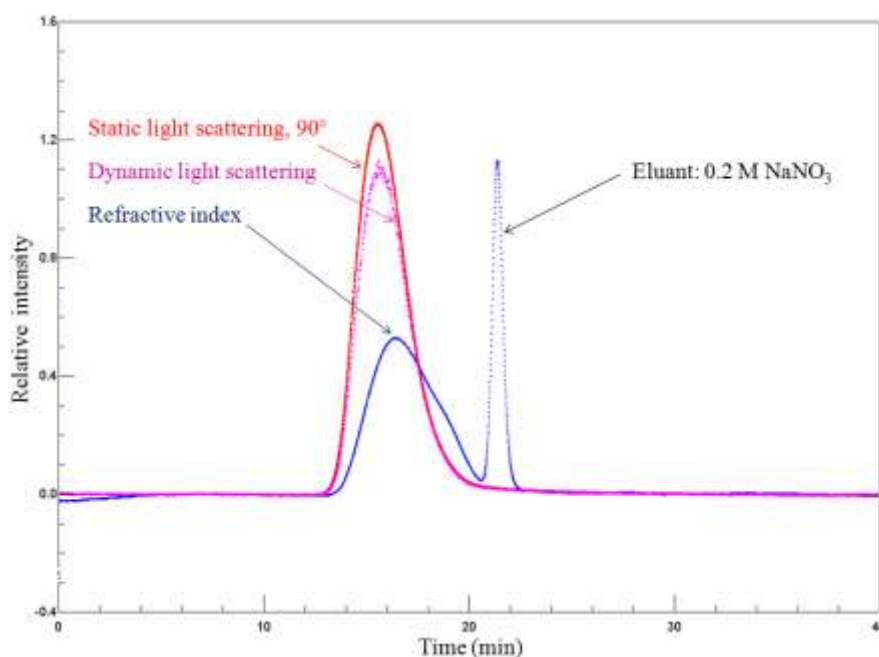
## 8 APPENDIX



SEC chromatogram of the synthesized terpolymer 1



SEC chromatogram of the synthesized terpolymer 2



SEC chromatogram of the synthesized terpolymer 3

#### Commercial samples used in this study

Name	Trade name	Usage	Supplier
Welan gum	Biozan <sup>®</sup>	Free water control agent	Kelco Oil Field Group, Houston, USA
Diutan gum	Kelco-Crete <sup>®</sup> DG	Free water control agent	CP Kelco UK Ltd., Surrey, United Kingdom
Ca <sup>2+</sup> lignosulfonate	Borrement Ca 120 <sup>®</sup>	Cement plasticizer and retarder	Borregaard Deutschland GmbH, Karlsruhe, Germany
Na <sup>+</sup> lignosulfonate	HR-5 <sup>®</sup>	Cement plasticizer and retarder	Halliburton GmbH, Celle, Germany

***Q* and *e* values of the monomers used for the preparation of the FLAs [93]**

Monomer	<i>Q</i>	<i>e</i>
AMPS <sup>®</sup>	0.39	0.22
NNDMA	0.41	-0.26
MA	0.86	3.69

**Correlation between polymer conformation and *Burchard* parameter [91]**

Conformation	<i>Burchard</i> parameter, $\rho$
Stiff chains	2.20
Linear statistic bundles	1.50 to 2.05
Star-like branched molecules	1.00
Compact balls	0.78
Microgel, globular structures	0.30 to 0.50

## 9 REFERENCES

- [1] P.A. Dickey, *The first oil well*, Journal of Petroleum Technology, 11, **1959**, 14.
- [2] D.K. Smith, *Cementing*, Monograph Vol. 4, American Institute of Mining, Metallurgical and Petroleum Engineers, Inc.: New York, USA **1976**.
- [3] R.C. Smith, *Successful primary cementing can be a reality*, Journal of Petroleum Technology, 36, **1984**, 1851.
- [4] J.K. Fink, *Oil field chemicals*, Gulf Professional Publishing: Burlington, USA **2003**.
- [5] J. Plank, *Anwendung synthetischer Retentionsmittel in der Tiefbohrzementierung* in: Chemanager Spezial, Kunststoff Forschung: Bauchemie, M. Reubold; C.K. Schemel-Trumpfeller; GIT Verlag GmbH: Darmstadt, Germany **2000**.
- [6] P. Rao; J.F. Burkhalter, *Hydrolytically stable polymers for use in oil field cementing methods and compositions*, U.S. Patent No. 4,515,635; **1985**.
- [7] E.B. Nelson; D. Guillot, *Well cementing*, 2nd Edition, Schlumberger: Sugar Land, USA **2006**.
- [8] *Primary cementing course*, PetroSkill Alliance, Dubai, United Arab Emirates **2007**.
- [9] J. Plank, *Applications of biopolymers in construction engineering* in: Biopolymers, A. Steinbüchel; Wiley-VCH Verlag GmbH: Weinheim, Germany **2003**.
- [10] V.S. Ramachandran, *Interaction of calcium lignosulfonate with tricalcium silicate, hydrated tricalcium silicate, and calcium hydroxide*, Cement and Concrete Research, 2, **1972**, 179.
- [11] G.V. Chilingar; J.O. Robertson; S. Kumar, *Surface operations in petroleum production*, Elsevier Science Publishers: Amsterdam, The Netherlands **1989**.
- [12] <http://litoilinvestments.com/fundamentals.html> (15.12.09).

- [13] J. Plank; D. Stephan; C. Hirsch, *Bauchemie* in: Chemische Technik-Prozesse und Produkte, Band 7 (Industrieprodukte), Winnacker/Küchler; Verlag Wiley-VCH: Weinheim, Germany **2004**.
- [14] API Specification 10A, *Specification for cements and materials for well cementing*, 23rd Edition, American Petroleum Institute: Washington, USA **2002**.
- [15] P.C. Hewlett, *Lea's chemistry of cement and concrete*, 4th Edition, Elsevier Linacre House: Oxford, United Kingdom **2004**.
- [16] Z.-Q. Wu; J. Young, *The hydration of tricalcium silicate in the presence of colloidal silica*, Journal of Materials Science, 19, **1984**, 3477.
- [17] J.I. Escalante-Garcia; J.H. Sharp, *Variation in the composition of C-S-H gel in Portland cement pastes cured at various temperatures*, Journal of the American Ceramic Society, 82, **1999**, 3237.
- [18] D.L. Rayment; A.J. Majumdar, *The composition of the C-S-H phases in portland cement pastes*, Cement and Concrete Research, 12, **1982**, 753.
- [19] H.F.W. Taylor, *Cement chemistry*, 2nd Edition, Thomas Telford Publishing: London, United Kingdom **1997**.
- [20] P. Meredith; A.M. Donald; K. Luke, *Pre-induction and induction hydration of tricalcium silicate: an environmental scanning electron microscopy study*, Journal of Materials Science, 30, **1995**, 1921.
- [21] H. Taylor; P. Barret; P. Brown; D. Double; G. Frohnsdorff; V. Johansen; D. Ménétrier-Sorrentino; I. Odler; L. Parrott; J. Pommersheim; M. Regourd; J. Young, *The hydration of tricalcium silicate*, Materials and Structures, 17, **1984**, 457.
- [22] J.G.M. DeJong; H.N. Stein; J.M. Stevels, *Hydration of tricalcium silicate*, Journal of Applied Chemistry, 17, **1967**, 246.
- [23] J.D. Birchall; A.J. Howard; D.D. Double, *Some general considerations of a membrane/osmosis model for Portland cement hydration*, Cement and Concrete Research, 10, **1980**, 145.

- [24] L.S. Dent Glasser; E.E. Lachowski; K. Mohan; H.F.W. Taylor, *A multi-method study of  $C_3S$  hydration*, Cement and Concrete Research, 8, **1978**, 733.
- [25] M.E. Tadros; J. Skalny; R.S. Kalyoncu, *Early hydration of tricalcium silicate*, Journal of the American Ceramic Society, 59, **1976**, 344.
- [26] I. Odler; H. Dörr, *Early hydration of tricalcium silicate II. The induction period*, Cement and Concrete Research, 9, **1979**, 277.
- [27] M. Collepardi; G. Baldini; M. Pauri; M. Corradi, *Retardation of tricalcium aluminate hydration by calcium sulfate*, Journal of the American Ceramic Society, 62, **1979**, 33.
- [28] M. Collepardi; G. Baldini; M. Pauri; M. Corradi, *The effect of pozzolanas on the tricalcium aluminate hydration*, Cement and Concrete Research, 8, **1978**, 741.
- [29] J. Rose; A. Bénard; S. El Mrabet; A. Masion; I. Moulin; V. Briois; L. Olivi; J.Y. Bottero, *Evolution of iron speciation during hydration of  $C_4AF$* , Waste Management, 26, **2006**, 720.
- [30] D. Stephan; S. Dikoundou; G. Raudaschl-Sieber, *Influence of combined doping of tricalcium silicate with  $MgO$ ,  $Al_2O_3$  and  $Fe_2O_3$ : synthesis, grindability, X-ray diffraction and  $^{29}Si$  NMR*, Materials and Structures, 41, **2008**, 1729.
- [31] G. Le Saout; E. Lécolier; A. Rivereau; H. Zanni, *Chemical structure of cement aged at normal and elevated temperatures and pressures: Part I. Class G oilwell cement*, Cement and Concrete Research, 36, **2006**, 71.
- [32] A. Bentur; R.L. Berger; J.H. Kung; N.B. Milestone; J.F. Young, *Structural properties of calcium silicate pastes: II, effect of curing temperature*, Journal of the American Ceramic Society, 62, **1979**, 362.
- [33] K.L. Scrivener, *The effect of heat treatment of inner product C-S-H*, Cement and Concrete Research, 22, **1992**, 1224.
- [34] J.J. Thomas; D. Rothstein; H.M. Jennings; B.J. Christensen, *Effect of hydration temperature on the solubility behavior of Ca-, S-, Al-, and Si-bearing solid phases in Portland cement pastes*, Cement and Concrete Research, 33, **2003**, 2037.

- [35] D. Damidot; F.P. Glasser, *Thermodynamic investigation of the CaO-Al<sub>2</sub>O<sub>3</sub>-CaSO<sub>4</sub>-H<sub>2</sub>O system at 50°C and 85°C*, Cement and Concrete Research, 22, **1992**, 1179.
- [36] Q. Zhou; F.P. Glasser, *Thermal stability and decomposition mechanisms of ettringite at <120°C*, Cement and Concrete Research, 31, **2001**, 1333.
- [37] B. Bresson; F. Meducin; H. Zanni; C. Noik, *Hydration of tricalcium silicate (C<sub>3</sub>S) at high temperature and high pressure*, Journal of Materials Science, 37, **2002**, 5355.
- [38] M.A. Swayze, *Effect of high temperatures on strength of oil-well cements*, American Petroleum Institute, API 54-072, **1954**.
- [39] L.H. Eilers; R.L. Root, *Long-term effects of high temperature on strength retrogression of cements*, SPE California Regional Meeting, Long Beach, USA **1976**.
- [40] K. Luke; H.F.W. Taylor; G.L. Kalousek, *Some factors affecting formation of truscottite and xonotlite at 300-350°C*, Cement and Concrete Research, 11, **1981**, 197.
- [41] K. Luke; H.F.W. Taylor, *Equilibria and non-equilibria in the formation of xonotlite and truscottite*, Cement and Concrete Research, 14, **1984**, 657.
- [42] H.F.W. Taylor, *The chemistry of cements*, Academic Press Inc. Ltd.: London, United Kingdom **1964**.
- [43] L.H. Eilers; E.B. Nelson; L.K. Moran, *High-temperature cement compositions - pectolite, scawtite, truscottite, or xonotlite: Which do you want?*, Journal of Petroleum Technology, 35, **1983**, 1373.
- [44] J.P. Gallus; D.E. Pyle; L.T. Watters, *Performance of oilwell cementing compositions in geothermal wells*, SPE 7591, **1979**.
- [45] P.F.G. Banfill, *The rheology of fresh cement and concrete - a review*, 11th International Cement Chemistry Congress, Durban, South Africa **2003**.
- [46] J. Punkki; J. Golaszewski; O.E. Gjorv, *Workability loss of high-strength concrete*, Materials Journal, 93, **1996**, 427.
- [47] J.G. Savins; W.F. Roper, *A direct-indicating viscometer for drilling fluids*, American Petroleum Institute, API 54-007, **1954**.

- [48] D.G. Hill, *Clay stabilization - criteria for best performance*, SPE Formation Damage Control Symposium, Lafayette, USA **1982**.
- [49] K.A. Slagle; K. Dwight, *Salt cement for shale and bentonitic sands*, Journal of Petroleum Technology, 15, **1963**, 187.
- [50] N.C. Ludwig, *Effect of sodium chloride on setting properties of oil-well cements*, American Petroleum Institute, API 51-020, **1951**.
- [51] J. Plank; B. Sachsenhauser, *Impact of molecular structure on zeta potential and adsorbed conformation of  $\alpha$ -allyl- $\omega$ -methoxypolyethylene glycol - maleic anhydride superplasticizers*, Journal of Advanced Concrete Technology, 4, **2006**, 233.
- [52] J. Plank; C. Hirsch, *Impact of zeta potential of early cement hydration phases on superplasticizer adsorption*, Cement and Concrete Research, 37, **2007**, 537.
- [53] I. Iwasaki; P.L.D. Bruyn, *The electrochemical double layer on silver sulfide at pH 4.7. I. In the absence of specific adsorption*, The Journal of Physical Chemistry, 62, **1958**, 594.
- [54] M.Y.A. Mollah; W. Yu; R. Schennach; D.L. Cocks, *A Fourier transform infrared spectroscopic investigation of the early hydration of Portland cement and the influence of sodium lignosulfonate*, Cement and Concrete Research, 30, **2000**, 267.
- [55] S. Goni; M.P. Lorenzo; A. Guerrero; M.S. Hernandez, *Calcium hydroxide saturation factors in the pore solution of hydrated Portland cement fly ash pastes*, Journal of the American Ceramic Society, 79, **1996**, 1041.
- [56] M.Y.A. Mollah; R.K. Vempati; T.C. Lin; D.L. Cocks, *The interfacial chemistry of solidification/stabilization of metals in cement and pozzolanic material systems*, Waste Management, 15, **1995**, 137.
- [57] M.Y.A. Mollah; W.J. Adams; R. Schennach, *A review of cement-superplasticizer interactions and their models*, Advances in Cement Research, 12, **2000**, 153.
- [58] M. Mosquet; P. Maitresse; J.-P. Guicquero, *Ethoxylated di-phosphonate: An extreme molecule for extreme applications*, Seventh CANMET/ACI International Conference on Superplasticizers and Other Chemical Admixtures in Concrete, Berlin, Germany, ACI SP-217, **2003**, 161.

- [59] API Specification 10B, *Recommended Practice for Testing Well Cements*, 22nd Edition, American Petroleum Institute: Washington, USA **1997**.
- [60] J. Desbrières, *Cement cake properties in static filtration - influence of polymeric additives on cement filter cake permeability*, *Cement and Concrete Research*, 23, **1993**, 347.
- [61] J. Desbrières, *Cement cake properties in static filtration. On the role of fluid loss control additives on the cake porosity*, *Cement and Concrete Research*, 23, **1993**, 1431.
- [62] J. Plank; A. Brandl; Y.N. Zhai; A. Franke, *Adsorption behavior and effectiveness of poly(N,N-dimethylacrylamide-co-Ca 2-acrylamido-2-methylpropanesulfonate) as cement fluid loss additive in the presence of acetone-formaldehyde-sulfite dispersant*, *Journal of Applied Polymer Science*, 102, **2006**, 4341.
- [63] J. Plank; F. Dugonjic-Bilic; N. Recalde Lummer, *Modification of the molar anionic charge density of acetone-formaldehyde-sulfite dispersant to improve adsorption behavior and effectiveness in the presence of CaAMPS (R)-co-NNDMA cement fluid loss polymer*, *Journal of Applied Polymer Science*, 111, **2009**, 2018.
- [64] J. Plank; A. Brandl; N. Recalde Lummer, *Effect of different anchor groups on adsorption behavior and effectiveness of poly (N,N-dimethylacrylamide-co-Ca 2-acrylamido-2-methylpropanesulfonate) as cement fluid loss additive in presence of acetone-formaldehyde-sulfite dispersant*, *Journal of Applied Polymer Science*, 106, **2007**, 3889.
- [65] M. Saric-Coric; K.H. Khayat; A. Tagnit-Hamou, *Performance characteristics of cement grouts made with various combinations of high-range water reducer and cellulose-based viscosity modifier*, *Cement and Concrete Research*, 33, **2003**, 1999.
- [66] F.L. Allen; G.H. Best; T.A. Lindroth, *Welan gum in cement compositions*, U.S. Patent 4,963,668; **1990**.
- [67] B. Skaggs; M. O'brien, *Carrier fluid for the suspension and delivery of water soluble polymers*, US Patent 5,362,312; **1994**.

- [68] V. Crescenzi; M. Dentini; T. Coviello; R. Rizzo, *Comparative analysis of the behavior of gellan gum(S-60) and welan gum(S-130) in dilute aqueous solution*, Carbohydrate Research, 149, **1986**, 425.
- [69] J. Plank, *Applications of biopolymers and other biotechnological products in building materials*, Applied Microbiology and Biotechnology, 66, **2004**, 1.
- [70] S.P. Campana Filho; C. Andrade; M. Milas; M. Rinaudo, *Polyelectrolyte and rheological studies on the polysaccharide welan*, International Journal of Biological Macromolecules, 12, **1990**, 379.
- [71] R. Chandrasekaran; A. Radha, *Molecular architectures and functional properties of gellan gum and related polysaccharides*, Trends in Food Science & Technology, 6, **1995**, 143.
- [72] M. Tako, *Molecular origin for the thermal stability of S-657 polysaccharide produced by Xanthomonas ATCC 53159*, Polymer Gels and Networks, 2, **1994**, 91.
- [73] R. Coleman; Y. Patel; N. Harding, *Identification and organization of genes for diutan polysaccharide synthesis from Sphingomonas sp. ATCC 53159*, Journal of Industrial Microbiology and Biotechnology, 35, **2008**, 263.
- [74] R.C. Navarrete; J.M. Scheult, *New bio-polymers for drilling, drill-in, completions, spacer fluids and coiled tubing applications*, IADC/SPE Asia Pacific Drilling Technology, Kuala Lumpur, Malaysia **2000**.
- [75] A. Salhan; J. Billingham; A.C. King, *The effect of a retarder on the early stages of the hydration of tricalcium silicate*, Journal of Engineering Mathematics, 45, **2003**, 367.
- [76] N.L. Thomas; J.D. Birchall, *The retarding action of sugars on cement hydration*, Cement and Concrete Research, 13, **1983**, 830.
- [77] M.Y.A. Mollah; F. Lu; R. Schennach; D.L. Cocke, *An X-ray diffraction, Fourier-transform infrared spectroscopy, and scanning electron microscopy/energy-dispersive spectroscopic investigation of the effect of sodium lignosulfonate superplasticizer on the hydration of Portland cement type V*, Polymer-Plastics Technology and Engineering, 38, **1999**, 849.

- [78] D.D. Double; P.C. Hewlett; K.S.W. Sing; J.F. Raffle, *New developments in understanding the chemistry of cement hydration [and discussion]*, Philosophical Transactions of the Royal Society A: Physical, Mathematical and Engineering Sciences, 310, **1983**, 53.
- [79] M. Bishop; A.R. Barron, *Cement hydration inhibition with sucrose, tartaric acid, and lignosulfonate: An analytical and spectroscopic study*, Industrial & Engineering Chemistry Research, 45, **2006**, 7042.
- [80] X. Ouyang; X. Qiu; P. Chen, *Physicochemical characterization of calcium lignosulfonate - a potentially useful water reducer*, Colloids and Surfaces A: Physicochemical and Engineering Aspects, 282-283, **2006**, 489.
- [81] A.C. Jupe; A.P. Wilkinson; K. Luke; G.P. Funkhouser, *Class H Oil Well Cement Hydration at Elevated Temperatures in the Presence of Retarding Agents: An In Situ High-Energy X-ray Diffraction Study*, Industrial & Engineering Chemistry Research, 44, **2005**, 5579.
- [82] M.Y.A. Mollah; F. Lu; D.L. Cocco, *An X-ray diffraction (XRD) and Fourier transform infrared spectroscopic (FT-IR) characterization of the speciation of arsenic (V) in Portland cement type-V*, The Science of The Total Environment, 224, **1998**, 57.
- [83] L.B. McCusker; R.B. VonDreele; D.E. Cox; D. Louër; P. Scardi, *Rietveld refinement guidelines*, Journal of Applied Crystallography, 32, **1999**, 36.
- [84] M.B. Huglin, *Specific refractive index increments of polymers in dilute solution in: Polymer handbook*, 3rd. Edition, J. Brandrup; E.H. Immergut; John Wiley & Sons: New York, USA **1989**.
- [85] J. Plank; B. Sachsenhauser, *Experimental determination of the effective anionic charge density of polycarboxylate superplasticizers in cement pore solution*, Cement and Concrete Research, 39, **2009**, 1.
- [86] P.P. Rao; D.L. Sutton, *Method and apparatus for nondestructive testing of cement*, US Patent 4,259,868; **1981**.

- [87] K.H. Khayat; A. Yahia, *Simple field tests to characterize fluidity and washout resistance of structural cement grout*, Cement Concrete & Aggregates Australia, 20, **1998**, 145.
- [88] S.L. Colston; P. Barnes; A.C. Jupe; S.D.M. Jacques; C. Hall; P. Livesey; J. Dransfield; N. Meller; G.C. Maitland, *An in situ synchrotron energy-dispersive diffraction study of the hydration of oilwell cement systems under high temperature/autoclave conditions up to 130 °C*, Cement and Concrete Research, 35, **2005**, 2223.
- [89] C.L. McCormick; L.S. Park; G.S. Chen; H.H. Neidlinger, *Model acrylamide random and graft copolymers (I) – synthesis and characterization*, Polymer Preprints, 22, **1981**, 137.
- [90] L.-K. Bi; M.E. Dillon; C. Sharik, *N-dimethylacrylamide/2-acrylamido-2-methylpropane sulfonic acid copolymers for enhanced petroleum recovery*, U.S. Patent No. 4,404,111; **1983**.
- [91] W. Burchard, *Static and dynamic light scattering from branched polymers and biopolymers* in: Light scattering from polymers, Springer: Berlin, Germany **1983**.
- [92] G. Odian, *Principles of polymerization*, 3rd Edition, Wiley & Sons: New York, USA **1991**.
- [93] R.Z. Greenley, *Q and e values for free radical copolymerizations of vinyl monomers and telogens* in: Polymer handbook, 4 th Edition, J. Brandrup; E.H. Immergut; E.A. Grulke; Wiley & Sons: New York, USA **1999**.
- [94] J. Plank; N. Recalde Lummer; F. Dugonjic-Bilic, *Competitive adsorption between an AMPS®-based fluid loss polymer and welan gum biopolymer in oil well cement*, Journal of Applied Polymer Science 116, **2010**, 2913.
- [95] A. Sabhapondit; A. Borthakur; I. Haque, *Adsorption behavior of poly(N,N-dimethylacrylamide-co-Na 2-acrylamido-2-methylpropanesulfonate) on sand surface*, Journal of Applied Polymer Science, 91, **2004**, 2482.
- [96] A. Jada; R. Ait Akbour; J. Douch, *Surface charge and adsorption from water onto quartz sand of humic acid*, Chemosphere, 64, **2006**, 1287.

- [97] J. Plank; C. Schroeﬂ; M. Gruber; M. Lesti; R. Sieber, *Effectiveness of polycarboxylate superplasticizers in ultra-high strength concrete: The importance of PCE compatibility with silica fume*, Journal of Advanced Concrete Technology, 7, **2009**, 5.
- [98] K. Yamada; S. Ogawa; S. Hanehara, *Controlling of the adsorption and dispersing force of polycarboxylate-type superplasticizer by sulfate ion concentration in aqueous phase*, Cement and Concrete Research, 31, **2001**, 375.
- [99] S. Hanehara; K. Yamada, *Rheology and early age properties of cement systems*, Cement and Concrete Research, 38, **2008**, 175.
- [100] M. Sonebi, *Rheological properties of grouts with viscosity modifying agents as diutan gum and welan gum incorporating pulverised fly ash*, Cement and Concrete Research, 36, **2006**, 1609.
- [101] J. Plank; C. Winter, *Competitive adsorption between superplasticizer and retarder molecules on mineral binder surface*, Cement and Concrete Research, 38, **2008**, 599.

...ῥρκια δ' αὖ κατόπισθε μετ' ἀμφοτέροισιν ἔθηκε

Παλλὰς Ἀθηναίη, κούρη Διὸς αἰγιόχοιο,

Μέντορι εἰδομένη ἡμὲν δέμας ἠδὲ καὶ αὐδήν.

Homer, *Odyssey*, Book 24, Lines 546 to 548